Chapter 4: Ozonesondes: Instrumentation and Data Applications – Final Version 14 Dec 2021

Anne M. Thompson[1,2], Herman G. J. Smit[3], Debra E. Kollonige[1,4], Ryan M. Stauffer[1]

[1]NASA-Goddard Space Flight Center, Earth Sciences Division, Greenbelt, MD USA; [2]Joint Center for Environmental Technology, University of Maryland – Baltimore County, MD USA; [3]Forschungszentrum-Jülich, Jülich, Germany; [4]SSAI, Lanham, MD USA

"Nobody can be uncheered with a balloon" A. A. Milne, *Winnie the Pooh*

1. The Role of Ozonesondes in the Global Ozone Measurement Framework

1.1 Sondes in the Context of a Global Ozone Measurement Strategy

The ozonesonde instrument, although more than 50 years old in design, and simple to operate, remains an essential component of the global observing strategy for stratospheric and tropospheric ozone. The profiles from ozonesondes are foundational in the development of satellite ozone retrievals and are used for validating satellite products from a growing constellation of ozone-measuring sensors. The ozonesonde instrument is unique in providing readings at (5-10)% uncertainty or better throughout the troposphere to the mid-stratosphere at 100-150 m resolution independent of conditions of cloudiness or precipitation (**Figure 1**). Because it is relatively inexpensive and easy to operate – launching with a standard radiosonde instrument -- the ozonesonde can be used virtually anywhere. Ozone sounding records provide the longest record of the vertical distribution of ozone and thus play a key role in monitoring changes in stratospheric ozone in accordance with the Montreal Protocol (*WMO/UNEP*, 2019).

Figure 2 illustrates how ozonesondes fit into the global ozone observing strategy that employs various ground-based spectroscopic and lidar techniques, ozone instruments on aircraft and balloons as well as from space-borne platforms. The altitude ranges of sonde operation, aircraft, and Low-Earth Orbit (LEO) satellites are illustrated. Note that ozone-measuring instruments have been hosted on the International Space Station (SAGE III is currently operational). Geostationary satellites (e.g., the Korean GEMS, NOAA's GOES series) also carry ozone measuring instruments; these are typically 36,000 km above earth. The tropospheric and stratospheric segments of the atmosphere are usually measured by two separate lidar instruments (*McDermid et al.*, 1990; *McGee et al.*, 1991). An advantage of ozonesondes is that a single sounding encompasses the troposphere and lower and middle stratosphere.

In addition to monitoring and validation of other sensors, ozonesonde data are important in understanding atmospheric dynamics, lifetimes, and sources and sinks of ozone. Above the atmospheric boundary layer, the ozone lifetime is weeks to months. Thus, in the troposphere, sonde data are used to study the transport of pollution throughout the troposphere and lowermost stratosphere. Pollution from biomass fires in the tropics (*Thompson et al.*, 1996; 2001; 2003a,b), throughout mid-latitudes by intercontinental transport (*Stauffer et al.*, 2017) and from boreal fires (*Moeini et al.*, 2020) has been investigated. Recently sonde data across the midlatitude northern hemisphere quantified a significant drop in tropospheric ozone due to the global economic crisis instigated by the 2020 COVID-19 pandemic (*Steinbrecht et al.*, 2021).

1.2 Chapter Overview

The purpose of this chapter is to present the capabilities and applications of the ozonesonde measurement as they relate to remote sensing (**Sections 3 and 4**). We begin with a description of the ozonesonde instrument and ongoing research related to the quaality assurance (QA) of the data (**Section 2**).

2. The Ozonesonde Instrument, Operation and Data Quality Control

2.1 Electrochemical Ozonesondes

Ozonesondes are small, light-weight instruments that are flown on weather balloons coupled via interfacing electronics to radiosondes for data transmission and measurements of meteorological parameters: pressure, temperature, humidity, wind, and position. The total weight of the ozonesonde-radiosonde flight package is ~1 kg so the payload can be flown on relatively small balloons (typically 1200-1500 g). Using the telemetry of the radiosonde, the measured data are transmitted to the ground station for further processing. Normally, data are taken during ascent at a rise rate of about 5 m/s to a balloon burst altitude of 30-33 km altitude. The inherent response time of the chemical measurement of the ozonesonde is 20-30 s, which provides an effective height resolution in the ozone profile data of 100-150 m.

Since their first design in the 1960's, the most commonly used ozonesonde instruments are based on electrochemical detection methods that convert the sampled ozone into an electrical current. *Smit* (2014) describes the common ozonesonde types in use over the past 50 years. At the present time, the most widely used ozonesonde type is the Electrochemical Concentration Cell (ECC). Although widely deployed in the past, the Brewer Mast sonde is presently only launched at the Meteorological Observatory Hohenpeissenberg in Germany in a time series that started in 1967. Two other major electrochemical sonde types, developed by the India Meteorological Department and the Japan Meteorological Agency, are no longer used.

Each ozonesonde instrument is unique and is prepared and provisionally calibrated prior to launch. It is important for remote sensing researchers to understand operational aspects of the ozonesonde and the procedures that sonde data providers take to minimize uncertainties within an individual profile and to ensure consistency of the global ozonesonde record over time. The instrument and data treatment are described in the following sections.

2.2 The ECC Ozonesonde: Principles of Operation and Sources of Uncertainty

The ECC ozonesonde (**Figure 3**) developed by *Komhyr* (1969) consists of two cells, made of Teflon or molded plastic, which serve as a cathode and anode chamber. There are two widely used ECC ozonesonde types, manufactured by Science Pump Corporation and the EN-SCI Corporation, producing the SPC-6A and EN-SCI instrument, respectively. The design of both ECCs resembles **Figure 3** but there is a consistent 4-5% difference in their performance (**Figures 4A and 4B)** when the different instrument types are operated under the same conditions (*Smit et al*., 2007; *Thompson et al.*, 2007c; *Smit*, 2014). Both cells contain platinum mesh electrodes. They are immersed in aqueous potassium iodide (KI) solutions of different concentrations, whereby the cathode cell is charged with a solution of low KI concentration and the anode cell with a solution saturated with KI. The two chambers are linked together by an ion-bridge to provide an ion-pathway and to prevent mixing of the cathode and anode electrolytes. The detection is based on the titration of ozone in KI according to the redox reaction:

$$2\,KI + O_3 + H_2O \rightarrow I_2 + O_2 + 2\,KOH \qquad \text{(R-1)}$$

In the cathode cell, the iodine (I_2) is converted back into two iodide ions (I^-) by the uptake of two electrons from the platinum electrode surface. Continuous sampling is achieved by a small battery-driven gas pump made of Teflon that bubbles ambient air through the sensing solution of the electrochemical cell. The iodine molecules that are produced by the reaction are transported towards the cathode electrode to be converted back to I^-; this process generates an electrical current in an external circuit that is proportional to the sampled ozone per unit time. Given the pump flow rate ($\boldsymbol{\Phi_P}$ in $cm^3\ s^{-1}$), the pump temperature ($\boldsymbol{T_P}$ in K), the overall efficiency ($\boldsymbol{\eta_T}$) of the sensor cell, the measured electrical current ($\boldsymbol{I_M}$ *in* μA), after a correction for a background current ($\boldsymbol{I_B}$ in μA), is converted to the ozone partial pressure ($\boldsymbol{P_{O3}}$ in *mPa***):**

$$P_{O3} = 0.043085 * \frac{T_P}{(\eta_T * \Phi_P)} * (I_M - I_B) \qquad \text{(E-1)}$$

The constant 0.043085 is determined by the ratio of the gas constant (R) to two times the Faraday constant (for each O_3 molecule two electrons flow in the electrical circuit from reaction **R-1**). The overall efficiency, $\boldsymbol{\eta_T}$, includes: the absorption efficiency $\boldsymbol{\eta_A}$ of O_3 into the sensing solution (usually 1.00), the pressure dependent pump efficiency $\boldsymbol{\eta_P}$ and the conversion efficiency $\boldsymbol{\eta_C}$ of the ECC sensor cell. The last efficiency is predominantly determined by the stoichiometry of redox reaction **R-1** followed by the conversion of the produced iodine into the measured electrical current $\boldsymbol{I_M}$. In practice, most operators add a sodium-hydrogen phosphate buffer to the cathode KI-solution to maintain the pH at 7.0 to keep the stoichiometry of the redox reaction **R-1** close to one.

The uncertainty of the ECC sonde measurements of the ozone partial pressure ($\boldsymbol{P_{O3}}$) is a composite of the contributions of the individual uncertainties of the instrumental parameters ($\boldsymbol{I_M}$, $\boldsymbol{I_B}$, $\boldsymbol{T_P}$, $\boldsymbol{F_P}$, $\boldsymbol{\eta_T = \eta_A * \eta_P * \eta_C}$), as described in detail by *Tarasick et al.* (2021). *Tarasick et al.* (2021) assumed that all systematic uncertainty components are known and corrected for. All instrumental uncertainties are assumed to be random and uncorrelated such that they follow Gaussian statistics to determine the overall uncertainty of the measured $\boldsymbol{P_{O3}}$. In the troposphere the background current $\boldsymbol{I_B}$ is the dominant uncertainty, particularly in the upper troposphere where the ozone concentration is generally low (mid-latitudes) to very low (near the tropical tropopause).

In the stratosphere, uncertainties of pump characteristics (*Johnson et al.,* 2002) and conversion efficiencies are the major contributors to the overall uncertainty (*WMO/GAW Report No. 268,* 2021). Since 2000-2010, the radiosondes flown with the ozonesondes are equipped to measure GNSS altitude. This means that the ambient air pressure is determined from the altitude measurement (e.g. *Stauffer et al.* 2014) in which case the pressure uncertainty is better than 0.05-0.10 hPa above 50 hPa, making only a minor contribution to the overall uncertainty. However, in case of ozonesondes flown with non-GNSS radiosondes, generally those prior to ~2000, the uncertainty of the radiosonde pressure sensor measurement above 50 hPa could be the dominant source of error.

2.3 Quality Assurance (QA) of Ozonesondes: Approach and Current Status

There has been considerable research activity to understand the performance of the ozonesonde instrument and to establish standard operating procedures (SOP). Twenty-five years ago, the ozonesonde measurement was assigned a 15-20% accuracy *(SPARC/IOC/GAW, 1998)*. The total column ozone (TCO) amount is now typically accurate to within 2-3% when evaluated against co-located ground-based instruments. Accuracy throughout the column, when best practices are followed, is ~(5-10)%, with the potential to improve to (3-5)%.

2.3.1 Overview of Ozonesonde Community Quality Assurance (QA) Activities

The ozonesonde community, working together under the auspices of World Meteorological Organization/Global Atmospheric Watch (WMO/GAW) and groups like NDACC, the International Ozone Commission (IO3C), and, in the past decade, the GCOS Reference Upper Air Network (GRUAN), has organized QA research around three important activities. The first of these was the creation of a testing facility for ozonesondes. In the mid-1990s, as part of the WMO/GAW Quality Assurance plan (*WMO/GAW Report No. 104*, 1995), a World Calibration Centre for OzoneSondes (WCCOS) was established at Germany's Forschungszentrum-Jülich (*Smit et al.,* 2000). The heart of the WCCOS is an environmental simulation chamber in which up to four ozonesondes can be intercompared and calibrated against a dual beam UV-photometer (OPM; *Proffitt and McLaughlin*, 1983) that is traceable to the NIST standard for ozone. During testing, pressure, temperature and ozone concentration are varied at the rate of an actual ascent from the surface until burst altitude at 33-35 km altitude. In its first five years of operation a set of campaigns, each referred to as a Jülich Ozone Sonde Intercomparison Experiment (JOSIE; *WMO/GAW Report No. 130* (1998), *No. 157* (2004a) and *No. 158* (2004b)), quantified biases among ozonesonde types, ECC or otherwise, between the two major ECC types of instruments, among different sensing solution types (SST). *Smit et al.* (2007) summarized a JOSIE-2000 in which eight groups compared instruments and preparation methods over 10 simulations of various environments: polar, tropical, mid-latitude.

The second ozonesonde QA activity has been intercomparisons of ECC ozonesondes in the field. For example, JOSIE-2000 results on biases were confirmed in the field during the Balloon Experiment on Standards for Ozone (BESOS) campaign in 2004 (*Deshler et al.,* 2008), with 18 sondes flown on a single gondola along with the WCCOS standard OPM.

Examples from laboratory and field comparisons appear in **Figure 4.** In Figures **4A** and **4B,** offsets in the measurement of ozone between the two instruments from JOSIE-2000 and BESOS, respectively, are shown. The OPM was the absolute reference in both experiments.

2.3.2 Development of Consensus-based Standard Operating Procedures (ASOPOS)

The third component of enhancing QA was the establishment in 2004 of an international team of 15-20 sonde experts to review laboratory and field tests in an Assessment of Standard Operating Procedures (SOPs) for OzoneSondes (ASOPOS). The first ASOPOS led to a community consensus for SOPs. Largely based on the 1996-2000 JOSIE campaigns and BESOS, the recommended SOPs were published as *WMO/GAW Report No. 201* (2014).

The 2017 JOSIE campaign, with simulations of only tropical conditions (*Thompson et al.,* 2019), was the basis for a ASOPOS 2.0 evaluation (*WMO/GAW No. Report 268*, 2021). The ASOPOS 2.0 report outlines (1) an improved treatment to correct the pump flow rate that falls off at low pressures; (2) a correction of the ozone exposure dependent stoichiometry of the O_3+KI redox reaction (**R-1**) to account for both slow (≅20-25 min) and fast (≅20-25 sec) reactions that take place in the ECC during an ascent (*Vömel et al*., 2020); (3) a new conversion efficiency in **Eq. E-1** that relates the final calculation of ozone amount to the OPM used at the WCCOS, making every reported sounding traceable to a common standard; (4) an extended list of metadata to be collected at launch time so data can be reprocessed; (5) continuous monitoring of station QA by comparing sonde ozone amounts to ground-based and satellite overpass measurements for detecting problems like the post-2013 total ozone "dropoff" observed at a number of stations (*Stauffer et al.* 2020; see Section 4.2). **Figure 4C** displays some JOSIE-2017 results. Operators prepared their sondes used for determining the average labeled "nominal SOP" according to their home station practices; for 7 of 8 stations tested, the preparation followed the first ASOPOS Report (*WMO/GAW Report No. 201,* 2014). For the "Low Buffer" tests all operators used a sensing solution with 1% KI and 10% of the standard buffer solution. Ozone measured with the low-buffer solution, irrespective of instrument type, measured closer to the OPM near the simulated tropopause altitude (~15 km) but always lower than the OPM elsewhere in the profile.

2.3.3 Homogenization of Long Ozonesonde Time-Series

The bias effects, i.e., discontinuities and trends introduced by instrumental artifacts, as described in the first ASOPOS Report (*WMO/GAW Report No. 201*, 2014), need to be accounted for in calculating reliable ozone profile trends. ECC ozonesondes were first manufactured 50 years ago and have undergone modifications of the instrument and in some cases, operational procedures, resulting in inhomogeneities in some station records and biases among stations. Discontinuities in total ozone or profile segments have appeared in the time-series at various stations. This phenomenon was recognized in a 2011/2012 Ozone Sonde Data Quality Assessment (O3S-DQA) that reviewed 40 years of ozonesonde records from a number of stations. The O3S-DQA activity led to guidelines for data providers to resolve inhomogeneities in long-term sonde records (*Smit et al.*, 2012; https://www.wccos-josie.org/o3s-dqa). Generic transfer functions were developed (*Deshler et al.*, 2017) to aid the process of harmonizing sonde records to the common standard of the combinations recommended in the *WMO/GAW Report No. 201* (2014).

Since 2015, ~40 of the long-term ozonesonde records within the global network have been re-processed following the O3S-DQA guidelines, removing known inhomogeneities to achieve overall uncertainties of 5-10 %. These include the Canadian stations (*Tarasick et al.*, 2016), several European stations (*Van Malderen et al*., 2016), those of the SHADOZ network (*Witte et al*., 2017, 2018; *Thompson et al.*, 2017), Wallops Island, VA (*Witte et al.*, 2019), and eight stations in the NOAA network (*Sterling et al.*, 2018). **Figure 5** shows the result of the homogenization effort of the ozonesonde time series at Boulder, CO (cyan triangle on the **Figure 6 map**), by comparing the total ozone column (TCO) derived from the sondes with TCO measured by the Dobson spectrophotometer before (**Figure 5A**) and after the re-processing (**Figure 5B**).

3. Ozonesonde Networks

3.1. The Global Network: Long-term Sites

Stations launching ozonesondes on a regular basis are displayed in **Figure 6**. All except one launch ECC type ozonesonde instruments. WOUDC archives the sonde profiles along with co-located total column ozone amounts from Dobson, Brewer, and SAOZ spectrometers where these are available. NDACC is another repository for ozonesonde data. Other oft-used archives are NOAA/GML (https://gml.noaa.gov/aftp/data/ozwv/Ozonesonde/) and NASA’s SHADOZ (https://tropo.gsfc.nasa.gov/shadoz). Surface ozone concentrations are archived with other reactive gases at the WDCRG.

The global ozonesonde network, consisting of stations operated by meteorological services, space agencies, and several universities, has evolved over more than 80 years. A number of stations originated in the 1950s during the International Geophysical Year. Other sounding stations became operational as the number of ozone-measuring satellites increased after 1990 (**Figure 7**). Because most Antarctic ozonesonde stations began operating before the 1980s, a robust record exists of the lower stratospheric ozone depletion associated with the Antarctic “ozone hole” in the Austral winter to early spring when UV-based satellites have limited views. The discovery of extreme Antarctic ozone loss was first reported at the 1984 Quadrennial Ozone

Symposium (*Chubashi*, 1985) based on soundings from the Japanese Syowa station (black triangle on **Figure 6**) and on column ozone losses at the British Halley Bay station in 1985 (*Farman et al.*, 1985). **Figure 8A** displays an example from South Pole station (magenta triangle on the **Figure 6** map) in 2018 of the morphology of low-ozone profiles that occur during September and October when there is a sustained Antarctic polar vortex. The contrasting profiles are from July 2018 at South Pole.

3.2 Strategic Networks: Global and Campaign Operations

Ozonesondes have been organized for targeted purposes in what are referred to as strategic ozonesonde networks (*Thompson et al.*, 2011). The global SHADOZ network (blue circles in **Figure 6**), organized in 1998 (*Thompson et al.*, 2003a), consists of tropical and subtropical stations that launch 2-5 sondes monthly, generally coordinated with a midday overpass of one or more instruments on a polar-orbiting satellite. The zonal distribution of SHADOZ stations (*Thompson et al.*, 2003b) was chosen to investigate the wave-one pattern in tropical total column ozone (**Figure 9**) first reported in the 1980s by *Fishman et al.* (1987). An important contribution of SHADOZ has been the characterization of a distinct tropical tropopause layer (TTL, sometimes referred to as a tropopause transition layer [*Gettelman and Forster*, 2002; *Fuglistaler et al.*, 2009; *Thompson et al.*, 2012]). This region is typically given as between 13-18 km; note steep ozone gradients at ~ 13 km in **Figure 9).**

Other strategic ozonesonde networks operate on a campaign basis (*Thompson et al.*, 2011); a list of major campaigns is given in **Table 1**. These soundings provide fixed-site ozone profiles to complement the multi-species payloads that aircraft deploy to study chemical and meteorological processes influencing ozone in the stratosphere and/or troposphere. The Match campaigns (*von der Gathen et al.*, 1995; *Rex et al.*, 1999) have coordinated polar and midlatitude soundings to study in situ ozone losses during two Antarctic and 19 Arctic springs since the 1991-1992 Arctic winter (**Table 1**). Using forecast trajectories to predict where layers of depleted ozone observed in one sounding will travel, the projected arrival of such a parcel over another station triggers a timed launch. Match has also supported a number of international aircraft experiments (**Table 1**). For the first time, in the 2019-2020 winter-spring season, Match showed that the magnitude of Arctic ozone profile loss, recorded by soundings over Greenland, Ny-Ålesund (Svalbard, Norway), Canada and Finland, could approach the magnitude of Antarctic "ozone hole" loss, with ozone mixing ratio values at $\leq$ 0.2 ppmv at 18 km (**Figure 8B;** *Wohltmann et al.*, 2020).

Over North America, a series of Intensive Ozonesonde Network Studies (IONS**)** supported multi-aircraft and satellite validation studies from 2004 through 2013. For four IONS campaigns, sondes were coordinated at 6 to as many as 23 sites (August 2006) for midday satellite overpasses from 3-7 times/week. The IONS experiments led to a deeper understanding of tropospheric ozone during North American summers and have been especially useful in identifying stratosphere-troposphere exchange (STE) episodes. STE turns out to be more prevalent than previously thought, with significant intrusions of stratospheric air taking place after April-May, the typical "springtime" maximum in STE activity (*Ott et al.*, 2016; *Kuang et al.*, 2017; *Tarasick et al.*, 2019). During the July-August 2004 IONS, ozonesonde observations along with satellite data, showed that ~1/4 of the free tropospheric ozone budget from mid-Atlantic states to southeastern Canada originated from the stratosphere (*Thompson et al.*, 2007a,b). **Figure 8C** illustrates ozone profiles below 18 km at a Houston site during SEACIONS (2013). Varying ozone concentrations in the upper troposphere reflect stratospheric influences as well as lightning, as *Thompson et al.* (2008) showed with the identification of ozone laminae and satellite data analysis with IONS-06 summertime soundings over Houston. These same influences are reflected in the 2013 SEACIONS profiles (**Figure 8C)**.

4. Applications of Ozonesonde Data with Remote Sensing Observations

Ozonesonde observations and remote sensing observations have a symbiotic relationship in that they are both useful to each other for producing high quality datasets. The simple satellite retrieval flowchart of **Figure 10A** demonstrates that climatologies based on ozonesonde profiles (e.g., *McPeters and Labow*, 2012) are used in satellite algorithms as a priori or first guess information. Limb-measuring satellites rely on comparisons with sonde ozone profiles for validation of their products. With a number of ozone-measuring satellites lasting a decade or more (**Figure 7),** ozonesonde data are being used to evaluate drift in the satellite instruments (*Hubert et al.*, 2016). The latter application has been an important factor in increasing demand for sonde data with reduced uncertainty and more rapid data delivery. Total column ozone (TCO) or tropospheric column ozone (TrCO) from sondes, as well as ground-based spectrometers, are routinely compared with the satellite TCO or TrCO. Examples are given in the next section.

4.1 Satellite Ozone Product Evaluation using Ozonesonde Data

Ozonesonde data are typically used to evaluate two types of satellite products: profiles and column amounts. For example, stratospheric ozone profiles from the SAGE III instrument on the International Space Station (ISS/SAGE III) were recently examined by *Wang et al.*, (2020). The satellite profiles are based on limb-viewing observations at sunrise and sunset. Twenty ozonesonde stations (between ±55 degrees latitude) provided the statistics, using a total of 273 profiles. *Wang et al.* (2020) also compared the SAGE III data to ozone from four other limb-measuring satellites, OSIRIS, Aura/MLS, ACE-FTS and OMPS-LP. Agreement of the satellites as a whole was somewhat better at midlatitudes than in the tropics.

Extracting profiles from nadir-viewing UV-measuring satellites is challenging. *Huang et al.* (2017) presents a 10-year record of tropospheric profiles derived from OMI. The record is somewhat compromised due to a partial detector failure in 2009, which introduced a sampling bias into the ozone readings. For the newer TROPOMI (2017-), *Mettig et al.* (2021a) employed a novel technique (TOPAS, Tikhonov regularized Ozone Profile retrievAl with SCIATRAN) to nadir retrievals in tropical and mid-latitudes to estimate ozone throughout the troposphere and lower-mid stratosphere; the method follows the simple flowchart in **Figure 10A**. The vertical resolution of the TOPAS method is fairly coarse (~9 km on average) based on the averaging kernels reported with only 1-2 degrees of freedom (DOFs) in the troposphere, which is not unlike other UV-only satellite instruments. This indicates that similar instruments are highly dependent on the a priori profile (eg. an ozonesonde climatology) in the troposphere. However, agreement between the TROPOMI-retrieved ozone profiles and ozonesonde measurements is generally within 20% (**Figure 10B**). New retrievals that combine observations from UV-satellite instruments and IR instruments (eg. NOAA's CrIS) can improve both tropospheric and stratospheric comparisons with ozonesondes due to increased sensitivity throughout the ozone profile (*Mettig et al.*, 2021b).

Other techniques for estimating tropospheric ozone are based on column amounts, following the heritage of *Fishman et al.* (1991; 1996). Their "residual" approach to tropospheric ozone consists of subtracting the stratospheric column extracted from one satellite sensor from a highly accurate TCO from a backscattered UV instrument, initially from TOMS (several instruments from 1978-2005). The OMI/MLS series (*Ziemke et al.* 2006; 2019) is one of the most-used tropospheric column ozone (TrCO) datasets based on a residual technique. **Figure 11** shows the monthly mean TrCO from SHADOZ sondes from 10 tropical sites (latitude within ±20 degrees) compared to the corresponding monthly average OMI/MLS estimated tropospheric column. The offset is ~25% where the sonde TrCO is 40 DU although the correlation ($r^2 = 0.66$) is reasonably good. Part of the offset may be sampling differences (daily satellite data, with averaging over several pixels, vs. 2-4 sondes/month). The satellite measurements do not typically capture the full-range of ozone extremes measured by the sondes.

Cloud-slicing techniques (*Ziemke et al*., 2001; *Heue et al.*, 2017) constitute an alternative approach to estimating upper and lower tropospheric column amounts; this has been applied to TROPOMI (*Hubert et al.*, 2021). Agreement with ozonesonde-based totals is ~15%. A shortcoming of both cloud-slicing and residual methods is incomplete knowledge of the tropopause height, i.e., what the column actually represents. This limitation is particularly relevant in the extra-tropics where the tropopause height can vary greatly and change from < 10 km to more than 15 km within hours. Time-series with residual products (*Ziemke et al.,* 2019) capture seasonal variability and oscillations like the ENSO but caution is warranted for trends.

Figure 12 shows examples of ozonesonde comparisons from two instruments on the Aura satellite (OMI and MLS) that has operated for 17 years. The comparisons are for soundings taken at the Wallops Island, VA (green triangle marks location in **Figure 6**). Good agreement between the ozonesondes and MLS (**Figure 12A**) is observed throughout the stratosphere (*Witte et al.*, 2019. Dobson spectrophotometer measurements at Wallops Island are within ±5% of the ozonesonde TCO over the 25-year record illustrated (1995-2020), demonstrating the stability and high-quality of the sounding record); the Dobson is calibrated regularly against the world reference instrument at Boulder, CO. **Figure 12B** shows that agreement between OMI (October 2004-) and ozonesonde TCO also averages 5% or better to 2020.

4.2 Use of Satellite Ozone Data to Track the Performance of the Ozonesonde

The examples above illustrate how ozonesonde data are used for evaluation of satellite products. Conversely, because several satellite records have been processed and improved multiple times, high-accuracy satellite data can be useful in monitoring the quality of sonde data. The ozonesonde community has been systematically reprocessing long-term sonde records over the past decade. Comparisons in total column ozone between integrated total ozone from soundings and coincident satellite overpasses may show a discontinuity that signifies a problem in the sonde measurements. For example, *Witte et al.* (2017; 2018) showed that an inadvertent change in the sensing solution in soundings at La Réunion led to an artificial 18 DU increase in the mean TCO from 2007 to 2016 compared to the average TCO from 1998 to 2006. *Witte et al.* (2017; 2018) corrected the affected ozone profiles to remove the discontinuities, using the homogenization procedures recommended by ASOPOS in *Deshler et al.* (2017).

In the past 5 years there have been concerns about drifts or discontinuities in the ozonesonde TCO at ~20% of the global ozonesonde record since 2005. The direction of change is a loss of 3% or more in TCO since 2013. **Figure 13** illustrates how data from 5 operational satellite instruments, MLS (stratosphere), OMI, OMPS and two GOME-2 instruments (TCO), are used to evaluate the ozonesonde data quality in the Aura era. In the upper panels of **Figures 13A** and **13B**, comparisons of sonde stratospheric ozone are made with ozone at standard MLS pressure levels. The lower panels show TCO comparisons with the 4 UV-based satellite instruments. The Wallops Island record (**Figures 12 and 13A)** is stable in both TCO and stratospheric ozone above 50 hPa whereas, after 2013, the Samoa data (**Figure 13B**) display more variability and an overall TCO decline (lower panel in **Figure 13B**) that averages 3-4% (*Stauffer et al.*, 2020); the cause is partially due to changes in one sonde instrument type. The ASOPOS 2.0 Report (*WMO/GAW Report No. 268*, 2021), in which procedures are detailed to maximize quality in ozonesonde measurements, recommends ongoing comparisons of both the TCO and the stratospheric profile. The goal is to detect any change in procedure or instrument performance as quickly as possible.

5. Summary and Conclusions

5.1 Scientific Perspective: On-going Need for Profiles from Global Ozonesondes

The vertical profiles of the ozonesonde instrument provide unique information in the global ozone observing system for several reasons. First, no other widely used method is as free of weather effects. Second, although lidar has high vertical resolution, there are many fewer lidar stations compared to ozonesonde monitoring sites.

The near-real time measurement of the ozonesonde is ideal for tracking layers of stratospheric ozone (Match campaigns) and ozone pollution in the troposphere (IONS campaigns). Interest in ingesting sonde profiles into regional air-quality forecasts in near-real time and global chemistry-climate models is another motivator for adding to the number of ozonesonde stations. Unfortunately, numbers of sonde records have been declining in the past years. The combined WOUDC, NDACC, SHADOZ and NOAA/GML archives include >2800 soundings for 2017 but fewer than 2400 records in 2019. Key Arctic and mid-latitude stations have reduced or eliminated soundings.

The satellite community continues to be an important user of ozonesonde data as well as a driver for faster data delivery and more stringent quality assurance. With 5% uncertainty in TCO now achievable, ozonesonde data can be used to detect drifts of profiling ozone monitoring satellites and to evaluate new algorithms and satellite ozone products in a timely manner. Conversely, satellite data have been shown to be an important component in ensuring continuous evaluation of ozonesonde instrument and operational QA.

5.2 Quality Assurance: Need for Sonde Intercomparisons and a Global Ozone Reference

Changes in ozonesonde instrumentation is unavoidable as individual components may be modified by manufacturers. Operational and data processing practices may also change at individual stations. Accordingly, there is an ongoing need for periodic evaluation of ozonesonde performance and intercomparisons with a global ozone reference as the ASOPOS process has demonstrated. Essential elements of QA assessments are: (1) regular laboratory evaluation of instruments and operational practices, such as the JOSIE experiments; (2) field tests; (3) a process whereby global data and SOPs are continuously evaluated by a broad team of ozonesonde experts. These assessments must be supported by maintaining a world ozone standard photometer and one or more environmental test centers, e.g., the WCCOS. A strength of the ASOPOS process has been the inclusion of dedicated researchers who provide and archive ozone profiles, data users and instrument manufacturers. The recommendations, supported by analyses in the peer-reviewed literature, are consensus-based. The ASOPOS Reports are themselves peer-reviewed and are publicly available through the WMO/GAW website.

5.3 Conclusions

The ozonesonde instrument is unmatched in producing profiles of ozone with high vertical resolution throughout the troposphere and lower-mid stratosphere. Over the past 25 years, dedicated attention to ozonesonde QA has led to significant advances. This in turn led to new laboratory and field experiments to further refine SOP and guidelines for traceable ozonesonde records, bringing the target of 5% uncertainty throughout the ozone profile within reach. With reprocessed data, it has been possible to reduce residual uncertainties, biases, and discontinuities in ozonesonde time-series. We can expect that there will be further homogenization efforts of ozonesonde data and evaluation of the new data within the global network in the coming years.

Acknowledgments. Valuable comments were received from reviewer Holger Vömel (NCAR). Thanks to Peter von der Gathen (Alfred Wegener Institute, Potsdam) for information on the Match and related aircraft and ground campaigns.

References

Chubashi, S., A special ozone observation a Syowa station, Antarctica, from February 1982 to January, 1983. In Atmospheric Ozone, C. S. Zerefos and A. Ghazi, D. Reidel Publishers, Dordrecht, The Netherlands, 1985, pp. 285-289.

DeMazière, M., Thompson, A. M., Kurylo, M. J., Wild, J., Bernhard, G., Blumenstock, T., Hannigan, J., Lambert, J-C., Leblanc, T., McGee, T. J., Nedoluha, G., Petropavlovskikh, I., Seckmeyer, G., Simon, P. C., Steinbrecht, W., Strahan, S., Sullivan, J. T., 2018. The Network for the Detection of Atmospheric Composition Change (NDACC): History, status and perspectives, Atmos. Chem. Phys., 18, 4935–4964. https://doi.org/10.5194/acp-18-4935-2018.

Deshler, T., Mercer, J., Smit, H. G. J., Stubi, R., Levrat, G., Johnson, B J., Oltmans, S. J., Kivi, R., Thompson, A. M., Witte, J., Davies, J., Schmidlin, F. J., Brothers, G., Sasaki, T., 2008. Atmospheric comparison of electrochemical cell ozonesondes from different manufacturers, and with different cathode solution strengths: The Balloon Experiment on Standards for Ozonesondes, J. Geophys. Res., 113, D04307. http://doi.org/10.1029/2007JD008975.

Deshler, T., Stübi, R., Schmidlin, F. J., Mercer, J. L., Smit, H.G.J., Johnson, B.J., Kivi, R. and Nardi, B., 2017. Methods to homogenize ECC ozonesonde measurements across changes in sensing solution concentration or ozonesonde manufacturer, Atmos. Meas. Tech., 10, 2012-2043. http://doi.org/10.5194/amt-10-2021-2017.

Farman, J., Gardiner, B., Shanklin, J. Large losses of total ozone in Antarctica reveal seasonal ClO_x/NO_x interaction. Nature 315, 207–210 (1985). https://doi.org/10.1038/315207a0

Fishman, J., Larsen, J. C., 1987. Distribution of total ozone and stratospheric ozone in the tropics: Implications for the distribution of tropospheric ozone, J. Geophys. Res., 92, D6. https://doi.org/10.1029/JD092iD06p06627.

Fishman, J., Fakhruzzaman, K., Cros, B., Nganga, D., 1991. Identification of widespread pollution in the Southern Hemisphere deduced from satellite analyses, Science, 252 (5013), 1693-1696. http://doi.org/10.1126/science.252.5013.1693.

Fishman, J., Brackett, V. G., Browell, E. V., Grant, W. B., 1996. Tropospheric ozone derived from TOMS/SBUV measurements during TRACE-A, J. Geophys. Res., 101, D19. https://doi.org/10.1029/95JD03576.

Fuglistaler, S. Dessler, A. E., Dunkerton, T. J., Folkins, I., Fu, Q., Mote, P. W., 2009. Tropical tropopause layer, Rev. Geophysics, https://doi.org/10.1029/2008RG000267.

Gettelman, A., Forster, P. M. F., 2002. A climatology of the tropical tropopause layer, J. Meterol. Soc. Jpn., 80(4B), 911–924. http://doi.org/10.2151/jmsj.80.911.

Heue, K-P., Coldewey-Egbers, M., Delcloo, A., Lerot, C., Loyola, D., Valks, P., van Roozendael, M., 2016. Trends of tropical tropospheric ozone from 20 years of European satellite measurements and perspectives for the Sentinel-5 Precursor, Atmos. Meas. Tech., 9, 5037–5051. http://doi.org/10.5194/amt-9-5037-2016.

Huang, G., Liu, X., Chance, K., Yang, K., Bhartia, P. K., Cai, Z., Allaart, M., Acellet, G., Calpini, B., Coetzee, G. J. R., Cuevas-Agulló, E., Cupeiro, M., De Backer, H., Dubey, M. K., Fuelberg, H. E., Fujiwara, M., Godin-Beekmann, S., Hall, T. J., Johnson, B., Joseph, E., Kivi, R., Kois, B., Komala, N., König-Langlo, G., Laneve, G., Leblanc, T., Marchand, M., Minschwaner, K. R., Morris, G., Newchurch, M. J., Ogino, S-Y., Ohkawara, N., Piters, A. J. M., Posny, F., Querel, R., Scheele, R., Schmidlin, F. J., Schnell, R. C., Schrems, O., Selkirk, H., Shiotani, M., Skrivánková, P., Stübi, R., Taha, G., Tarasick, D. W., Thompson, A. M., Thouret, V., Tully, M. B., van Malderen, R., Vömel, H., von der Gathen, P., Witte, J. C., Yela, M., 2017. Validation of 10-year SAO OMI Ozone Profile (PROFOZ) product using ozonesonde observations, Atmos. Meas. Tech., 10, 2455–2475. https://doi.org/10.5194/amt-10-2455-2017.

Hubert, D., Lambert, J.-C., Verhoelst, T., Granville, J., Keppens, A., Baray, J.-L., Bourassa, A. E., Cortesi, U., Degenstein, D. A., Froidevaux, L., Godin-Beekmann, S., Hoppel, K. W., Johnson, B. J., Kyrölä, E., Leblanc, T., Lichtenberg, G., Marchand, M., McElroy, C. T., Murtagh, D., Nakane, H., Portafaix, T., Querel, R., Russell III, J. M., Salvador, J., Smit, H. G. J., Stebel, K., Steinbrecht, W., Strawbridge, K. B., Stübi, R., Swart, D. P. J., Taha, G., Tarasick, D. W., Thompson, A. M., Urban, J., van Gijsel, J. A. E., Van Malderen, R., von der Gathen, P., Walker, K. A., Wolfram, E., Zawodny, J. M., 2016. Ground-based assessment of the bias and long-term stability of 14 limb and occultation ozone profile data records, Atmos. Meas. Tech., 9, 2497–2534. https://doi.org/10.5194/amt-9-2497-2016.

Hubert, D., Heue, K.-P., Lambert, J.-C., Verhoelst, T., Allaart, M., Compernolle, S., Cullis, P. D., Dehn, A., Félix, C., Johnson, B. J., Keppens, A., Kollonige, D. E., Lerot, C., Loyola, D., Maata, M., Mitro, S., Mohamad, M., Piters, A., Romahn, F., Selkirk, H. B., da Silva, F. R., Stauffer, R. M., Thompson, A. M., Veefkind, J. P., Vömel, H., Witte, J. C., Zehner, C., 2021. TROPOMI tropospheric ozone column data: Geophysical assessment and comparison to ozonesondes, GOME-2B and OMI, Atmos. Meas. Tech, 14, 7405-7433, https://doi.org/10.5194/amt-14-7405-2021

Johnson, B.J., Oltmans, S. J., Vömel, H., Smit, H. G. J., T. Deshler, T., C. Kroeger, C., 2002. ECC Ozonesonde pump efficiency measurements and tests on the sensitivity to ozone of buffered and unbuffered ECC sensor cathode solutions, J. Geophys. Res., 107, D19 doi: 10.1029/2001JD000557.

Komhyr, W.D., 1969. Electrochemical concentration cells for gas analysis, Ann.Geoph., 25, 203-210.

Kuang, S., Newchurch, M. J., Thompson, A. M., Stauffer, R. M., Johnson, B. J., Wang, L., 2017. Ozone variability and anomalies observed during SENEX and SEAC4RS campaigns in 2013, J. Geophys. Res., 122(20), 11,227-11,241. https://doi.org/10.1002/2017JD027139.

McDermid, I. S., Godin, S. M., Lindqvist, L. O., Ground-based laser DIAL system for long-term measurements of stratospheric ozone, 1990. Applied Optics, 29, 3603-3612, https://doi.org/10.1364/AO.29.003603.

McGee, T. J., Newman,P., Ferrare, R., Whiteman, D., Butler, J. J., Burris, J., Godin, S. M., McDermid, I. S., 1990. Lidar observations of ozone changes induced by sub-polar airmass motion over Table Mountain (34.4N), J. Geophys. Res., 95, 20527-20530.

McPeters, R. D., Labow, G. J., 2012. Climatology 2011: An MLS and sonde derived ozone climatology for satellite retrieval algorithms, J. Geophys. Res., 117, D10303. http://doi.org/10.1029/2011JD017006.

Mettig, N., Weber, M., Rozanov, A., Arosio, C., Burrows, J. P., Veefkind, P., Thompson, A. M., Querel, R., Leblanc, T., Godin-Beekman, S., Kivi, R., Tully, M. B., 2021a. Ozone profile retrieval from nadir TROPOMI measurements in the UV range, Atmos. Meas. Tech., 14, 6057-6082, https://doi.org/10.5194/amt-14-6057-2021, 2021.

Mettig, N., Weber, M., Rozanov, A., Burrows, J. P., Veefkind, P., Barnet, C., Thompson, A. M., Stauffer, R. M., Leblanc, T., Ancellet, G., Newchurch, M., Kivi, R., Tully, M. B., Van Malderen, R., Steinbrecht, W., Piters, A., Allaart, M., Kois, B., Stübi, R., Davies, J., Skrivankova, P., 2021b. Combined UV and IR ozone profile retrieval from TROPOMI and CrIS measurements, Atmos. Meas. Tech. Disc, https://doi.org/10.5194/amt-2021-412.

Moeini, O., Tarasick, D. W., McElroy, C. T., Liu, J., Osman, M. K., Thompson, A. M., Parrington, M., Palmer, P. I., Johnson, B., Oltmans, S. J., Merrill, J., 2020. Estimating boreal fire-generated ozone over North American using ozonesonde profiles and a differential back trajectory technique, Atmos. Environ. https://doi.org/10.1016/j.aeaoa.2020.100078.

Ott, L. E., Duncan, B. N., Thompson, A. M., Diskin, G., Fasnacht, Z., Langford, A. O., Lin, M., Molod, A. M., Nielsen, J. E., Pusede, S. E., Wargan, K., Weinheimer, A. J., Yoshida, Y., 2016. Frequency and impact of summertime stratospheric intrusions over Maryland during DISCOVER-AQ (2011): New evidence from NASA's GEOS-5 simulations, J. Geophys. Res.,121(7), 3687-3706. https://doi.org/10.1002/2015JD024052.

Proffitt, M.H., McLaughlin, R. J., 1983. Fast response dual-beam UV-absorption photometer suitable for use on stratospheric balloons, Rev. Sci. Instrum., 54, 1719-1728.

Rex, M., von der Gathen, P., Braathen, G., Harris, N. R. P., Reimer, E., Beck, A., Alfier, R., Krüger-carstensen, R., Chipperfield, M., De Backer, H., Balis, D., O'Connor, F., Dier, H., Dorokhov, V., Fast, H., Gamma, A., Gil, M., Kyrö, E., Litynska, Z., Mikkelsen, I. S., Molyneux, M., Murphy, G., Reid, S. J., Rummukainen, M., Zerefos, C., 1999. Chemical Ozone Loss in the Arctic Winter 1994/95 as Determined by the Match Technique, J. Atmos. Chem., 32, 35–59. https://doi.org/10.1023/A:1006093826861.

Smit, H.G.J., 2014. Ozone Sondes, in Encyclopedia of Atmospheric Sciences, Second Edition, edited by G.R. North, J.A. Pyle, and F. Zhang, 1, 372-378, Academic Press, London.

Smit, H.G.J., Sträter, W., Helten, M., Kley, D., 2000. Environmental simulation facility to calibrate airborne ozone and humidity sensors. Jül Berichte Nr 3796, Forschungszentrum Jülich.

Smit, H.G.J., Straeter, W., Johnson, B. J., Oltmans, S. J., Davies, J., Tarasick, D. W., Hoegger, B., Stubi, R., Schmidlin, F. J., Northam, T., Thompson, A. M., Witte, J. C., Boyd, I., Posny, F., 2007. Assessment of the performance of ECC-ozonesondes under quasi-flight conditions in the environmental simulation chamber: Insights from the Jülich Ozone Sonde Intercomparison Experiment (JOSIE), J. Geophys. Res., 112, D19306. https://doi.org/10.1029/2006JD007308.

Smit, H. G. J., O3S-DQA, 2012. Guidelines for homogenization of ozonesonde data, SI2N/O3S-DQA activity as part of “Past changes in the vertical distribution of ozone assessment”, available at https://www.wccos-josie.org/o3s-dqa/.

SPARC/IOC/GAW, 1998. Assessment of Trends in the Vertical Distribution of Ozone, SPARC Report No.1, WMO Global Ozone Research and Monitoring Project Report No. 43, World Meteorological Organization, Geneva.

SPARC/IO3C/GAW, 2019. Report on Long-term Ozone Trends and Uncertainties in the Stratosphere, I. Petropavlovskikh, S. Godin-Beekmann, D. Hubert, R. Damadeo, B. Hassler, V. Sofieva (Eds.), SPARC Report No. 9, GAW Report No. 241, WCRP-17/2018, http://doi.org/10.17874/f899e57a20b.

Stauffer, R. M., Morris, G. A., Thompson, A. M., Joseph, E., Coetzee, G. J. R., Nalli, N. R., 2014. Propagation of radiosonde pressure sensor errors to ozonesonde measurements, Atmos. Meas. Tech., 7, 65–79, https://doi.org/10.5194/amt-7-65-2014.

Stauffer, R. M., Thompson, A. M., Oltmans, S. J., Johnson, B. J., 2017. Tropospheric ozonesonde profiles at long-term US monitoring sites: 2. Links between Trinidad, CA, profile clusters and inland surface ozone measurements, J. Geophys. Res., 122. http://doi.org/10.1002/2016JD025254.

Stauffer, R. M., Thompson, A. M., Kollonige, D. E., Witte, J. C., Tarasick, D. W., Davies, J. M., Vömel, H., Morris, G. A., Van Malderen, R., Johnson, B. J., Querel, R. R., Selkirk, H. B., Stübi, R., Smit, H. G. J., 2020. A post-2013 drop-off in total ozone at a third of global ozonesonde stations: Electrochemical Concentration Cell Instrument Artifacts?, Geophys. Res. Lett., 47(11). http://doi.org/10.1029/2019/GL086791.

Steinbrecht, W., Kubistin, D., Plass-Dülmer, C., Davies, J., Tarasick, D. W., von der Gathen, P., Deckelmann, H., Jepsen, N., Kivi, R., Lyall, N., Palm, M., Notholt, J., Kois, B., Oelsner, P., Allaart, M., Piters, A., Gill, M., Van Malderen, R., Delcloo, A. W., Sussmann, R., Mahieu, E., Servais, C., Romanens, G., Stübi, R., Ancellet, G., Godin-Beekmann, S., Yamanouchi, S., Strong, K., Johnson, B., Cullis, P., Petropavlovskikh, I., Hannigan, J. W., Hernandez, J.-L., Rodriguez, A. D., Nakano, T., Chouza, F., Leblanc, T., Torres, C., Garcia, O., Röhling, A. N., Schneider, M., Blumenstock, T., Tully, M., Paton-Walsh, C., Jones, N., Querel, R., Strahan, S., Stauffer, R. M., Thompson, A. M., Inness, A., Engelen, R., Chang, K.-L., Cooper, O. R., 2021. Did the COVID-19 crisis reduce free tropospheric ozone across the Northern Hemisphere? Geophys. Res. Lett., 48, e2020GL091987. https://doi.org/10.1029/2020GL091987.

Sterling, C. W., Johnson, B. J., Oltmans, S. J., Smit, H. G. J., Jordan, A. F., Cullis, P. D., Hall, E. G., Thompson, A. M., Witte, J. C., 2018. Homogenizing and estimating the uncertainty in NOAA's long-term vertical ozone profile records measured with the electrochemical concentration cell ozonesonde, Atmos. Meas. Tech., 11, 3661–3687. https://doi.org/10.5194/amt-11-3661-2018.

Sullivan, J. T., McGee, T. J., Leblanc, T., Sumnicht, G. K., Twigg, L. W., 2015. Optimization of the GSFC TROPOZ DIAL retrieval using synthetic lidar returns and ozonesondes – Part 1: Algorithm validation, Atmos. Meas. Tech., 8, 4133–4143. https://doi.org/10.5194/amt-8-4133-2015, 2015.

Tarasick, D. W., Davies, J., Smit, H. G. J., Oltmans, S. J., 2016. A re-evaluated Canadian ozonesonde record: measurements of the vertical distribution of ozone over Canada from 1966 to 2013. Atmos. Meas. Tech., 9, 195–214, https://doi.org/10.5194/amt-9-195-2016.

Tarasick, D. W., Carey-Smith, T. K., Hocking, W. K., Moeini, O., He, H., Liu, J., Osman, M. K., Thompson, A. M., Johnson, B. J., Oltmans, S. J., Merrill, T. J., 2019. Quantifying stratosphere-troposphere transport of ozone using balloon-borne ozonesondes, radar windprofilers and trajectory models. Atmos. Envir., 198(2019), 496–509. https://doi.org/10.1016/j.atmosenv.2018.10.040

Tarasick, D. W., Smit, H. G. J., Thompson, A. M., Morris, G. A., Witte, J. C., Davies, J., Nakano, T., Van Malderen, R., Stauffer, R. M., Johnson, B. J., Stübi, R., Oltmans, S. J., Vömel. H., 2021. Improving ECC Ozonesonde Data Quality: Assessment of Current Methods and Outstanding Issues. Earth and Space Science, 8, e2019EA000914, https://doi.org/10.1029/2019EA000914
Thompson, A. M., Pickering, K. E., McNamara, D. P., Schoeberl, M. R., Hudson, R. D., Kim, J. H., Browell, E. V., Kirchhoff, V. W. J. H., Nganga, D., 1996. Where did tropospheric ozone over southern Africa and the tropical Atlantic come from in October 1992? Insights from TOMS, GTE TRACE A, and SAFARI 1992. J. Geophys. Res., 101(D19), 24251– 24278, https://doi.org/10.1029/96JD01463.
Thompson, A. M., Witte, J. C., Hudson, R. D., Guo, H., Herman, J. R., Fujiwara, M., 2001. Tropical tropospheric ozone and biomass burning, Science, 291, 2128-2132 https://doi.org/10.1126/science.291.5511.2128.
Thompson, A. M., Witte, J. C., McPeters, R. D., Oltmans, S. J., Schmidlin, F. J., Logan, J. A., Fujiwara, M., Kirchhoff, V. W. J. H., Posny, F., Coetzee, G. J. R., Hoegger, B., Kawakami, S., Ogawa, T., Johnson, B. J., Vömel, H., Labow, G., 2003a. Southern Hemisphere Additional Ozonesondes (SHADOZ) 1998-2000 tropical ozone climatology 1. Comparison with Total Ozone Mapping Spectrometer (TOMS) and ground-based measurements. J. Geophys. Res., 108, 8238, https://doi.org/10.1029/2001JD000967.
Thompson, A. M., Witte, J. C., Oltmans, S. J., Schmidlin, F. J., Logan, J. A., Fujiwara, M., Kirchhoff, V. W. J. H., Posny, F., Coetzee, G. J. R., Hoegger, B., Kawakami, S., Ogawa, T. Fortuin, J. P. F., Kelder, H. M., 2003b: Southern Hemisphere Additional Ozonesondes (SHADOZ) 1998–2000 tropical ozone climatology. 2. Tropospheric Variability and the Zonal Wave-One, J. Geophys. Res., 108, 8241, doi: 10.1029/2002JD002241.
Thompson, A. M., Stone, J. B., Witte, J. C., Miller, S. K., Pierce, R. B., Chatfield, R. B., Oltmans, S. J., Cooper, O. R., Loucks, A. L., Taubman, B. F., Johnson, B. J., Joseph, E., Kucsera, T. L., Merrill, J. T., Morris, G. A., Hersey, S., Forbes, G., Newchurch, M. J., Schmidlin, F. J., Tarasick, D. W., Thouret, V., Cammas, J.-P., 2007a. Intercontinental Chemical Transport Experiment Ozonesonde Network Study (IONS) 2004: 1 Summertime upper troposphere/lower stratosphere ozone over northeastern North America. J. Geophys. Res., 112, D12S12, https://doi.org/10.1029/2006JD007441.
Thompson, A. M., Stone, J. B., Witte, J. C., Miller, S. K., Oltmans, S. J., Ross, K. L., Kucsera, T. L., Merrill, J. T., Forbes, G., Tarasick, D. W., Joseph, E., Schmidlin, F. J., McMillan, W. W., Warner, J., Hintsa, E. J., Johnson J. E., 2007b. Intercontinental Transport Experiment Ozonesonde Network Study (IONS, 2004): 2. Tropospheric Ozone Budgets and Variability over Northeastern North America. J. Geophys. Res., 112, D12S13, https://doi.org/10.1029/2006JD007670.
Thompson, A. M., Witte, J. C., Smit, H. G. J., Oltmans, S. J., Johnson, B. J., Kirchhoff, V. W. J. H., Schmidlin, F. J., 2007c. Southern Hemisphere Additional Ozonesondes (SHADOZ) 1998-2004 tropical ozone climatology. 3. Instrumentation, Station Variability, Evaluation with Simulated Flight Profiles. J. Geophys. Res., 112, D03304, https://doi.org/10.1029/2005JD007042.
Thompson, A. M., Yorks, J. E., Miller, S. K., Witte, J. C., Dougherty, K. M., Morris, G. A., Baumgardner, D., Ladino, L., Rappenglueck, B., 2008. Tropospheric ozone sources and wave activity over Mexico City and Houston during Milagro/Intercontinental Transport Experiment (INTEX-B) Ozonesonde Network Study, 2006 (IONS-06), Atmos. Chem. Phys., 8, 5113-5126.

Thompson, A. M., Oltmans, S. J., Tarasick, D. W., von der Gathen, P., Smit, H. G. J., Witte, J. C., 2011. Strategic ozone sounding networks: Review of design and accomplishments. Atmos. Envir., 45, 2145-2163, https://doi.org/10.1016/j.atmosenv.2010.05.002.

Thompson, A. M., Miller, S. K., Tilmes, S., Kollonige, D. W., Witte, J. C., Oltmans, S. J., Johnson, B. J., Fujiwara, M., Schmidlin, F. J., Coetzee, G. J. R., Komala, N., Maata, M., Mohamad, M. bt, Nguyo, J., Mutai, C., Ogino, S-Y., Raimundo Da Silva, F., Paes Leme, N. M., Posny, F., Scheele, R., Selkirk, H. B., Shiotani, M., Stübi, R., Levrat, G., Calpini, B., Thouret, V., Tsuruta, H., Valverde Canossa, J., Vömel, H., Yonemura, S., Andrés Diaz, J., Tan Thanh, H. T., Thuy Ha, H. T., 2012. Southern Hemisphere Additional Ozonesondes (SHADOZ) ozone climatology (2005-2009): Tropospheric and tropical tropopause layer (TTL) profiles with comparisons to OMI-based ozone products. J. Geophys. Res., 117, D23301, https://doi.org/10.1029/2011JD016911.

Thompson, A. M., Witte, J. C., Sterling, C., Jordan, A., Johnson, B. J., Oltmans, S. J., Fujiwara, M., Vömel, H., Allaart, M., Piters, A., Coetzee, G. J. R., Posny, F., Corrales, E., Diaz, J. A., Félix, C., Komala, N., Lai, N., Ahn Nguyen, H. T., Maata, M., Mani, F., Zainal, Z., Ogino, S-Y., Paredes, F., Penha, T. L. B., da Silva, F. R., Sallons-Mitro, S., Selkirk, H. B., Schmidlin, F. J. Stübi, R., Thiongo, K., 2017. First reprocessing of Southern Hemisphere ADditional OZonesondes (SHADOZ) Ozone Profiles (1998-2016). 2. Comparisons with satellites and ground-based instruments, J. Geophys. Res., 122, https://doi.org/10.1002/2017JD027406.

Thompson, A. M., Smit, H. G. J., Witte, J. C., Stauffer, R. M., Johnson, B. J., Morris, G., von der Gathen, P., Van Malderen, R., Davies, J., Piters, A., Allaart, M., Posny, F., Kivi, R., Cullis, P., Anh, N. T. H., Corrales, E., Machinini, T., da Silva, F. R.,, Paiman, G., Thiong'o, K., Zainal, Z., Brothers, G. B., Wolff, K. R., Nakano, T., Stübi, R., Romanens, G., Coetzee, G. J. R., Diaz, J. A., Mitro, S., Mohamad, M., Ogino, S-Y., 2019. Ozonesonde Quality Assurance: The JOSIE-SHADOZ (2017) Experience, Bull. Am. Meteor. Society, 100(1), https://doi.org/10.1175/BAMS-D-17-0311.1.

Van Malderen, R., Allaart, M. A. F., De Backer, H., Smit, H. G. J., De Muer, D., 2016. On instrumental errors and related correction strategies of ozonesondes: possible effect on calculated ozone trends for the nearby sites Uccle and De Bilt, Atmos. Meas. Tech., 9, 3793–3816, https://doi.org/10.5194/amt-9-3793-2016.

Vömel, H., Smit, H. G. J., Tarasick, D., Johnson, B., Oltmans, S. J., Selkirk, H., Thompson, A. M., Stauffer, R. M., Witte, J. C., Davies, J., van Malderen, R., Morris, G. A., Nakano, T., Stübi, R., 2020. A new method to correct the ECC ozone sonde time response and its implications for "background current" and pump efficiency, Atmos. Meas. Tech.., 13(10), 5667-5680, doi.org/10.5194/amt-13-5667-2020.

von der Gathen, P., Rex, M., Harris, N. R. P., Lucic, D., Knudsen, B. M., Braathen, G. O., De Backer, H., Fabian, R., Fast, H., Gil, M., Kyrö, E., Mikkelsen, I. S., Rummukainen, M., Stähelin, J., Varotsos, C., 1995. Observational evidence for chemical ozone depletion over the Arctic in winter 1991–92. Nature, 375, 131–134, https://doi.org/10.1038/375131a0.

Wang, H. J. R., Damadeo, R., Flittner, D., Kramarova, N., Taha, G., Davis, S., Thompson, A. M., Strahan, S., Wang, Y., Froidevaux, L., Degenstein, D., Bourassa, A., Steinbrecht, W., Walker, K., Querel, R., Leblanc, T., Godin-Beekman, S., Hurst, D., Hall, E., 2020. Validation of SAGE III/ISS solar occultation ozone products with correlative satellite and ground based measurements, J. Geophys. Res., 125, https://doi.org/10.1029/2020JD032430.

Witte, J. C., Thompson, A. M., Smit, H. G. J., Fujiwara, M., Posny, F., Coetzee, G. J. R., Northam, E. T., Johnson, B. J., Sterling, C. W., Mohamad, M., Ogino, S-Y., Jordan, A., da Silva, F. R., 2017. First reprocessing of Southern Hemisphere ADditional OZonesondes

(SHADOZ) profile records (1998-2015) 1: Methodology and evaluation. J. Geophys. Res., 122, https://doi.org/10.1002/2016JD026403.

Witte, J. C., Thompson, A. M., Smit, H. G. J., Vömel, H., Posny, F., Stübi, R., 2018. First reprocessing of Southern Hemisphere Additional Ozonesondes (SHADOZ) Profile Records. 3. Uncertainty in ozone profile and total column. J. Geophys. Res., 123(6), 3243-3268, https://doi.org/10.1002/2017JD027791.

Witte, J. C., Thompson, A. M., Schmidlin, F. J., Northam, E. T., Wolff, K. R., Brothers, G. B., 2019. The NASA Wallops Flight Facility digital ozonesonde record: Reprocessing, uncertainties, and dual launches. J. Geophys. Res., 124, 3565–3582, https://doi.org/10.1029/2018JD030098.

WMO/GAW Report No. 104, 1996. Report of the Fourth WMO Meeting of Experts on the Quality Assurance/Science Activity Centers (QA/SACs) of the Global Atmosphere Watch. WMO Global Atmosphere Watch Report Series, No. 104, World Meteorological Organization, Geneva.

WMO/GAW Report No. 130, 1998: Smit H.G.J and D. Kley, JOSIE: The 1996 WMO International Intercomparison of Ozonesondes Under Quasi Flight Conditions in the Environmental Simulation Chamber at Jülich, WMO Global Atmosphere Watch Report Series, No. 130, WMO/TD No. 926, World Meteorological Organization, Geneva.

WMO/GAW Report No. 157, 2004a: Smit, H.G.J., and W. Straeter, JOSIE-1998, Performance of ECC Ozone Sondes of SPC-6A and ENSCI-Z Type, WMO Global Atmosphere Watch Report Series, No. 157, WMO/TD No. 1218, World Meteorological Organization, Geneva. [Available online at https://library.wmo.int/index.php?lvl=notice_display&id=11089#.Ya-MV1MxlUM]

WMO/GAW Report No. 158, 2004b: Smit, H.G.J., and W. Straeter, JOSIE-2000, Jülich Ozone Sonde Intercomparison Experiment 2000, The 2000 WMO International Intercomparison of Operating Procedures for ECC Ozonesondes at the Environmental Simulation Facility at Jülich, WMO Global Atmosphere Watch Report Series, No. 158, WMO TD No. 1225, World Meteorological Organization, Geneva. [Available online at https://library.wmo.int/index.php?lvl=notice_display&id=11090#.Ya-M6FMxlUM]

WMO/GAW Report No. 201, 2014: Smit, H.G.J., and ASOPOS panel, Quality assurance and quality control for ozonesonde measurements in GAW, WMO Global Atmosphere Watch report series, No. 201, World Meteorological Organization, Geneva. [Available online at https://library.wmo.int/doc_num.php?explnum_id=7167]

WMO/GAW Report No. 268, 2021: Smit, H. G. J., Thompson, A. M., and ASOPOS panel, Ozonesonde Measurement Principles and Best Operational Practices, ASOPOS (Assessment of Standard Operating Procedures for Ozonesondes) 2.0, WMO Global Atmosphere Watch report series, No. 268, World Meteorological Organization, Geneva. [Available online at https://library.wmo.int/index.php?lvl=notice_display&id=21986#.YaFNSbpOlc8]

WMO/UNEP, 1995: Scientific Assessment of Ozone Depletion: 1994, Global Ozone Research and Monitoring Project – Report No. 37, World Meteorological Organization, Geneva.

WMO/UNEP, 2019: Scientific Assessment of Ozone Depletion: 2018, Global Ozone Research and Monitoring Project – Report No. 58, World Meteorological Organization, Geneva. [Available online at https://library.wmo.int/index.php?lvl=notice_display&id=20763#.Ya-O8lMxlUM]

Wohltmann, I., von der Gathen, P., Lehmann, R., Maturilli, M., Deckelmann, H., Manney, G. L., Davies, J., Tarasick, D., Jepsen, N., Kivi, R., Lyall, N., Rex, M., 2020. Near complete local

reduction of Arctic stratospheric ozone by record chemical loss in spring 2020. Geophys. Res. Lett., 47(20), https://doi.org/10.1029/2020GL089547.
Ziemke, J. R., Chandra, S., Bhartia, P. K., 2001. “Cloud slicing”: A new technique to derive upper tropospheric ozone from satellite measurements, J. Geophy. Res., 106, D9, 9853–9867, https://doi.org/10.1029/2000JD900768.
Ziemke, J. R., Chandra, S., Duncan, B. N., Froidevaux, L., Bhartia, P. K., Levelt, P. F., Waters, J. W., 2006. Tropospheric ozone determined from Aura OMI and MLS: Evaluation of measurements and comparison with the Global Modeling Initiative’s Chemical Transport Model, J. Geophys. Res., 111, D19303, https://doi.org/10.1029/2006JD007089.
Ziemke, J. R., Oman, L. D., Strode, S. A., Douglass, A. R., Olsen, M. A., McPeters, R. D., Bhartia, P. K., Froidevaux, L., Labow, G. J., Witte, J. C., Thompson, A. M., Haffner, D. P., Kramarova, N. A., Frith, S. M., Huang, L. K., Jaross, G. R., Seftor, C. J., Deland, M. T., Taylor, S. L., 2019. Trends in global tropospheric ozone Inferred from a composite record of TOMS/OMI/MLS/OMPS satellite measurements and the MERRA-2 GMI simulation, Atmos. Chem. Phys., 19, 3257–3269, https://doi.org/10.5194/acp-19-3257-2019.

Table 1 Caption. Strategic ozonesonde networks and related campaigns. Campaigns aligned with Match are in black (European-sponsored) and red (NASA-sponsored)

Observation Years	Campaign	Observation Years	Campaign
1991-1992	**Match** (Arctic Spring) *with EASOE & AASE II*	**July-Aug 2004**	**IONS-04** (Intensive Ozonesonde Network Study, INTEX-A, ICARTT)
1992-1993	**Match** (Arctic Spring)		
1993-1994	**Match** (Arctic Spring) *with SESAME*		
1994-1995	**Match** (Arctic Spring) *with SESAME*	**March, May, Aug-Sept 2006**	**IONS-06** (Intensive Ozonesonde Network Study, INTEX-B, MILAGRO)
1995-1996	**Match** (Arctic Spring)		
1996-1997	**Match** (Arctic Spring)		
1997-1998	**Match** (Arctic Spring)		
1998-1999	**Match** (Arctic Spring) *with THESEO*	**April 2008, June-July 2008**	**ARCIONS** (ARCTAS IONS)
1999-2000	**Match** (Arctic Spring) *with THESEO 2000 & SOLVE*		
2002-2003	**Match** (Arctic Spring) *with VINTERSOL & SOLVE II*		
2004-2005	**Match** (Arctic Spring) *with SCOUT-O3*		
2006-2007	**Match** (Arctic Spring) *with SCOUT-O3*	**July-Aug 2010, 2011**	**BORTAS**
2007-2008	**Match** (Arctic Spring) *with SCOUT-O3*		
2009-2010	**Match** (Arctic Spring) *with RECONCILE*		
2010-2011	**Match** (Arctic Spring) *with RECONCILE*		
2013-2014	**Match** (Arctic Spring) *with StratoClim*		
2015-2016	**Match** (Arctic Spring) *with StratoClim*		
2017-2018	**Match** (Arctic Spring) *with StratoClim*		
2019-2020	**Match** (Arctic Spring)		
2003	**Match** (Antarctic Spring)	**Aug-Sept 2013**	**SEACIONS** (SEAC4RS IONS)
2007			

Figure Captions:

Figure 1: Ozone profile from an ECC ozonesonde with the temperature and humidity recorded by the accompanying radiosonde. The radiosonde also measures wind speed and direction. Data from a launch at Wallops Island, VA (37.9N, 75.5W) on 17 July 2019.

Figure 2: Altitude ranges of techniques used to measure ozone, ground-based, airborne and satellites. Other ground-based instrumentation (lidar, surface monitors) show context for the ozonesonde measurement. The schematic shows lidar that measure in the troposphere only (*Sullivan et al*., 2015) and that cover troposphere and stratosphere. In fact, only one or two of the most widely used ozone lidar instruments, e.g., within NDACC, detect both troposphere and stratosphere; most ozone lidars report data only in the stratosphere.

Figure 3: (A) Cross-section of the electrochemical concentration cells (ECC) in (B) the ozonesonde sensor. There are two widely used ECC ozonesonde types, manufactured by Science Pump Corporation and the EN-SCI Corporation, producing the SPC-6A and EN-SCI instrument, respectively. The design of both ECCs is similar but there is a consistent 4-5% difference in their performance (**Figures 4A and 4B)** when launched under the same conditions (*Smit et al*., 2007; *Thompson et al.,* 2007c; *Smit*, 2014). Since 2014, a third ECC-type instrument manufactured at the Institute of Atmospheric Physics (IAP), Beijing, China, has been flown at several East Asian stations; the new instrument has not been extensively intercompared with the SPC-6A or EN-SCI in laboratory or field tests.

Figure 4: (A) JOSIE 2000 & BESOS (B): Relative differences between measurements of ozone by EN-SCI and SPC-6A using different combinations of 1%KI & full buffer and 0.5%KI & half buffer sensing solution strength. Data are averaged over 5 km altitude. All profiles were first referenced to the WMO/GAW standard ozone photometer (OPM). In JOSIE-2000 the OPM was in the Jülich (Germany) WCCOS facility; in BESOS the OPM flew on a gondola with 18 ozonesonde instruments in Laramie, Wyoming (US). (C) Mean percent differences between ozone measured by EN-SCI and SPC-6A sondes following WMO/GAW (2014) recommendations and sondes using 1%KI and 0.1buffer, during JOSIE-2017. Both sets of measurements were referenced to the OPM.

Figure 5: Total column ozone (TCO) derived from Boulder, CO, sondes compared with TCO measured by the Boulder Dobson spectrophotometer before (A) and after (B) re-processing of sonde data (Source: *Sterling et al.* 2018). An artifact step-function drop has been eliminated with the reprocessing.

Figure 6: Distribution of 64 most active ozone sounding stations in the global network (after *WMO/GAW Report No. 268*, 2021). These stations deposit data in major public archives. The latter include the archive WOUDC (World Ozone and Ultraviolet Data Center) sponsored by the World Meteorological Organization Global Atmospheric Watch (WMO/GAW; see Acronym List). Other commonly used archives are those of the Network for Detection of Atmospheric Composition Change (NDACC; *deMazière et al.*, 2018), at the websites of NASA for the Southern Hemisphere ADditional OZonesonde Network (SHADOZ; *Thompson et al.*, 2012; 2017), or at the NOAA/Global Monitoring Laboratory (GML).

Figure 7: Ozone-measuring satellites that have used sonde data for algorithm development and validation since 1995.

Figure 8: Examples of dynamic and/or chemical processes affecting the ozone profile, as captured by soundings. (A) Ozonesonde profiles over NOAA's South Pole station that illustrate extreme ozone loss due to catalytic chemical destruction in the region ~15-20 km [above 100

hPa] in October of 2018, compared to July 2018 (pre-ozone hole); (B) 2019-2020 winter-spring season Match ozone soundings over Greenland, Ny-Ålesund (Svalbard, Norway), Canada, and Finland (Source: *Wohltmann et al.*, 2020); Used by permission from AGU. (C) A series of ozone profiles during the 2013 SEACIONS campaign (https://tropo.gsfc.nasa.gov/seacions/) at Ellington Field, Texas (29.6N, 95.2W). STE influences appear in profiles of 7. 9 August and 4 September (green line) 2013. An example of low-ozone air lofted in convection appears in the profile of 4 September (maroon).

Figure 9: Composite data from a strategic global network, SHADOZ, displaying the zonal ozone structure (mixing ratios) that gives rise to the wave-one pattern in satellite TCO. The contours are based on annually averaged profile data over 1998-2020.

Figure 10: (A) Generalized flowchart indicating how ozonesonde data is used for a first guess or a priori profile in the retrieval process and for validation of the final satellite product. (B) Comparison of ozone profiles retrieved from TROPOMI and those from ozonesondes for different zonal bands. The relative mean difference between the retrieval results and the high-resolution sonde data (solid line), as well as the standard deviation of the differences (dashed line), is shown in black. The comparison with the sonde profiles convolved with the averaging kernels is shown in red. In grey, the relative difference between the a priori ozone profiles and high-resolution ozonesonde profiles is displayed, along with the corresponding standard deviations. (Source: *Mettig et al.*, 2021a).

Figure 11: Scatterplot of monthly mean TrCO estimated by the tropospheric residual OMI/MLS product (*Ziemke et al.*, 2019) vs the corresponding TrCO from 10 SHADOZ sites, the latter computed by integrating ozone from surface to tropopause determined from the coupled radiosonde. Comparisons are for SHADOZ stations with latitude within + 20 degrees.

Figure 12: (A) Comparison of ozone from Wallops Island, VA, USA, ozonesondes (red) and Aura/MLS data (black) at the standard levels of the MLS measurement (mean over 2004-2020) with standard deviations indicated by horizontal bars; (B) TCO from Wallops sondes (red) compared to TCO from the Aura/OMI (black), 2004-2020, and Dobson spectrophotometer (blue), 1995-2020.

Figure 13: Comparisons between data from ECC sondes and Aura MLS stratospheric ozone profiles (top panels), and OMI, GOME 2A and GOME 2B (blue dots), and OMPS (red dots) TCO (bottom panels). (A) Wallops Island, VA, record; (B) Samoa SHADOZ record. Red (blue) colors in the top panels indicate where the ECC ozone is greater (less) than MLS. Horizontal dashed lines in the lower panels indicate the 0% line for TCO differences. Note a post-2014 drop in Samoa TCO relative to satellite measurements.

Acronym List

AASE II	Airborne Arctic Stratospheric Experiment II
ACE-FTS	Atmospheric Chemistry Experiment – Fourier Transform Spectrometer on Canadian SCISAT satellite
ASOPOS	Assessment of Standard Operating Procedures for OzoneSondes
BESOS	Balloon Experiment on Standards for OzoneSondes

BORTAS	Quantifying the impaoct of BOReal forest fires on Tropospheric oxidants over the Atlantic using Aircraft and Satellites
DU	Dobson Unit, the unit to express vertical ozone column abundances,1 DU= $2.69x10^{16}$ molecules per cm^2 at STP $1x10^{-3}$ atm.cm at STP)
EASOE	European Arctic Stratospheric Ozone Experiment
ECC	Electrochemical Concentration Cell
EN-SCI	Environmental Science Corporation; ECC ozonesonde manufacturer
ESRL	Earth System Research Laboratories
GAW	Global Atmospheric Watch
GCOS	Global Climate Observing System
GEMS	Geostationary Environment Monitoring Spectrometer
GML	Global Monitoring Laboratory (division of NOAA's ESRL; formerly GMD)
GOES	Geostationary Operational Environmental Satellites
GOME	Global Ozone Monitoring Experiment (onboard MetOp satellites)
GNSS	Global Navigational Satellite System
GRUAN	GCOS Reference Upper Air Network
IAP	Institute of Atmospheric Physics, Beijing, China
IGACO	Integrated Global Atmospheric Chemistry Observations
IOC	International Ozone Commission
IONS	Intensive Ozonesonde Network Study
IPCC	Intergovernmental Panel on Climate Change
ISS	International Space Station
JOSIE	Jülich OzoneSonde Intercomparison Experiment
KI	Potassium Iodide
LEO	Low Earth Orbit
MLS	Microwave Limb Sounder (on Aura satellite)
NASA	National Aeronautics and Space Administration
NDACC	Network for the Detection of Atmospheric Composition Change
NOAA	National Oceanic and Atmospheric Administration
OMI	Ozone Monitoring Instrument (on Aura satellite)
OMPS-LP	Ozone Mapping and Profiler Suite – Limb Profiler (onboard Suomi-NPP and JPSS satellites)
OPM	Ozone PhotoMeter Instrument (used as UV-reference)
OSIRIS	Optical Spectrograph and InfraRed Imaging **S**ystem, on Odin satellite
O3S-DQA	Ozone Sonde Data Quality Assessment
QA	Quality Assurance
RECONCILE	Reconciliation of essential process parameters for an enhanced predictability of Arctic stratospheric ozone loss and its climate interactions
SAGE III	Stratospheric Aerosol and Gas Experiment (fourth generation on ISS)
SBUV	Solar Backscatter Ultraviolet (referring to instrument type on satellites measuring ozone)
SCIAMACHY	SCanning Imaging Absorption SpectroMeter for Atmospheric CHartographY
SCIATRAN	Radiative transfer and retrieval code used by Univ. Bremen SCIAMACHY and TROPOMI algorithm group
SCOUT-O3	Stratospheric-Climate links with emphasis On the Upper Troposphere and lower stratosphere
SEACIONS	Southeast America Consortium for Intensive Ozonesonde Network Study

SESAME	Second European Stratospheric Arctic and Mid-latitude Experiment
SHADOZ	Southern Hemisphere ADditional OZonesondes
SI^{2}N	Ozone trend assessment study supported by SPARC, IOC, IGACO, and NDACC
SMILES	Submillimeter-Wave Limb Emission Sounder onboard ISS
SOLVE	SAGE III Ozone Loss and Validation Experiment
SOP	Standard Operating Procedure
SPARC	Stratosphere-troposphere Processes And their Role in Climate
SPC	Science Pump Corporation; ECC ozonesonde manufacturer
SST	Sensing Solution Type
STP	Standard Temperature (=273.15 K) and Pressure (=1013.25 hPa) conditions
StratoClim	Stratospheric and upper tropospheric processes for better climate predictions
TCO	Total Column Ozone
TEMPO	Tropospheric Emissions: Monitoring of Pollution
THESEO	Third European Stratospheric Experiment on Ozone
TOMS	Total Ozone Mapping Spectrometer
TOPAS	Tikhonov regularized Ozone Profile retrievAl with SCIATRAN
TROPOMI	TROPOspheric Monitoring Instrument
TrCO	Tropospheric Column Ozone
UNEP	United Nations Environment Programme
UV	Ultraviolet
VINTERSOL	Validation of INTERnational satellites and Study of Ozone Loss
WCCOS	World Calibration Center for OzoneSonde
WDCRG	World Data Centre for Reactive Gases
WMO	World Meteorological Organization
WOUDC	World Ozonesonde and Ultraviolet Data Centre

Chapter 4: Ozonesondes

Version 14 Dec 2021

Anne M. Thompson[1,2], Herman G. J. Smit[3], Debra E. Kollonige[1,4], Ryan M. Stauffer[1]

[1]NASA-Goddard Space Flight Center, Earth Sciences Division, Greenbelt, MD USA; [2]Joint Center for Environmental Technology, University of Maryland – Baltimore County, MD USA; [3]Forschungszentrum-Jülich, Jülich, Germany; [4]SSAI, Lanham, MD USA

"Nobody can be uncheered with a balloon" A. A. Milne, *Winnie the Pooh*

1. The Role of Ozonesondes in the Global Ozone Measurement Framework

1.1 Sondes in the Context of a Global Ozone Measurement Strategy

The ozonesonde instrument, although more than 50 years old in design, and simple to operate, remains an essential component of the global observing strategy for stratospheric and tropospheric ozone. The profiles from ozonesondes are foundational in the development of satellite ozone retrievals and are used for validating satellite products from a growing constellation of ozone-measuring sensors. The ozonesonde instrument is unique in providing readings at (5-10)% uncertainty or better throughout the troposphere to the mid-stratosphere at 100-150 m resolution independent of conditions of cloudiness or precipitation (**Figure 1**). Because it is relatively inexpensive and easy to operate – launching with a standard radiosonde instrument -- the ozonesonde can be used virtually anywhere. Ozone sounding records provide the longest record of the vertical distribution of ozone and thus play a key role in monitoring changes in stratospheric ozone in accordance with the Montreal Protocol (*WMO/UNEP*, 2019).

Figure 2 illustrates how ozonesondes fit into the global ozone observing strategy that employs various ground-based spectroscopic and lidar techniques, ozone instruments on aircraft and balloons as well as from space-borne platforms. The altitude ranges of sonde operation, aircraft, and Low-Earth Orbit (LEO) satellites are illustrated. Note that ozone-measuring instruments have been hosted on the International Space Station (SAGE III is currently operational). Geostationary satellites (e.g., the Korean GEMS, NOAA's GOES series) also carry ozone measuring instruments; these are typically 36,000 km above earth. The tropospheric and stratospheric segments of the atmosphere are usually measured by two separate lidar instruments (*McDermid et al.*, 1990; *McGee et al.*, 1991). An advantage of ozonesondes is that a single sounding encompasses the troposphere and lower and middle stratosphere.

In addition to monitoring and validation of other sensors, ozonesonde data are important in understanding atmospheric dynamics, lifetimes, and sources and sinks of ozone. Above the atmospheric boundary layer, the ozone lifetime is weeks to months. Thus, in the troposphere, sonde data are used to study the transport of pollution throughout the troposphere and lowermost stratosphere. Pollution from biomass fires in the tropics (*Thompson et al.*, 1996; 2001; 2003a,b), throughout mid-latitudes by intercontinental transport (*Stauffer et al.*, 2017) and from boreal fires (*Moeini et al.*, 2020) has been investigated. Recently sonde data across the midlatitude northern hemisphere quantified a significant drop in tropospheric ozone due to the global economic crisis instigated by the 2020 COVID-19 pandemic (*Steinbrecht et al.*, 2021).

1.2 Chapter Overview

The purpose of this chapter is to present the capabilities and applications of the ozonesonde measurement as they relate to remote sensing (**Sections 3 and 4**). We begin with a description of the ozonesonde instrument and ongoing research related to the quaality assurance (QA) of the data (**Section 2**).

2. The Ozonesonde Instrument, Operation and Data Quality Control

2.1 Electrochemical Ozonesondes

Ozonesondes are small, light-weight instruments that are flown on weather balloons coupled via interfacing electronics to radiosondes for data transmission and measurements of meteorological parameters: pressure, temperature, humidity, wind, and position. The total weight of the ozonesonde-radiosonde flight package is ~1 kg so the payload can be flown on relatively small balloons (typically 1200-1500 g). Using the telemetry of the radiosonde, the measured data are transmitted to the ground station for further processing. Normally, data are taken during ascent at a rise rate of about 5 m/s to a balloon burst altitude of 30-33 km altitude. The inherent response time of the chemical measurement of the ozonesonde is 20-30 s, which provides an effective height resolution in the ozone profile data of 100-150 m.

Since their first design in the 1960's, the most commonly used ozonesonde instruments are based on electrochemical detection methods that convert the sampled ozone into an electrical current. *Smit* (2014) describes the common ozonesonde types in use over the past 50 years. At the present time, the most widely used ozonesonde type is the Electrochemical Concentration Cell (ECC). Although widely deployed in the past, the Brewer Mast sonde is presently only launched at the Meteorological Observatory Hohenpeissenberg in Germany in a time series that started in 1967. Two other major electrochemical sonde types, developed by the India Meteorological Department and the Japan Meteorological Agency, are no longer used.

Each ozonesonde instrument is unique and is prepared and provisionally calibrated prior to launch. It is important for remote sensing researchers to understand operational aspects of the ozonesonde and the procedures that sonde data providers take to minimize uncertainties within an individual profile and to ensure consistency of the global ozonesonde record over time. The instrument and data treatment are described in the following sections.

2.2 The ECC Ozonesonde: Principles of Operation and Sources of Uncertainty

The ECC ozonesonde (**Figure 3**) developed by *Komhyr* (1969) consists of two cells, made of Teflon or molded plastic, which serve as a cathode and anode chamber. There are two widely used ECC ozonesonde types, manufactured by Science Pump Corporation and the EN-SCI Corporation, producing the SPC-6A and EN-SCI instrument, respectively. The design of both ECCs resembles **Figure 3** but there is a consistent 4-5% difference in their performance (**Figures 4A and 4B)** when the different instrument types are operated under the same conditions (*Smit et al*., 2007; *Thompson et al.*, 2007c; *Smit*, 2014). Both cells contain platinum mesh electrodes. They are immersed in aqueous potassium iodide (KI) solutions of different concentrations, whereby the cathode cell is charged with a solution of low KI concentration and the anode cell with a solution saturated with KI. The two chambers are linked together by an ion-bridge to provide an ion-pathway and to prevent mixing of the cathode and anode electrolytes. The detection is based on the titration of ozone in KI according to the redox reaction:

$$2\,KI + O_3 + H_2O \rightarrow I_2 + O_2 + 2\,KOH \qquad \text{(R-1)}$$

In the cathode cell, the iodine (I_2) is converted back into two iodide ions (I^-) by the uptake of two electrons from the platinum electrode surface. Continuous sampling is achieved by a small battery-driven gas pump made of Teflon that bubbles ambient air through the sensing solution of the electrochemical cell. The iodine molecules that are produced by the reaction are transported towards the cathode electrode to be converted back to I^-; this process generates an electrical current in an external circuit that is proportional to the sampled ozone per unit time. Given the pump flow rate ($\boldsymbol{\Phi_P}$ in $cm^3\ s^{-1}$), the pump temperature ($\boldsymbol{T_P}$ in K), the overall efficiency ($\boldsymbol{\eta_T}$) of the sensor cell, the measured electrical current ($\boldsymbol{I_M}$ *in* μA), after a correction for a background current ($\boldsymbol{I_B}$ in μA), is converted to the ozone partial pressure ($\boldsymbol{P_{O3}}$ in *mPa)*:

$$P_{O3} = 0.043085 * \frac{T_P}{(\eta_T * \Phi_P)} * (I_M - I_B) \qquad \text{(E-1)}$$

The constant 0.043085 is determined by the ratio of the gas constant (R) to two times the Faraday constant (for each O_3 molecule two electrons flow in the electrical circuit from reaction **R-1**). The overall efficiency, $\boldsymbol{\eta_T}$, includes: the absorption efficiency $\boldsymbol{\eta_A}$ of O_3 into the sensing solution (usually 1.00), the pressure dependent pump efficiency $\boldsymbol{\eta_P}$ and the conversion efficiency $\boldsymbol{\eta_C}$ of the ECC sensor cell. The last efficiency is predominantly determined by the stoichiometry of redox reaction **R-1** followed by the conversion of the produced iodine into the measured electrical current $\boldsymbol{I_M}$. In practice, most operators add a sodium-hydrogen phosphate buffer to the cathode KI-solution to maintain the pH at 7.0 to keep the stoichiometry of the redox reaction **R-1** close to one.

The uncertainty of the ECC sonde measurements of the ozone partial pressure ($\boldsymbol{P_{O3}}$) is a composite of the contributions of the individual uncertainties of the instrumental parameters ($\boldsymbol{I_M}$, $\boldsymbol{I_B}$, $\boldsymbol{T_P}$, $\boldsymbol{F_P}$, $\boldsymbol{\eta_T = \eta_A * \eta_P * \eta_C}$), as described in detail by *Tarasick et al.* (2021). *Tarasick et al.* (2021) assumed that all systematic uncertainty components are known and corrected for. All instrumental uncertainties are assumed to be random and uncorrelated such that they follow Gaussian statistics to determine the overall uncertainty of the measured $\boldsymbol{P_{O3}}$. In the troposphere the background current $\boldsymbol{I_B}$ is the dominant uncertainty, particularly in the upper troposphere where the ozone concentration is generally low (mid-latitudes) to very low (near the tropical tropopause).

In the stratosphere, uncertainties of pump characteristics (*Johnson et al.,* 2002) and conversion efficiencies are the major contributors to the overall uncertainty (*WMO/GAW Report No. 268,* 2021). Since 2000-2010, the radiosondes flown with the ozonesondes are equipped to measure GNSS altitude. This means that the ambient air pressure is determined from the altitude measurement (e.g. *Stauffer et al.* 2014) in which case the pressure uncertainty is better than 0.05-0.10 hPa above 50 hPa, making only a minor contribution to the overall uncertainty. However, in case of ozonesondes flown with non-GNSS radiosondes, generally those prior to ~2000, the uncertainty of the radiosonde pressure sensor measurement above 50 hPa could be the dominant source of error.

2.3 Quality Assurance (QA) of Ozonesondes: Approach and Current Status

There has been considerable research activity to understand the performance of the ozonesonde instrument and to establish standard operating procedures (SOP). Twenty-five years ago, the ozonesonde measurement was assigned a 15-20% accuracy *(SPARC/IOC/GAW, 1998)*. The total column ozone (TCO) amount is now typically accurate to within 2-3% when evaluated against co-located ground-based instruments. Accuracy throughout the column, when best practices are followed, is ~(5-10)%, with the potential to improve to (3-5)%.

2.3.1 Overview of Ozonesonde Community Quality Assurance (QA) Activities

The ozonesonde community, working together under the auspices of World Meteorological Organization/Global Atmospheric Watch (WMO/GAW) and groups like NDACC, the International Ozone Commission (IO3C), and, in the past decade, the GCOS Reference Upper Air Network (GRUAN), has organized QA research around three important activities. The first of these was the creation of a testing facility for ozonesondes. In the mid-1990s, as part of the WMO/GAW Quality Assurance plan (*WMO/GAW Report No. 104*, 1995), a World Calibration Centre for OzoneSondes (WCCOS) was established at Germany's Forschungszentrum-Jülich (*Smit et al.,* 2000). The heart of the WCCOS is an environmental simulation chamber in which up to four ozonesondes can be intercompared and calibrated against a dual beam UV-photometer (OPM; *Proffitt and McLaughlin*, 1983) that is traceable to the NIST standard for ozone. During testing, pressure, temperature and ozone concentration are varied at the rate of an actual ascent from the surface until burst altitude at 33-35 km altitude. In its first five years of operation a set of campaigns, each referred to as a Jülich Ozone Sonde Intercomparison Experiment (JOSIE; *WMO/GAW Report No. 130* (1998), *No. 157* (2004a) and *No. 158* (2004b)), quantified biases among ozonesonde types, ECC or otherwise, between the two major ECC types of instruments, among different sensing solution types (SST). *Smit et al.* (2007) summarized a JOSIE-2000 in which eight groups compared instruments and preparation methods over 10 simulations of various environments: polar, tropical, mid-latitude.

The second ozonesonde QA activity has been intercomparisons of ECC ozonesondes in the field. For example, JOSIE-2000 results on biases were confirmed in the field during the Balloon Experiment on Standards for Ozone (BESOS) campaign in 2004 (*Deshler et al.,* 2008), with 18 sondes flown on a single gondola along with the WCCOS standard OPM.

Examples from laboratory and field comparisons appear in **Figure 4.** In Figures **4A** and **4B,** offsets in the measurement of ozone between the two instruments from JOSIE-2000 and BESOS, respectively, are shown. The OPM was the absolute reference in both experiments.

2.3.2 Development of Consensus-based Standard Operating Procedures (ASOPOS)

The third component of enhancing QA was the establishment in 2004 of an international team of 15-20 sonde experts to review laboratory and field tests in an Assessment of Standard Operating Procedures (SOPs) for OzoneSondes (ASOPOS). The first ASOPOS led to a community consensus for SOPs. Largely based on the 1996-2000 JOSIE campaigns and BESOS, the recommended SOPs were published as *WMO/GAW Report No. 201* (2014).

The 2017 JOSIE campaign, with simulations of only tropical conditions (*Thompson et al.,* 2019), was the basis for a ASOPOS 2.0 evaluation (*WMO/GAW No. Report 268*, 2021). The ASOPOS 2.0 report outlines (1) an improved treatment to correct the pump flow rate that falls off at low pressures; (2) a correction of the ozone exposure dependent stoichiometry of the O_3+KI redox reaction (**R-1**) to account for both slow (≅20-25 min) and fast (≅20-25 sec) reactions that take place in the ECC during an ascent (*Vömel et al*., 2020); (3) a new conversion efficiency in **Eq. E-1** that relates the final calculation of ozone amount to the OPM used at the WCCOS, making every reported sounding traceable to a common standard; (4) an extended list of metadata to be collected at launch time so data can be reprocessed; (5) continuous monitoring of station QA by comparing sonde ozone amounts to ground-based and satellite overpass measurements for detecting problems like the post-2013 total ozone "dropoff" observed at a number of stations (*Stauffer et al.* 2020; see Section 4.2). **Figure 4C** displays some JOSIE-2017 results. Operators prepared their sondes used for determining the average labeled "nominal SOP" according to their home station practices; for 7 of 8 stations tested, the preparation followed the first ASOPOS Report (*WMO/GAW Report No. 201,* 2014). For the "Low Buffer" tests all operators used a sensing solution with 1% KI and 10% of the standard buffer solution. Ozone measured with the low-buffer solution, irrespective of instrument type, measured closer to the OPM near the simulated tropopause altitude (~15 km) but always lower than the OPM elsewhere in the profile.

2.3.3 Homogenization of Long Ozonesonde Time-Series

The bias effects, i.e., discontinuities and trends introduced by instrumental artifacts, as described in the first ASOPOS Report (*WMO/GAW Report No. 201*, 2014), need to be accounted for in calculating reliable ozone profile trends. ECC ozonesondes were first manufactured 50 years ago and have undergone modifications of the instrument and in some cases, operational procedures, resulting in inhomogeneities in some station records and biases among stations. Discontinuities in total ozone or profile segments have appeared in the time-series at various stations. This phenomenon was recognized in a 2011/2012 Ozone Sonde Data Quality Assessment (O3S-DQA) that reviewed 40 years of ozonesonde records from a number of stations. The O3S-DQA activity led to guidelines for data providers to resolve inhomogeneities in long-term sonde records (*Smit et al.*, 2012; https://www.wccos-josie.org/o3s-dqa). Generic transfer functions were developed (*Deshler et al.*, 2017) to aid the process of harmonizing sonde records to the common standard of the combinations recommended in the *WMO/GAW Report No. 201* (2014).

Since 2015, ~40 of the long-term ozonesonde records within the global network have been re-processed following the O3S-DQA guidelines, removing known inhomogeneities to achieve overall uncertainties of 5-10 %. These include the Canadian stations (*Tarasick et al.*, 2016), several European stations (*Van Malderen et al*., 2016), those of the SHADOZ network (*Witte et al*., 2017, 2018; *Thompson et al.*, 2017), Wallops Island, VA (*Witte et al.*, 2019), and eight stations in the NOAA network (*Sterling et al.*, 2018). **Figure 5** shows the result of the homogenization effort of the ozonesonde time series at Boulder, CO (cyan triangle on the **Figure 6 map**), by comparing the total ozone column (TCO) derived from the sondes with TCO measured by the Dobson spectrophotometer before (**Figure 5A**) and after the re-processing (**Figure 5B**).

3. Ozonesonde Networks

3.1. The Global Network: Long-term Sites

Stations launching ozonesondes on a regular basis are displayed in **Figure 6**. All except one launch ECC type ozonesonde instruments. WOUDC archives the sonde profiles along with co-located total column ozone amounts from Dobson, Brewer, and SAOZ spectrometers where these are available. NDACC is another repository for ozonesonde data. Other oft-used archives are NOAA/GML (https://gml.noaa.gov/aftp/data/ozwv/Ozonesonde/) and NASA's SHADOZ (https://tropo.gsfc.nasa.gov/shadoz). Surface ozone concentrations are archived with other reactive gases at the WDCRG.

The global ozonesonde network, consisting of stations operated by meteorological services, space agencies, and several universities, has evolved over more than 80 years. A number of stations originated in the 1950s during the International Geophysical Year. Other sounding stations became operational as the number of ozone-measuring satellites increased after 1990 (**Figure 7**). Because most Antarctic ozonesonde stations began operating before the 1980s, a robust record exists of the lower stratospheric ozone depletion associated with the Antarctic "ozone hole" in the Austral winter to early spring when UV-based satellites have limited views. The discovery of extreme Antarctic ozone loss was first reported at the 1984 Quadrennial Ozone

Symposium (*Chubashi*, 1985) based on soundings from the Japanese Syowa station (black triangle on **Figure 6**) and on column ozone losses at the British Halley Bay station in 1985 (*Farman et al.*, 1985). **Figure 8A** displays an example from South Pole station (magenta triangle on the **Figure 6** map) in 2018 of the morphology of low-ozone profiles that occur during September and October when there is a sustained Antarctic polar vortex. The contrasting profiles are from July 2018 at South Pole.

3.2 Strategic Networks: Global and Campaign Operations

Ozonesondes have been organized for targeted purposes in what are referred to as strategic ozonesonde networks (*Thompson et al.*, 2011). The global SHADOZ network (blue circles in **Figure 6**), organized in 1998 (*Thompson et al.*, 2003a), consists of tropical and subtropical stations that launch 2-5 sondes monthly, generally coordinated with a midday overpass of one or more instruments on a polar-orbiting satellite. The zonal distribution of SHADOZ stations (*Thompson et al.*, 2003b) was chosen to investigate the wave-one pattern in tropical total column ozone (**Figure 9**) first reported in the 1980s by *Fishman et al.* (1987). An important contribution of SHADOZ has been the characterization of a distinct tropical tropopause layer (TTL, sometimes referred to as a tropopause transition layer [*Gettelman and Forster*, 2002; *Fuglistaler et al.*, 2009; *Thompson et al.*, 2012]). This region is typically given as between 13-18 km; note steep ozone gradients at ~ 13 km in **Figure 9).**

Other strategic ozonesonde networks operate on a campaign basis (*Thompson et al.*, 2011); a list of major campaigns is given in **Table 1**. These soundings provide fixed-site ozone profiles to complement the multi-species payloads that aircraft deploy to study chemical and meteorological processes influencing ozone in the stratosphere and/or troposphere. The Match campaigns (*von der Gathen et al.*, 1995; *Rex et al.*, 1999) have coordinated polar and midlatitude soundings to study in situ ozone losses during two Antarctic and 19 Arctic springs since the 1991-1992 Arctic winter (**Table 1**). Using forecast trajectories to predict where layers of depleted ozone observed in one sounding will travel, the projected arrival of such a parcel over another station triggers a timed launch. Match has also supported a number of international aircraft experiments (**Table 1**). For the first time, in the 2019-2020 winter-spring season, Match showed that the magnitude of Arctic ozone profile loss, recorded by soundings over Greenland, Ny-Ålesund (Svalbard, Norway), Canada and Finland, could approach the magnitude of Antarctic "ozone hole" loss, with ozone mixing ratio values at $\leq$ 0.2 ppmv at 18 km (**Figure 8B;** *Wohltmann et al.*, 2020).

Over North America, a series of Intensive Ozonesonde Network Studies (IONS**)** supported multi-aircraft and satellite validation studies from 2004 through 2013. For four IONS campaigns, sondes were coordinated at 6 to as many as 23 sites (August 2006) for midday satellite overpasses from 3-7 times/week. The IONS experiments led to a deeper understanding of tropospheric ozone during North American summers and have been especially useful in identifying stratosphere-troposphere exchange (STE) episodes. STE turns out to be more prevalent than previously thought, with significant intrusions of stratospheric air taking place after April-May, the typical "springtime" maximum in STE activity (*Ott et al.*, 2016; *Kuang et al.*, 2017; *Tarasick et al.*, 2019). During the July-August 2004 IONS, ozonesonde observations along with satellite data, showed that ~1/4 of the free tropospheric ozone budget from mid-Atlantic states to southeastern Canada originated from the stratosphere (*Thompson et al.*, 2007a,b). **Figure 8C** illustrates ozone profiles below 18 km at a Houston site during SEACIONS (2013). Varying ozone concentrations in the upper troposphere reflect stratospheric influences as well as lightning, as *Thompson et al.* (2008) showed with the identification of ozone laminae and satellite data analysis with IONS-06 summertime soundings over Houston. These same influences are reflected in the 2013 SEACIONS profiles (**Figure 8C)**.

4. Applications of Ozonesonde Data with Remote Sensing Observations

Ozonesonde observations and remote sensing observations have a symbiotic relationship in that they are both useful to each other for producing high quality datasets. The simple satellite retrieval flowchart of **Figure 10A** demonstrates that climatologies based on ozonesonde profiles (e.g., *McPeters and Labow*, 2012) are used in satellite algorithms as a priori or first guess information. Limb-measuring satellites rely on comparisons with sonde ozone profiles for validation of their products. With a number of ozone-measuring satellites lasting a decade or more (**Figure 7),** ozonesonde data are being used to evaluate drift in the satellite instruments (*Hubert et al.*, 2016). The latter application has been an important factor in increasing demand for sonde data with reduced uncertainty and more rapid data delivery. Total column ozone (TCO) or tropospheric column ozone (TrCO) from sondes, as well as ground-based spectrometers, are routinely compared with the satellite TCO or TrCO. Examples are given in the next section.

4.1 Satellite Ozone Product Evaluation using Ozonesonde Data

Ozonesonde data are typically used to evaluate two types of satellite products: profiles and column amounts. For example, stratospheric ozone profiles from the SAGE III instrument on the International Space Station (ISS/SAGE III) were recently examined by *Wang et al.*, (2020). The satellite profiles are based on limb-viewing observations at sunrise and sunset. Twenty ozonesonde stations (between ±55 degrees latitude) provided the statistics, using a total of 273 profiles. *Wang et al.* (2020) also compared the SAGE III data to ozone from four other limb-measuring satellites, OSIRIS, Aura/MLS, ACE-FTS and OMPS-LP. Agreement of the satellites as a whole was somewhat better at midlatitudes than in the tropics.

Extracting profiles from nadir-viewing UV-measuring satellites is challenging. *Huang et al.* (2017) presents a 10-year record of tropospheric profiles derived from OMI. The record is somewhat compromised due to a partial detector failure in 2009, which introduced a sampling bias into the ozone readings. For the newer TROPOMI (2017-), *Mettig et al.* (2021a) employed a novel technique (TOPAS, Tikhonov regularized Ozone Profile retrievAl with SCIATRAN) to nadir retrievals in tropical and mid-latitudes to estimate ozone throughout the troposphere and lower-mid stratosphere; the method follows the simple flowchart in **Figure 10A**. The vertical resolution of the TOPAS method is fairly coarse (~9 km on average) based on the averaging kernels reported with only 1-2 degrees of freedom (DOFs) in the troposphere, which is not unlike other UV-only satellite instruments. This indicates that similar instruments are highly dependent on the a priori profile (eg. an ozonesonde climatology) in the troposphere. However, agreement between the TROPOMI-retrieved ozone profiles and ozonesonde measurements is generally within 20% (**Figure 10B**). New retrievals that combine observations from UV-satellite instruments and IR instruments (eg. NOAA's CrIS) can improve both tropospheric and stratospheric comparisons with ozonesondes due to increased sensitivity throughout the ozone profile (*Mettig et al.*, 2021b).

Other techniques for estimating tropospheric ozone are based on column amounts, following the heritage of *Fishman et al.* (1991; 1996). Their "residual" approach to tropospheric ozone consists of subtracting the stratospheric column extracted from one satellite sensor from a highly accurate TCO from a backscattered UV instrument, initially from TOMS (several instruments from 1978-2005). The OMI/MLS series (*Ziemke et al.* 2006; 2019) is one of the most-used tropospheric column ozone (TrCO) datasets based on a residual technique. **Figure 11** shows the monthly mean TrCO from SHADOZ sondes from 10 tropical sites (latitude within ±20 degrees) compared to the corresponding monthly average OMI/MLS estimated tropospheric column. The offset is ~25% where the sonde TrCO is 40 DU although the correlation ($r^2 = 0.66$) is reasonably good. Part of the offset may be sampling differences (daily satellite data, with averaging over several pixels, vs. 2-4 sondes/month). The satellite measurements do not typically capture the full-range of ozone extremes measured by the sondes.

Cloud-slicing techniques (*Ziemke et al*., 2001; *Heue et al.*, 2017) constitute an alternative approach to estimating upper and lower tropospheric column amounts; this has been applied to TROPOMI (*Hubert et al.*, 2021). Agreement with ozonesonde-based totals is ~15%. A shortcoming of both cloud-slicing and residual methods is incomplete knowledge of the tropopause height, i.e., what the column actually represents. This limitation is particularly relevant in the extra-tropics where the tropopause height can vary greatly and change from < 10 km to more than 15 km within hours. Time-series with residual products (*Ziemke et al.,* 2019) capture seasonal variability and oscillations like the ENSO but caution is warranted for trends.

Figure 12 shows examples of ozonesonde comparisons from two instruments on the Aura satellite (OMI and MLS) that has operated for 17 years. The comparisons are for soundings taken at the Wallops Island, VA (green triangle marks location in **Figure 6**). Good agreement between the ozonesondes and MLS (**Figure 12A**) is observed throughout the stratosphere (*Witte et al.*, 2019. Dobson spectrophotometer measurements at Wallops Island are within ±5% of the ozonesonde TCO over the 25-year record illustrated (1995-2020), demonstrating the stability and high-quality of the sounding record); the Dobson is calibrated regularly against the world reference instrument at Boulder, CO. **Figure 12B** shows that agreement between OMI (October 2004-) and ozonesonde TCO also averages 5% or better to 2020.

4.2 Use of Satellite Ozone Data to Track the Performance of the Ozonesonde

The examples above illustrate how ozonesonde data are used for evaluation of satellite products. Conversely, because several satellite records have been processed and improved multiple times, high-accuracy satellite data can be useful in monitoring the quality of sonde data. The ozonesonde community has been systematically reprocessing long-term sonde records over the past decade. Comparisons in total column ozone between integrated total ozone from soundings and coincident satellite overpasses may show a discontinuity that signifies a problem in the sonde measurements. For example, *Witte et al.* (2017; 2018) showed that an inadvertent change in the sensing solution in soundings at La Réunion led to an artificial 18 DU increase in the mean TCO from 2007 to 2016 compared to the average TCO from 1998 to 2006. *Witte et al.* (2017; 2018) corrected the affected ozone profiles to remove the discontinuities, using the homogenization procedures recommended by ASOPOS in *Deshler et al.* (2017).

In the past 5 years there have been concerns about drifts or discontinuities in the ozonesonde TCO at ~20% of the global ozonesonde record since 2005. The direction of change is a loss of 3% or more in TCO since 2013. **Figure 13** illustrates how data from 5 operational satellite instruments, MLS (stratosphere), OMI, OMPS and two GOME-2 instruments (TCO), are used to evaluate the ozonesonde data quality in the Aura era. In the upper panels of **Figures 13A** and **13B**, comparisons of sonde stratospheric ozone are made with ozone at standard MLS pressure levels. The lower panels show TCO comparisons with the 4 UV-based satellite instruments. The Wallops Island record (**Figures 12 and 13A)** is stable in both TCO and stratospheric ozone above 50 hPa whereas, after 2013, the Samoa data (**Figure 13B**) display more variability and an overall TCO decline (lower panel in **Figure 13B**) that averages 3-4% (*Stauffer et al.*, 2020); the cause is partially due to changes in one sonde instrument type. The ASOPOS 2.0 Report (*WMO/GAW Report No. 268*, 2021), in which procedures are detailed to maximize quality in ozonesonde measurements, recommends ongoing comparisons of both the TCO and the stratospheric profile. The goal is to detect any change in procedure or instrument performance as quickly as possible.

5. Summary and Conclusions

5.1 Scientific Perspective: On-going Need for Profiles from Global Ozonesondes

The vertical profiles of the ozonesonde instrument provide unique information in the global ozone observing system for several reasons. First, no other widely used method is as free of weather effects. Second, although lidar has high vertical resolution, there are many fewer lidar stations compared to ozonesonde monitoring sites.

The near-real time measurement of the ozonesonde is ideal for tracking layers of stratospheric ozone (Match campaigns) and ozone pollution in the troposphere (IONS campaigns). Interest in ingesting sonde profiles into regional air-quality forecasts in near-real time and global chemistry-climate models is another motivator for adding to the number of ozonesonde stations. Unfortunately, numbers of sonde records have been declining in the past years. The combined WOUDC, NDACC, SHADOZ and NOAA/GML archives include >2800 soundings for 2017 but fewer than 2400 records in 2019. Key Arctic and mid-latitude stations have reduced or eliminated soundings.

The satellite community continues to be an important user of ozonesonde data as well as a driver for faster data delivery and more stringent quality assurance. With 5% uncertainty in TCO now achievable, ozonesonde data can be used to detect drifts of profiling ozone monitoring satellites and to evaluate new algorithms and satellite ozone products in a timely manner. Conversely, satellite data have been shown to be an important component in ensuring continuous evaluation of ozonesonde instrument and operational QA.

5.2 Quality Assurance: Need for Sonde Intercomparisons and a Global Ozone Reference

Changes in ozonesonde instrumentation is unavoidable as individual components may be modified by manufacturers. Operational and data processing practices may also change at individual stations. Accordingly, there is an ongoing need for periodic evaluation of ozonesonde performance and intercomparisons with a global ozone reference as the ASOPOS process has demonstrated. Essential elements of QA assessments are: (1) regular laboratory evaluation of instruments and operational practices, such as the JOSIE experiments; (2) field tests; (3) a process whereby global data and SOPs are continuously evaluated by a broad team of ozonesonde experts. These assessments must be supported by maintaining a world ozone standard photometer and one or more environmental test centers, e.g., the WCCOS. A strength of the ASOPOS process has been the inclusion of dedicated researchers who provide and archive ozone profiles, data users and instrument manufacturers. The recommendations, supported by analyses in the peer-reviewed literature, are consensus-based. The ASOPOS Reports are themselves peer-reviewed and are publicly available through the WMO/GAW website.

5.3 Conclusions

The ozonesonde instrument is unmatched in producing profiles of ozone with high vertical resolution throughout the troposphere and lower-mid stratosphere. Over the past 25 years, dedicated attention to ozonesonde QA has led to significant advances. This in turn led to new laboratory and field experiments to further refine SOP and guidelines for traceable ozonesonde records, bringing the target of 5% uncertainty throughout the ozone profile within reach. With reprocessed data, it has been possible to reduce residual uncertainties, biases, and discontinuities in ozonesonde time-series. We can expect that there will be further homogenization efforts of ozonesonde data and evaluation of the new data within the global network in the coming years.

Acknowledgments. Valuable comments were received from reviewer Holger Vömel (NCAR). Thanks to Peter von der Gathen (Alfred Wegener Institute, Potsdam) for information on the Match and related aircraft and ground campaigns.

References

Chubashi, S., A special ozone observation a Syowa station, Antarctica, from February 1982 to January, 1983. In Atmospheric Ozone, C. S. Zerefos and A. Ghazi, D. Reidel Publishers, Dordrecht, The Netherlands, 1985, pp. 285-289.

DeMazière, M., Thompson, A. M., Kurylo, M. J., Wild, J., Bernhard, G., Blumenstock, T., Hannigan, J., Lambert, J-C., Leblanc, T., McGee, T. J., Nedoluha, G., Petropavlovskikh, I., Seckmeyer, G., Simon, P. C., Steinbrecht, W., Strahan, S., Sullivan, J. T., 2018. The Network for the Detection of Atmospheric Composition Change (NDACC): History, status and perspectives, Atmos. Chem. Phys., 18, 4935–4964. https://doi.org/10.5194/acp-18-4935-2018.

Deshler, T., Mercer, J., Smit, H. G. J., Stubi, R., Levrat, G., Johnson, B J., Oltmans, S. J., Kivi, R., Thompson, A. M., Witte, J., Davies, J., Schmidlin, F. J., Brothers, G., Sasaki, T., 2008. Atmospheric comparison of electrochemical cell ozonesondes from different manufacturers, and with different cathode solution strengths: The Balloon Experiment on Standards for Ozonesondes, J. Geophys. Res., 113, D04307. http://doi.org/10.1029/2007JD008975.

Deshler, T., Stübi, R., Schmidlin, F. J., Mercer, J. L., Smit, H.G.J., Johnson, B.J., Kivi, R. and Nardi, B., 2017. Methods to homogenize ECC ozonesonde measurements across changes in sensing solution concentration or ozonesonde manufacturer, Atmos. Meas. Tech., 10, 2012-2043. http://doi.org/10.5194/amt-10-2021-2017.

Farman, J., Gardiner, B., Shanklin, J. Large losses of total ozone in Antarctica reveal seasonal ClO_x/NO_x interaction. Nature 315, 207–210 (1985). https://doi.org/10.1038/315207a0

Fishman, J., Larsen, J. C., 1987. Distribution of total ozone and stratospheric ozone in the tropics: Implications for the distribution of tropospheric ozone, J. Geophys. Res., 92, D6. https://doi.org/10.1029/JD092iD06p06627.

Fishman, J., Fakhruzzaman, K., Cros, B., Nganga, D., 1991. Identification of widespread pollution in the Southern Hemisphere deduced from satellite analyses, Science, 252 (5013), 1693-1696. http://doi.org/10.1126/science.252.5013.1693.

Fishman, J., Brackett, V. G., Browell, E. V., Grant, W. B., 1996. Tropospheric ozone derived from TOMS/SBUV measurements during TRACE-A, J. Geophys. Res., 101, D19. https://doi.org/10.1029/95JD03576.

Fuglistaler, S. Dessler, A. E., Dunkerton, T. J., Folkins, I., Fu, Q., Mote, P. W., 2009. Tropical tropopause layer, Rev. Geophysics, https://doi.org/10.1029/2008RG000267.

Gettelman, A., Forster, P. M. F., 2002. A climatology of the tropical tropopause layer, J. Meterol. Soc. Jpn., 80(4B), 911–924. http://doi.org/10.2151/jmsj.80.911.

Heue, K-P., Coldewey-Egbers, M., Delcloo, A., Lerot, C., Loyola, D., Valks, P., van Roozendael, M., 2016. Trends of tropical tropospheric ozone from 20 years of European satellite measurements and perspectives for the Sentinel-5 Precursor, Atmos. Meas. Tech., 9, 5037–5051. http://doi.org/10.5194/amt-9-5037-2016.

Huang, G., Liu, X., Chance, K., Yang, K., Bhartia, P. K., Cai, Z., Allaart, M., Acellet, G., Calpini, B., Coetzee, G. J. R., Cuevas-Agulló, E., Cupeiro, M., De Backer, H., Dubey, M. K., Fuelberg, H. E., Fujiwara, M., Godin-Beekmann, S., Hall, T. J., Johnson, B., Joseph, E., Kivi, R., Kois, B., Komala, N., König-Langlo, G., Laneve, G., Leblanc, T., Marchand, M., Minschwaner, K. R., Morris, G., Newchurch, M. J., Ogino, S-Y., Ohkawara, N., Piters, A. J. M., Posny, F., Querel, R., Scheele, R., Schmidlin, F. J., Schnell, R. C., Schrems, O., Selkirk, H., Shiotani, M., Skrivánková, P., Stübi, R., Taha, G., Tarasick, D. W., Thompson, A. M., Thouret, V., Tully, M. B., van Malderen, R., Vömel, H., von der Gathen, P., Witte, J. C., Yela, M., 2017. Validation of 10-year SAO OMI Ozone Profile (PROFOZ) product using ozonesonde observations, Atmos. Meas. Tech., 10, 2455–2475. https://doi.org/10.5194/amt-10-2455-2017.

Hubert, D., Lambert, J.-C., Verhoelst, T., Granville, J., Keppens, A., Baray, J.-L., Bourassa, A. E., Cortesi, U., Degenstein, D. A., Froidevaux, L., Godin-Beekmann, S., Hoppel, K. W., Johnson, B. J., Kyrölä, E., Leblanc, T., Lichtenberg, G., Marchand, M., McElroy, C. T., Murtagh, D., Nakane, H., Portafaix, T., Querel, R., Russell III, J. M., Salvador, J., Smit, H. G. J., Stebel, K., Steinbrecht, W., Strawbridge, K. B., Stübi, R., Swart, D. P. J., Taha, G., Tarasick, D. W., Thompson, A. M., Urban, J., van Gijsel, J. A. E., Van Malderen, R., von der Gathen, P., Walker, K. A., Wolfram, E., Zawodny, J. M., 2016. Ground-based assessment of the bias and long-term stability of 14 limb and occultation ozone profile data records, Atmos. Meas. Tech., 9, 2497–2534. https://doi.org/10.5194/amt-9-2497-2016.

Hubert, D., Heue, K.-P., Lambert, J.-C., Verhoelst, T., Allaart, M., Compernolle, S., Cullis, P. D., Dehn, A., Félix, C., Johnson, B. J., Keppens, A., Kollonige, D. E., Lerot, C., Loyola, D., Maata, M., Mitro, S., Mohamad, M., Piters, A., Romahn, F., Selkirk, H. B., da Silva, F. R., Stauffer, R. M., Thompson, A. M., Veefkind, J. P., Vömel, H., Witte, J. C., Zehner, C., 2021. TROPOMI tropospheric ozone column data: Geophysical assessment and comparison to ozonesondes, GOME-2B and OMI, Atmos. Meas. Tech, 14, 7405-7433, https://doi.org/10.5194/amt-14-7405-2021

Johnson, B.J., Oltmans, S. J., Vömel, H., Smit, H. G. J., T. Deshler, T., C. Kroeger, C., 2002. ECC Ozonesonde pump efficiency measurements and tests on the sensitivity to ozone of buffered and unbuffered ECC sensor cathode solutions, J. Geophys. Res., 107, D19 doi: 10.1029/2001JD000557.

Komhyr, W.D., 1969. Electrochemical concentration cells for gas analysis, Ann.Geoph., 25, 203-210.

Kuang, S., Newchurch, M. J., Thompson, A. M., Stauffer, R. M., Johnson, B. J., Wang, L., 2017. Ozone variability and anomalies observed during SENEX and SEAC4RS campaigns in 2013, J. Geophys. Res., 122(20), 11,227-11,241. https://doi.org/10.1002/2017JD027139.

McDermid, I. S., Godin, S. M., Lindqvist, L. O., Ground-based laser DIAL system for long-term measurements of stratospheric ozone, 1990. Applied Optics, 29, 3603-3612, https://doi.org/10.1364/AO.29.003603.

McGee, T. J., Newman,P., Ferrare, R., Whiteman, D., Butler, J. J., Burris, J., Godin, S. M., McDermid, I. S., 1990. Lidar observations of ozone changes induced by sub-polar airmass motion over Table Mountain (34.4N), J. Geophys. Res., 95, 20527-20530.

McPeters, R. D., Labow, G. J., 2012. Climatology 2011: An MLS and sonde derived ozone climatology for satellite retrieval algorithms, J. Geophys. Res., 117, D10303. http://doi.org/10.1029/2011JD017006.

Mettig, N., Weber, M., Rozanov, A., Arosio, C., Burrows, J. P., Veefkind, P., Thompson, A. M., Querel, R., Leblanc, T., Godin-Beekman, S., Kivi, R., Tully, M. B., 2021a. Ozone profile retrieval from nadir TROPOMI measurements in the UV range, Atmos. Meas. Tech., 14, 6057-6082, https://doi.org/10.5194/amt-14-6057-2021, 2021.

Mettig, N., Weber, M., Rozanov, A., Burrows, J. P., Veefkind, P., Barnet, C., Thompson, A. M., Stauffer, R. M., Leblanc, T., Ancellet, G., Newchurch, M., Kivi, R., Tully, M. B., Van Malderen, R., Steinbrecht, W., Piters, A., Allaart, M., Kois, B., Stübi, R., Davies, J., Skrivankova, P., 2021b. Combined UV and IR ozone profile retrieval from TROPOMI and CrIS measurements, Atmos. Meas. Tech. Disc, https://doi.org/10.5194/amt-2021-412.

Moeini, O., Tarasick, D. W., McElroy, C. T., Liu, J., Osman, M. K., Thompson, A. M., Parrington, M., Palmer, P. I., Johnson, B., Oltmans, S. J., Merrill, J., 2020. Estimating boreal fire-generated ozone over North American using ozonesonde profiles and a differential back trajectory technique, Atmos. Environ. https://doi.org/10.1016/j.aeaoa.2020.100078.

Ott, L. E., Duncan, B. N., Thompson, A. M., Diskin, G., Fasnacht, Z., Langford, A. O., Lin, M., Molod, A. M., Nielsen, J. E., Pusede, S. E., Wargan, K., Weinheimer, A. J., Yoshida, Y., 2016. Frequency and impact of summertime stratospheric intrusions over Maryland during DISCOVER-AQ (2011): New evidence from NASA's GEOS-5 simulations, J. Geophys. Res.,121(7), 3687-3706. https://doi.org/10.1002/2015JD024052.

Proffitt, M.H., McLaughlin, R. J., 1983. Fast response dual-beam UV-absorption photometer suitable for use on stratospheric balloons, Rev. Sci. Instrum., 54, 1719-1728.

Rex, M., von der Gathen, P., Braathen, G., Harris, N. R. P., Reimer, E., Beck, A., Alfier, R., Krüger-carstensen, R., Chipperfield, M., De Backer, H., Balis, D., O'Connor, F., Dier, H., Dorokhov, V., Fast, H., Gamma, A., Gil, M., Kyrö, E., Litynska, Z., Mikkelsen, I. S., Molyneux, M., Murphy, G., Reid, S. J., Rummukainen, M., Zerefos, C., 1999. Chemical Ozone Loss in the Arctic Winter 1994/95 as Determined by the Match Technique, J. Atmos. Chem., 32, 35–59. https://doi.org/10.1023/A:1006093826861.

Smit, H.G.J., 2014. Ozone Sondes, in Encyclopedia of Atmospheric Sciences, Second Edition, edited by G.R. North, J.A. Pyle, and F. Zhang, 1, 372-378, Academic Press, London.

Smit, H.G.J., Sträter, W., Helten, M., Kley, D., 2000. Environmental simulation facility to calibrate airborne ozone and humidity sensors. Jül Berichte Nr 3796, Forschungszentrum Jülich.

Smit, H.G.J., Straeter, W., Johnson, B. J., Oltmans, S. J., Davies, J., Tarasick, D. W., Hoegger, B., Stubi, R., Schmidlin, F. J., Northam, T., Thompson, A. M., Witte, J. C., Boyd, I., Posny, F., 2007. Assessment of the performance of ECC-ozonesondes under quasi-flight conditions in the environmental simulation chamber: Insights from the Jülich Ozone Sonde Intercomparison Experiment (JOSIE), J. Geophys. Res., 112, D19306. https://doi.org/10.1029/2006JD007308.

Smit, H. G. J., O3S-DQA, 2012. Guidelines for homogenization of ozonesonde data, SI2N/O3S-DQA activity as part of “Past changes in the vertical distribution of ozone assessment”, available at https://www.wccos-josie.org/o3s-dqa/.

SPARC/IOC/GAW, 1998. Assessment of Trends in the Vertical Distribution of Ozone, SPARC Report No.1, WMO Global Ozone Research and Monitoring Project Report No. 43, World Meteorological Organization, Geneva.

SPARC/IO3C/GAW, 2019. Report on Long-term Ozone Trends and Uncertainties in the Stratosphere, I. Petropavlovskikh, S. Godin-Beekmann, D. Hubert, R. Damadeo, B. Hassler, V. Sofieva (Eds.), SPARC Report No. 9, GAW Report No. 241, WCRP-17/2018, http://doi.org/10.17874/f899e57a20b.

Stauffer, R. M., Morris, G. A., Thompson, A. M., Joseph, E., Coetzee, G. J. R., Nalli, N. R., 2014. Propagation of radiosonde pressure sensor errors to ozonesonde measurements, Atmos. Meas. Tech., 7, 65–79, https://doi.org/10.5194/amt-7-65-2014.

Stauffer, R. M., Thompson, A. M., Oltmans, S. J., Johnson, B. J., 2017. Tropospheric ozonesonde profiles at long-term US monitoring sites: 2. Links between Trinidad, CA, profile clusters and inland surface ozone measurements, J. Geophys. Res., 122. http://doi.org/10.1002/2016JD025254.

Stauffer, R. M., Thompson, A. M., Kollonige, D. E., Witte, J. C., Tarasick, D. W., Davies, J. M., Vömel, H., Morris, G. A., Van Malderen, R., Johnson, B. J., Querel, R. R., Selkirk, H. B., Stübi, R., Smit, H. G. J., 2020. A post-2013 drop-off in total ozone at a third of global ozonesonde stations: Electrochemical Concentration Cell Instrument Artifacts?, Geophys. Res. Lett., 47(11). http://doi.org/10.1029/2019/GL086791.

Steinbrecht, W., Kubistin, D., Plass-Dülmer, C., Davies, J., Tarasick, D. W., von der Gathen, P., Deckelmann, H., Jepsen, N., Kivi, R., Lyall, N., Palm, M., Notholt, J., Kois, B., Oelsner, P., Allaart, M., Piters, A., Gill, M., Van Malderen, R., Delcloo, A. W., Sussmann, R., Mahieu, E., Servais, C., Romanens, G., Stübi, R., Ancellet, G., Godin-Beekmann, S., Yamanouchi, S., Strong, K., Johnson, B., Cullis, P., Petropavlovskikh, I., Hannigan, J. W., Hernandez, J.-L., Rodriguez, A. D., Nakano, T., Chouza, F., Leblanc, T., Torres, C., Garcia, O., Röhling, A. N., Schneider, M., Blumenstock, T., Tully, M., Paton-Walsh, C., Jones, N., Querel, R., Strahan, S., Stauffer, R. M., Thompson, A. M., Inness, A., Engelen, R., Chang, K.-L., Cooper, O. R., 2021. Did the COVID-19 crisis reduce free tropospheric ozone across the Northern Hemisphere? Geophys. Res. Lett., 48, e2020GL091987. https://doi.org/10.1029/2020GL091987.

Sterling, C. W., Johnson, B. J., Oltmans, S. J., Smit, H. G. J., Jordan, A. F., Cullis, P. D., Hall, E. G., Thompson, A. M., Witte, J. C., 2018. Homogenizing and estimating the uncertainty in NOAA's long-term vertical ozone profile records measured with the electrochemical concentration cell ozonesonde, Atmos. Meas. Tech., 11, 3661–3687. https://doi.org/10.5194/amt-11-3661-2018.

Sullivan, J. T., McGee, T. J., Leblanc, T., Sumnicht, G. K., Twigg, L. W., 2015. Optimization of the GSFC TROPOZ DIAL retrieval using synthetic lidar returns and ozonesondes – Part 1: Algorithm validation, Atmos. Meas. Tech., 8, 4133–4143. https://doi.org/10.5194/amt-8-4133-2015, 2015.

Tarasick, D. W., Davies, J., Smit, H. G. J., Oltmans, S. J., 2016. A re-evaluated Canadian ozonesonde record: measurements of the vertical distribution of ozone over Canada from 1966 to 2013. Atmos. Meas. Tech., 9, 195–214, https://doi.org/10.5194/amt-9-195-2016.

Tarasick, D. W., Carey-Smith, T. K., Hocking, W. K., Moeini, O., He, H., Liu, J., Osman, M. K., Thompson, A. M., Johnson, B. J., Oltmans, S. J., Merrill, T. J., 2019. Quantifying stratosphere-troposphere transport of ozone using balloon-borne ozonesondes, radar windprofilers and trajectory models. Atmos. Envir., 198(2019), 496–509. https://doi.org/10.1016/j.atmosenv.2018.10.040

Tarasick, D. W., Smit, H. G. J., Thompson, A. M., Morris, G. A., Witte, J. C., Davies, J., Nakano, T., Van Malderen, R., Stauffer, R. M., Johnson, B. J., Stübi, R., Oltmans, S. J., Vömel. H., 2021. Improving ECC Ozonesonde Data Quality: Assessment of Current Methods and Outstanding Issues. Earth and Space Science, 8, e2019EA000914, https://doi.org/10.1029/2019EA000914

Thompson, A. M., Pickering, K. E., McNamara, D. P., Schoeberl, M. R., Hudson, R. D., Kim, J. H., Browell, E. V., Kirchhoff, V. W. J. H., Nganga, D., 1996. Where did tropospheric ozone over southern Africa and the tropical Atlantic come from in October 1992? Insights from TOMS, GTE TRACE A, and SAFARI 1992. J. Geophys. Res., 101(D19), 24251– 24278, https://doi.org/10.1029/96JD01463.

Thompson, A. M., Witte, J. C., Hudson, R. D., Guo, H., Herman, J. R., Fujiwara, M., 2001. Tropical tropospheric ozone and biomass burning, Science, 291, 2128-2132 https://doi.org/10.1126/science.291.5511.2128.

Thompson, A. M., Witte, J. C., McPeters, R. D., Oltmans, S. J., Schmidlin, F. J., Logan, J. A., Fujiwara, M., Kirchhoff, V. W. J. H., Posny, F., Coetzee, G. J. R., Hoegger, B., Kawakami, S., Ogawa, T., Johnson, B. J., Vömel, H., Labow, G., 2003a. Southern Hemisphere Additional Ozonesondes (SHADOZ) 1998-2000 tropical ozone climatology 1. Comparison with Total Ozone Mapping Spectrometer (TOMS) and ground-based measurements. J. Geophys. Res., 108, 8238, https://doi.org/10.1029/2001JD000967.

Thompson, A. M., Witte, J. C., Oltmans, S. J., Schmidlin, F. J., Logan, J. A., Fujiwara, M., Kirchhoff, V. W. J. H., Posny, F., Coetzee, G. J. R., Hoegger, B., Kawakami, S., Ogawa, T. Fortuin, J. P. F., Kelder, H. M., 2003b: Southern Hemisphere Additional Ozonesondes (SHADOZ) 1998–2000 tropical ozone climatology. 2. Tropospheric Variability and the Zonal Wave-One, J. Geophys. Res., 108, 8241, doi: 10.1029/2002JD002241.

Thompson, A. M., Stone, J. B., Witte, J. C., Miller, S. K., Pierce, R. B., Chatfield, R. B., Oltmans, S. J., Cooper, O. R., Loucks, A. L., Taubman, B. F., Johnson, B. J., Joseph, E., Kucsera, T. L., Merrill, J. T., Morris, G. A., Hersey, S., Forbes, G., Newchurch, M. J., Schmidlin, F. J., Tarasick, D. W., Thouret, V., Cammas, J.-P., 2007a. Intercontinental Chemical Transport Experiment Ozonesonde Network Study (IONS) 2004: 1 Summertime upper troposphere/lower stratosphere ozone over northeastern North America. J. Geophys. Res., 112, D12S12, https://doi.org/10.1029/2006JD007441.

Thompson, A. M., Stone, J. B., Witte, J. C., Miller, S. K., Oltmans, S. J., Ross, K. L., Kucsera, T. L., Merrill, J. T., Forbes, G., Tarasick, D. W., Joseph, E., Schmidlin, F. J., McMillan, W. W., Warner, J., Hintsa, E. J., Johnson J. E., 2007b. Intercontinental Transport Experiment Ozonesonde Network Study (IONS, 2004): 2. Tropospheric Ozone Budgets and Variability over Northeastern North America. J. Geophys. Res., 112, D12S13, https://doi.org/10.1029/2006JD007670.

Thompson, A. M., Witte, J. C., Smit, H. G. J., Oltmans, S. J., Johnson, B. J., Kirchhoff, V. W. J. H., Schmidlin, F. J., 2007c. Southern Hemisphere Additional Ozonesondes (SHADOZ) 1998-2004 tropical ozone climatology. 3. Instrumentation, Station Variability, Evaluation with Simulated Flight Profiles. J. Geophys. Res., 112, D03304, https://doi.org/10.1029/2005JD007042.

Thompson, A. M., Yorks, J. E., Miller, S. K., Witte, J. C., Dougherty, K. M., Morris, G. A., Baumgardner, D., Ladino, L., Rappenglueck, B., 2008. Tropospheric ozone sources and wave activity over Mexico City and Houston during Milagro/Intercontinental Transport Experiment (INTEX-B) Ozonesonde Network Study, 2006 (IONS-06), Atmos. Chem. Phys., 8, 5113-5126.

Thompson, A. M., Oltmans, S. J., Tarasick, D. W., von der Gathen, P., Smit, H. G. J., Witte, J. C., 2011. Strategic ozone sounding networks: Review of design and accomplishments. Atmos. Envir., 45, 2145-2163, https://doi.org/10.1016/j.atmosenv.2010.05.002.

Thompson, A. M., Miller, S. K., Tilmes, S., Kollonige, D. W., Witte, J. C., Oltmans, S. J., Johnson, B. J., Fujiwara, M., Schmidlin, F. J., Coetzee, G. J. R., Komala, N., Maata, M., Mohamad, M. bt, Nguyo, J., Mutai, C., Ogino, S-Y., Raimundo Da Silva, F., Paes Leme, N. M., Posny, F., Scheele, R., Selkirk, H. B., Shiotani, M., Stübi, R., Levrat, G., Calpini, B., Thouret, V., Tsuruta, H., Valverde Canossa, J., Vömel, H., Yonemura, S., Andrés Diaz, J., Tan Thanh, H. T., Thuy Ha, H. T., 2012. Southern Hemisphere Additional Ozonesondes (SHADOZ) ozone climatology (2005-2009): Tropospheric and tropical tropopause layer (TTL) profiles with comparisons to OMI-based ozone products. J. Geophys. Res., 117, D23301, https://doi.org/10.1029/2011JD016911.

Thompson, A. M., Witte, J. C., Sterling, C., Jordan, A., Johnson, B. J., Oltmans, S. J., Fujiwara, M., Vömel, H., Allaart, M., Piters, A., Coetzee, G. J. R., Posny, F., Corrales, E., Diaz, J. A., Félix, C., Komala, N., Lai, N., Ahn Nguyen, H. T., Maata, M., Mani, F., Zainal, Z., Ogino, S-Y., Paredes, F., Penha, T. L. B., da Silva, F. R., Sallons-Mitro, S., Selkirk, H. B., Schmidlin, F. J. Stübi, R., Thiongo, K., 2017. First reprocessing of Southern Hemisphere ADditional OZonesondes (SHADOZ) Ozone Profiles (1998-2016). 2. Comparisons with satellites and ground-based instruments, J. Geophys. Res., 122, https://doi.org/10.1002/2017JD027406.

Thompson, A. M., Smit, H. G. J., Witte, J. C., Stauffer, R. M., Johnson, B. J., Morris, G., von der Gathen, P., Van Malderen, R., Davies, J., Piters, A., Allaart, M., Posny, F., Kivi, R., Cullis, P., Anh, N. T. H., Corrales, E., Machinini, T., da Silva, F. R.,, Paiman, G., Thiong'o, K., Zainal, Z., Brothers, G. B., Wolff, K. R., Nakano, T., Stübi, R., Romanens, G., Coetzee, G. J. R., Diaz, J. A., Mitro, S., Mohamad, M., Ogino, S-Y., 2019. Ozonesonde Quality Assurance: The JOSIE-SHADOZ (2017) Experience, Bull. Am. Meteor. Society, 100(1), https://doi.org/10.1175/BAMS-D-17-0311.1.

Van Malderen, R., Allaart, M. A. F., De Backer, H., Smit, H. G. J., De Muer, D., 2016. On instrumental errors and related correction strategies of ozonesondes: possible effect on calculated ozone trends for the nearby sites Uccle and De Bilt, Atmos. Meas. Tech., 9, 3793–3816, https://doi.org/10.5194/amt-9-3793-2016.

Vömel, H., Smit, H. G. J., Tarasick, D., Johnson, B., Oltmans, S. J., Selkirk, H., Thompson, A. M., Stauffer, R. M., Witte, J. C., Davies, J., van Malderen, R., Morris, G. A., Nakano, T., Stübi, R., 2020. A new method to correct the ECC ozone sonde time response and its implications for "background current" and pump efficiency, Atmos. Meas. Tech.., 13(10), 5667-5680, doi.org/10.5194/amt-13-5667-2020.

von der Gathen, P., Rex, M., Harris, N. R. P., Lucic, D., Knudsen, B. M., Braathen, G. O., De Backer, H., Fabian, R., Fast, H., Gil, M., Kyrö, E., Mikkelsen, I. S., Rummukainen, M., Stähelin, J., Varotsos, C., 1995. Observational evidence for chemical ozone depletion over the Arctic in winter 1991–92. Nature, 375, 131–134, https://doi.org/10.1038/375131a0.

Wang, H. J. R., Damadeo, R., Flittner, D., Kramarova, N., Taha, G., Davis, S., Thompson, A. M., Strahan, S., Wang, Y., Froidevaux, L., Degenstein, D., Bourassa, A., Steinbrecht, W., Walker, K., Querel, R., Leblanc, T., Godin-Beekman, S., Hurst, D., Hall, E., 2020. Validation of SAGE III/ISS solar occultation ozone products with correlative satellite and ground based measurements, J. Geophys. Res., 125, https://doi.org/10.1029/2020JD032430.

Witte, J. C., Thompson, A. M., Smit, H. G. J., Fujiwara, M., Posny, F., Coetzee, G. J. R., Northam, E. T., Johnson, B. J., Sterling, C. W., Mohamad, M., Ogino, S-Y., Jordan, A., da Silva, F. R., 2017. First reprocessing of Southern Hemisphere ADditional OZonesondes

(SHADOZ) profile records (1998-2015) 1: Methodology and evaluation. J. Geophys. Res., 122, https://doi.org/10.1002/2016JD026403.

Witte, J. C., Thompson, A. M., Smit, H. G. J., Vömel, H., Posny, F., Stübi, R., 2018. First reprocessing of Southern Hemisphere Additional Ozonesondes (SHADOZ) Profile Records. 3. Uncertainty in ozone profile and total column. J. Geophys. Res., 123(6), 3243-3268, https://doi.org/10.1002/2017JD027791.

Witte, J. C., Thompson, A. M., Schmidlin, F. J., Northam, E. T., Wolff, K. R., Brothers, G. B., 2019. The NASA Wallops Flight Facility digital ozonesonde record: Reprocessing, uncertainties, and dual launches. J. Geophys. Res., 124, 3565–3582, https://doi.org/10.1029/2018JD030098.

WMO/GAW Report No. 104, 1996. Report of the Fourth WMO Meeting of Experts on the Quality Assurance/Science Activity Centers (QA/SACs) of the Global Atmosphere Watch. WMO Global Atmosphere Watch Report Series, No. 104, World Meteorological Organization, Geneva.

WMO/GAW Report No. 130, 1998: Smit H.G.J and D. Kley, JOSIE: The 1996 WMO International Intercomparison of Ozonesondes Under Quasi Flight Conditions in the Environmental Simulation Chamber at Jülich, WMO Global Atmosphere Watch Report Series, No. 130, WMO/TD No. 926, World Meteorological Organization, Geneva.

WMO/GAW Report No. 157, 2004a: Smit, H.G.J., and W. Straeter, JOSIE-1998, Performance of ECC Ozone Sondes of SPC-6A and ENSCI-Z Type, WMO Global Atmosphere Watch Report Series, No. 157, WMO/TD No. 1218, World Meteorological Organization, Geneva. [Available online at https://library.wmo.int/index.php?lvl=notice_display&id=11089#.Ya-MV1MxlUM]

WMO/GAW Report No. 158, 2004b: Smit, H.G.J., and W. Straeter, JOSIE-2000, Jülich Ozone Sonde Intercomparison Experiment 2000, The 2000 WMO International Intercomparison of Operating Procedures for ECC Ozonesondes at the Environmental Simulation Facility at Jülich, WMO Global Atmosphere Watch Report Series, No. 158, WMO TD No. 1225, World Meteorological Organization, Geneva. [Available online at https://library.wmo.int/index.php?lvl=notice_display&id=11090#.Ya-M6FMxlUM]

WMO/GAW Report No. 201, 2014: Smit, H.G.J., and ASOPOS panel, Quality assurance and quality control for ozonesonde measurements in GAW, WMO Global Atmosphere Watch report series, No. 201, World Meteorological Organization, Geneva. [Available online at https://library.wmo.int/doc_num.php?explnum_id=7167]

WMO/GAW Report No. 268, 2021: Smit, H. G. J., Thompson, A. M., and ASOPOS panel, Ozonesonde Measurement Principles and Best Operational Practices, ASOPOS (Assessment of Standard Operating Procedures for Ozonesondes) 2.0, WMO Global Atmosphere Watch report series, No. 268, World Meteorological Organization, Geneva. [Available online at https://library.wmo.int/index.php?lvl=notice_display&id=21986#.YaFNSbpOlc8]

WMO/UNEP, 1995: Scientific Assessment of Ozone Depletion: 1994, Global Ozone Research and Monitoring Project – Report No. 37, World Meteorological Organization, Geneva.

WMO/UNEP, 2019: Scientific Assessment of Ozone Depletion: 2018, Global Ozone Research and Monitoring Project – Report No. 58, World Meteorological Organization, Geneva. [Available online at https://library.wmo.int/index.php?lvl=notice_display&id=20763#.Ya-O8lMxlUM]

Wohltmann, I., von der Gathen, P., Lehmann, R., Maturilli, M., Deckelmann, H., Manney, G. L., Davies, J., Tarasick, D., Jepsen, N., Kivi, R., Lyall, N., Rex, M., 2020. Near complete local reduction of Arctic stratospheric ozone by record chemical loss in spring 2020. Geophys. Res. Lett., 47(20), https://doi.org/10.1029/2020GL089547.

Ziemke, J. R., Chandra, S., Bhartia, P. K., 2001. "Cloud slicing": A new technique to derive upper tropospheric ozone from satellite measurements, J. Geophy. Res., 106, D9, 9853–9867, https://doi.org/10.1029/2000JD900768.

Ziemke, J. R., Chandra, S., Duncan, B. N., Froidevaux, L., Bhartia, P. K., Levelt, P. F., Waters, J. W., 2006. Tropospheric ozone determined from Aura OMI and MLS: Evaluation of measurements and comparison with the Global Modeling Initiative's Chemical Transport Model, J. Geophys. Res., 111, D19303, https://doi.org/10.1029/2006JD007089.

Ziemke, J. R., Oman, L. D., Strode, S. A., Douglass, A. R., Olsen, M. A., McPeters, R. D., Bhartia, P. K., Froidevaux, L., Labow, G. J., Witte, J. C., Thompson, A. M., Haffner, D. P., Kramarova, N. A., Frith, S. M., Huang, L. K., Jaross, G. R., Seftor, C. J., Deland, M. T., Taylor, S. L., 2019. Trends in global tropospheric ozone Inferred from a composite record of TOMS/OMI/MLS/OMPS satellite measurements and the MERRA-2 GMI simulation, Atmos. Chem. Phys., 19, 3257–3269, https://doi.org/10.5194/acp-19-3257-2019.

Table 1   Caption. Strategic ozonesonde networks and related campaigns. Campaigns aligned with Match are in black (European-sponsored) and red (NASA-sponsored)

Observation Years	Campaign	Observation Years	Campaign
1991-1992	**Match** (Arctic Spring) *with EASOE & AASE II*	**July-Aug 2004**	**IONS-04** (Intensive Ozonesonde Network Study, INTEX-A, ICARTT)
1992-1993	**Match** (Arctic Spring)		
1993-1994	**Match** (Arctic Spring) *with SESAME*		
1994-1995	**Match** (Arctic Spring) *with SESAME*	**March, May, Aug-Sept 2006**	**IONS-06** (Intensive Ozonesonde Network Study, INTEX-B, MILAGRO)
1995-1996	**Match** (Arctic Spring)		
1996-1997	**Match** (Arctic Spring)		
1997-1998	**Match** (Arctic Spring)		
1998-1999	**Match** (Arctic Spring) *with THESEO*	**April 2008, June-July 2008**	**ARCIONS** (ARCTAS IONS)
1999-2000	**Match** (Arctic Spring) *with THESEO 2000 & SOLVE*		
2002-2003	**Match** (Arctic Spring) *with VINTERSOL & SOLVE II*		
2004-2005	**Match** (Arctic Spring) *with SCOUT-O3*		
2006-2007	**Match** (Arctic Spring) *with SCOUT-O3*	**July-Aug 2010, 2011**	**BORTAS**
2007-2008	**Match** (Arctic Spring) *with SCOUT-O3*		
2009-2010	**Match** (Arctic Spring) *with RECONCILE*		
2010-2011	**Match** (Arctic Spring) *with RECONCILE*		
2013-2014	**Match** (Arctic Spring) *with StratoClim*		
2015-2016	**Match** (Arctic Spring) *with StratoClim*		
2017-2018	**Match** (Arctic Spring) *with StratoClim*		
2019-2020	**Match** (Arctic Spring)		
2003	**Match** (Antarctic Spring)	**Aug-Sept 2013**	**SEACIONS** (SEAC4RS IONS)
2007			

Figure Captions:

Figure 1: Ozone profile from an ECC ozonesonde with the temperature and humidity recorded by the accompanying radiosonde. The radiosonde also measures wind speed and direction. Data from a launch at Wallops Island, VA (37.9N, 75.5W) on 17 July 2019.

Figure 2: Altitude ranges of techniques used to measure ozone, ground-based, airborne and satellites. Other ground-based instrumentation (lidar, surface monitors) show context for the ozonesonde measurement. The schematic shows lidar that measure in the troposphere only (*Sullivan et al.*, 2015) and that cover troposphere and stratosphere. In fact, only one or two of the most widely used ozone lidar instruments, e.g., within NDACC, detect both troposphere and stratosphere; most ozone lidars report data only in the stratosphere.

Figure 3: (A) Cross-section of the electrochemical concentration cells (ECC) in (B) the ozonesonde sensor. There are two widely used ECC ozonesonde types, manufactured by Science Pump Corporation and the EN-SCI Corporation, producing the SPC-6A and EN-SCI instrument, respectively. The design of both ECCs is similar but there is a consistent 4-5% difference in their performance (**Figures 4A and 4B)** when launched under the same conditions (*Smit et al*., 2007; *Thompson et al.,* 2007c; *Smit*, 2014). Since 2014, a third ECC-type instrument manufactured at the Institute of Atmospheric Physics (IAP), Beijing, China, has been flown at several East Asian stations; the new instrument has not been extensively intercompared with the SPC-6A or EN-SCI in laboratory or field tests.

Figure 4: (A) JOSIE 2000 & BESOS (B): Relative differences between measurements of ozone by EN-SCI and SPC-6A using different combinations of 1%KI & full buffer and 0.5%KI & half buffer sensing solution strength. Data are averaged over 5 km altitude. All profiles were first referenced to the WMO/GAW standard ozone photometer (OPM). In JOSIE-2000 the OPM was in the Jülich (Germany) WCCOS facility; in BESOS the OPM flew on a gondola with 18 ozonesonde instruments in Laramie, Wyoming (US). (C) Mean percent differences between ozone measured by EN-SCI and SPC-6A sondes following WMO/GAW (2014) recommendations and sondes using 1%KI and 0.1buffer, during JOSIE-2017. Both sets of measurements were referenced to the OPM.

Figure 5: Total column ozone (TCO) derived from Boulder, CO, sondes compared with TCO measured by the Boulder Dobson spectrophotometer before (A) and after (B) re-processing of sonde data (Source: *Sterling et al.* 2018). An artifact step-function drop has been eliminated with the reprocessing.

Figure 6: Distribution of 64 most active ozone sounding stations in the global network (after *WMO/GAW Report No. 268*, 2021). These stations deposit data in major public archives. The latter include the archive WOUDC (World Ozone and Ultraviolet Data Center) sponsored by the World Meteorological Organization Global Atmospheric Watch (WMO/GAW; see Acronym List). Other commonly used archives are those of the Network for Detection of Atmospheric Composition Change (NDACC; *deMazière et al.*, 2018), at the websites of NASA for the Southern Hemisphere ADditional OZonesonde Network (SHADOZ; *Thompson et al.*, 2012; 2017), or at the NOAA/Global Monitoring Laboratory (GML).

Figure 7: Ozone-measuring satellites that have used sonde data for algorithm development and validation since 1995.

Figure 8: Examples of dynamic and/or chemical processes affecting the ozone profile, as captured by soundings. (A) Ozonesonde profiles over NOAA's South Pole station that illustrate extreme ozone loss due to catalytic chemical destruction in the region ~15-20 km [above 100

hPa] in October of 2018, compared to July 2018 (pre-ozone hole); (B) 2019-2020 winter-spring season Match ozone soundings over Greenland, Ny-Ålesund (Svalbard, Norway), Canada, and Finland (Source: *Wohltmann et al.*, 2020); Used by permission from AGU. (C) A series of ozone profiles during the 2013 SEACIONS campaign (https://tropo.gsfc.nasa.gov/seacions/) at Ellington Field, Texas (29.6N, 95.2W). STE influences appear in profiles of 7. 9 August and 4 September (green line) 2013. An example of low-ozone air lofted in convection appears in the profile of 4 September (maroon).

Figure 9: Composite data from a strategic global network, SHADOZ, displaying the zonal ozone structure (mixing ratios) that gives rise to the wave-one pattern in satellite TCO. The contours are based on annually averaged profile data over 1998-2020.

Figure 10: (A) Generalized flowchart indicating how ozonesonde data is used for a first guess or a priori profile in the retrieval process and for validation of the final satellite product. (B) Comparison of ozone profiles retrieved from TROPOMI and those from ozonesondes for different zonal bands. The relative mean difference between the retrieval results and the high-resolution sonde data (solid line), as well as the standard deviation of the differences (dashed line), is shown in black. The comparison with the sonde profiles convolved with the averaging kernels is shown in red. In grey, the relative difference between the a priori ozone profiles and high-resolution ozonesonde profiles is displayed, along with the corresponding standard deviations. (Source: *Mettig et al.*, 2021a).

Figure 11: Scatterplot of monthly mean TrCO estimated by the tropospheric residual OMI/MLS product (*Ziemke et al.*, 2019) vs the corresponding TrCO from 10 SHADOZ sites, the latter computed by integrating ozone from surface to tropopause determined from the coupled radiosonde. Comparisons are for SHADOZ stations with latitude within + 20 degrees.

Figure 12: (A) Comparison of ozone from Wallops Island, VA, USA, ozonesondes (red) and Aura/MLS data (black) at the standard levels of the MLS measurement (mean over 2004-2020) with standard deviations indicated by horizontal bars; (B) TCO from Wallops sondes (red) compared to TCO from the Aura/OMI (black), 2004-2020, and Dobson spectrophotometer (blue), 1995-2020.

Figure 13: Comparisons between data from ECC sondes and Aura MLS stratospheric ozone profiles (top panels), and OMI, GOME 2A and GOME 2B (blue dots), and OMPS (red dots) TCO (bottom panels). (A) Wallops Island, VA, record; (B) Samoa SHADOZ record. Red (blue) colors in the top panels indicate where the ECC ozone is greater (less) than MLS. Horizontal dashed lines in the lower panels indicate the 0% line for TCO differences. Note a post-2014 drop in Samoa TCO relative to satellite measurements.

Acronym List

AASE II Airborne Arctic Stratospheric Experiment II

ACE-FTS Atmospheric Chemistry Experiment – Fourier Transform Spectrometer on Canadian SCISAT satellite

ASOPOS Assessment of Standard Operating Procedures for OzoneSondes

BESOS Balloon Experiment on Standards for OzoneSondes

BORTAS	Quantifying the impaoct of BOReal forest fires on Tropospheric oxidants over the Atlantic using Aircraft and Satellites
DU	Dobson Unit, the unit to express vertical ozone column abundances,1 DU= 2.69×10^{16} molecules per cm^2 at STP 1×10^{-3} atm.cm at STP)
EASOE	European Arctic Stratospheric Ozone Experiment
ECC	Electrochemical Concentration Cell
EN-SCI	Environmental Science Corporation; ECC ozonesonde manufacturer
ESRL	Earth System Research Laboratories
GAW	Global Atmospheric Watch
GCOS	Global Climate Observing System
GEMS	Geostationary Environment Monitoring Spectrometer
GML	Global Monitoring Laboratory (division of NOAA's ESRL; formerly GMD)
GOES	Geostationary Operational Environmental Satellites
GOME	Global Ozone Monitoring Experiment (onboard MetOp satellites)
GNSS	Global Navigational Satellite System
GRUAN	GCOS Reference Upper Air Network
IAP	Institute of Atmospheric Physics, Beijing, China
IGACO	Integrated Global Atmospheric Chemistry Observations
IOC	International Ozone Commission
IONS	Intensive Ozonesonde Network Study
IPCC	Intergovernmental Panel on Climate Change
ISS	International Space Station
JOSIE	Jülich OzoneSonde Intercomparison Experiment
KI	Potassium Iodide
LEO	Low Earth Orbit
MLS	Microwave Limb Sounder (on Aura satellite)
NASA	National Aeronautics and Space Administration
NDACC	Network for the Detection of Atmospheric Composition Change
NOAA	National Oceanic and Atmospheric Administration
OMI	Ozone Monitoring Instrument (on Aura satellite)
OMPS-LP	Ozone Mapping and Profiler Suite – Limb Profiler (onboard Suomi-NPP and JPSS satellites)
OPM	Ozone PhotoMeter Instrument (used as UV-reference)
OSIRIS	Optical Spectrograph and InfraRed Imaging **S**ystem, on Odin satellite
O3S-DQA	Ozone Sonde Data Quality Assessment
QA	Quality Assurance
RECONCILE	Reconciliation of essential process parameters for an enhanced predictability of Arctic stratospheric ozone loss and its climate interactions
SAGE III	Stratospheric Aerosol and Gas Experiment (fourth generation on ISS)
SBUV	Solar Backscatter Ultraviolet (referring to instrument type on satellites measuring ozone)
SCIAMACHY	SCanning Imaging Absorption SpectroMeter for Atmospheric CHartographY
SCIATRAN	Radiative transfer and retrieval code used by Univ. Bremen SCIAMACHY and TROPOMI algorithm group
SCOUT-O3	Stratospheric-Climate links with emphasis On the Upper Troposphere and lower stratosphere
SEACIONS	Southeast America Consortium for Intensive Ozonesonde Network Study

SESAME	Second European Stratospheric Arctic and Mid-latitude Experiment
SHADOZ	Southern Hemisphere ADditional OZonesondes
SI^{2}N	Ozone trend assessment study supported by SPARC, IOC, IGACO, and NDACC
SMILES	Submillimeter-Wave Limb Emission Sounder onboard ISS
SOLVE	SAGE III Ozone Loss and Validation Experiment
SOP	Standard Operating Procedure
SPARC	Stratosphere-troposphere Processes And their Role in Climate
SPC	Science Pump Corporation; ECC ozonesonde manufacturer
SST	Sensing Solution Type
STP	Standard Temperature (=273.15 K) and Pressure (=1013.25 hPa) conditions
StratoClim	Stratospheric and upper tropospheric processes for better climate predictions
TCO	Total Column Ozone
TEMPO	Tropospheric Emissions: Monitoring of Pollution
THESEO	Third European Stratospheric Experiment on Ozone
TOMS	Total Ozone Mapping Spectrometer
TOPAS	Tikhonov regularized Ozone Profile retrievAl with SCIATRAN
TROPOMI	TROPOspheric Monitoring Instrument
TrCO	Tropospheric Column Ozone
UNEP	United Nations Environment Programme
UV	Ultraviolet
VINTERSOL	Validation of INTERnational satellites and Study of Ozone Loss
WCCOS	World Calibration Center for OzoneSonde
WDCRG	World Data Centre for Reactive Gases
WMO	World Meteorological Organization
WOUDC	World Ozonesonde and Ultraviolet Data Centre

Figure 1

Station: Wallops Island, Virginia, USA
Launch Date: 17 July 2019, 17 UTC

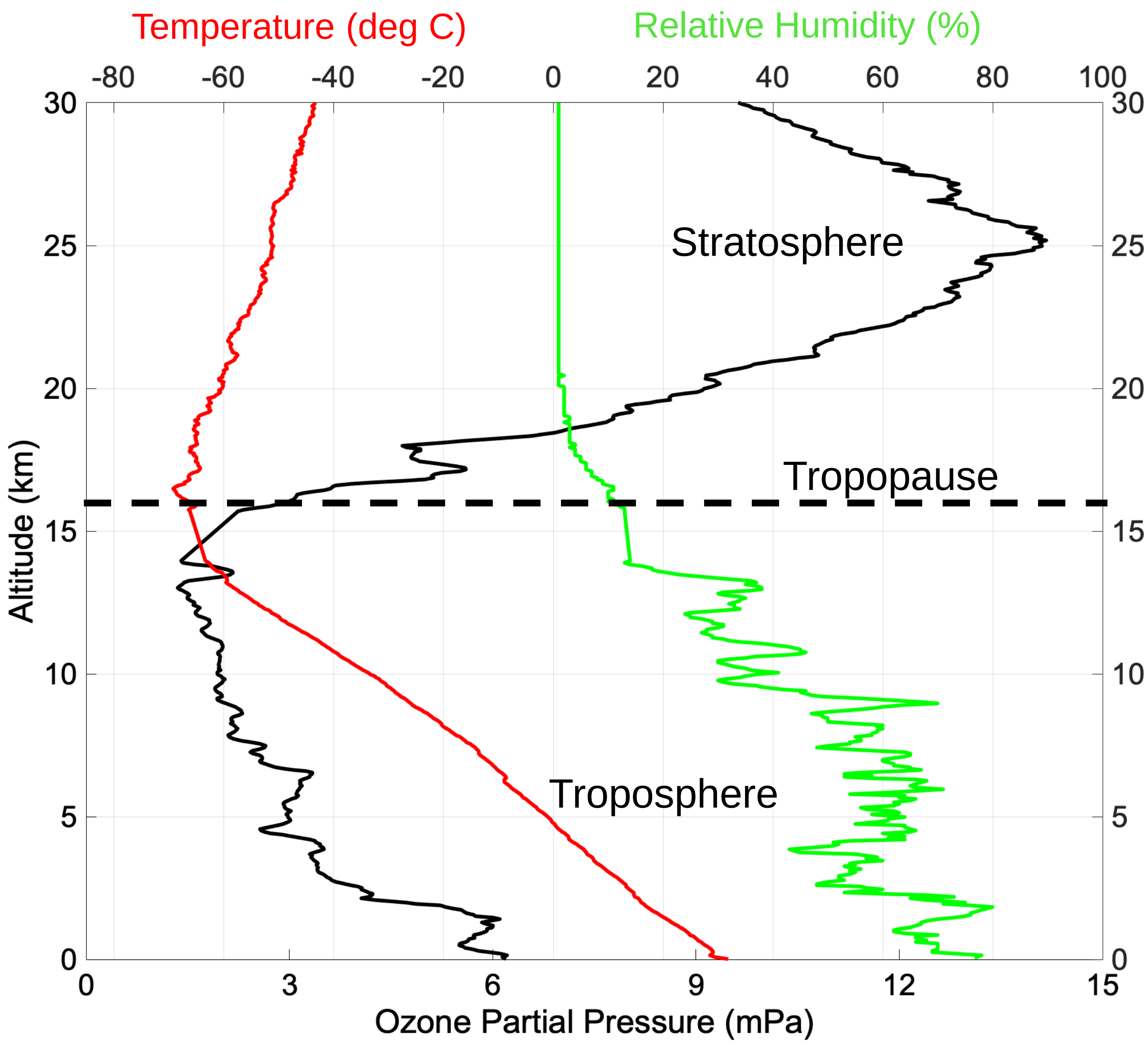

Figure 2

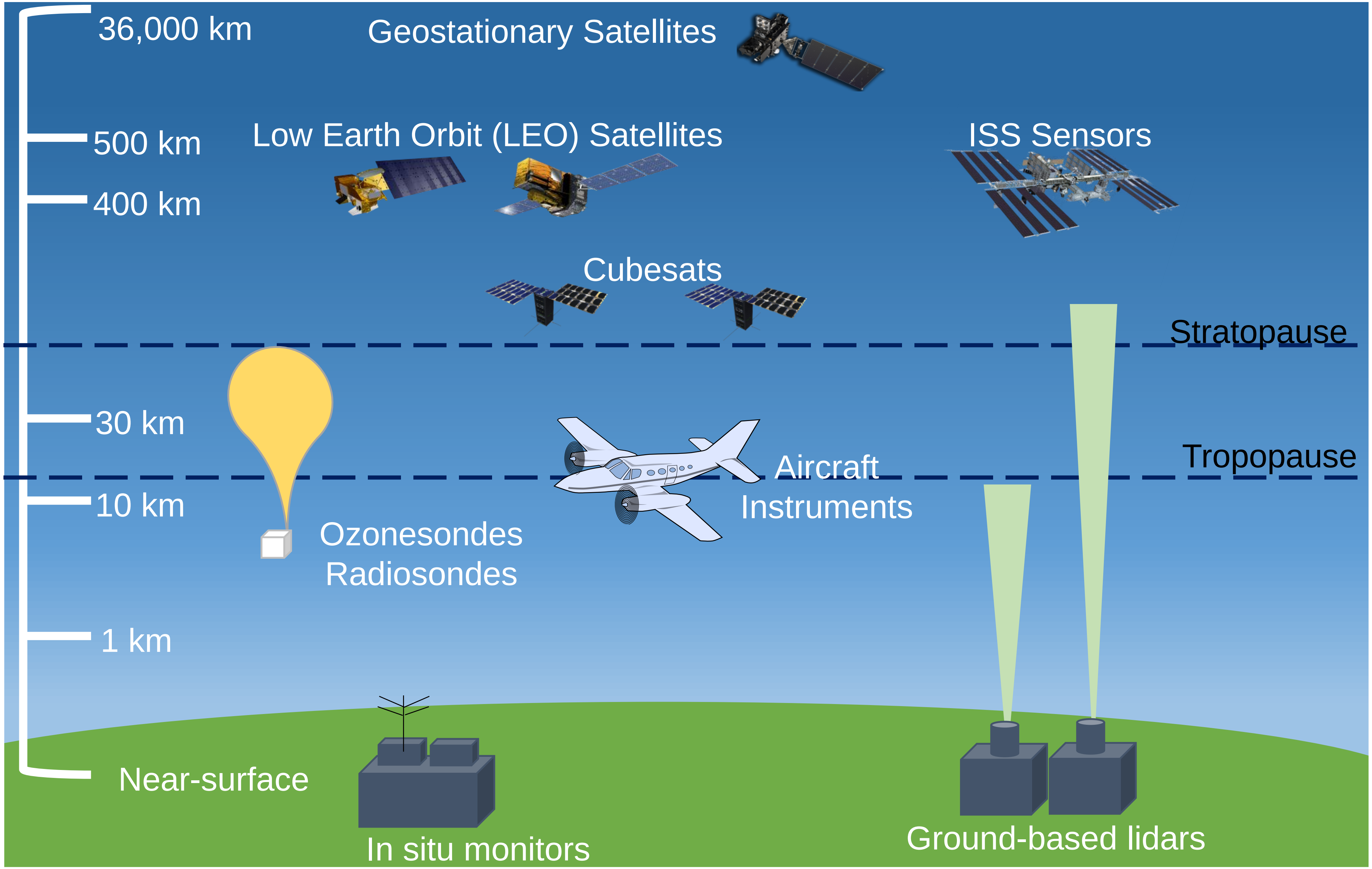
36,000 km
Geostationary Satellites
500 km
Low Earth Orbit (LEO) Satellites
ISS Sensors
400 km
Cubesats
Stratopause
30 km
Tropopause
Aircraft
Instruments
10 km
Ozonesondes
Radiosondes
1 km
Near-surface
In situ monitors
Ground-based lidars

Figure 3

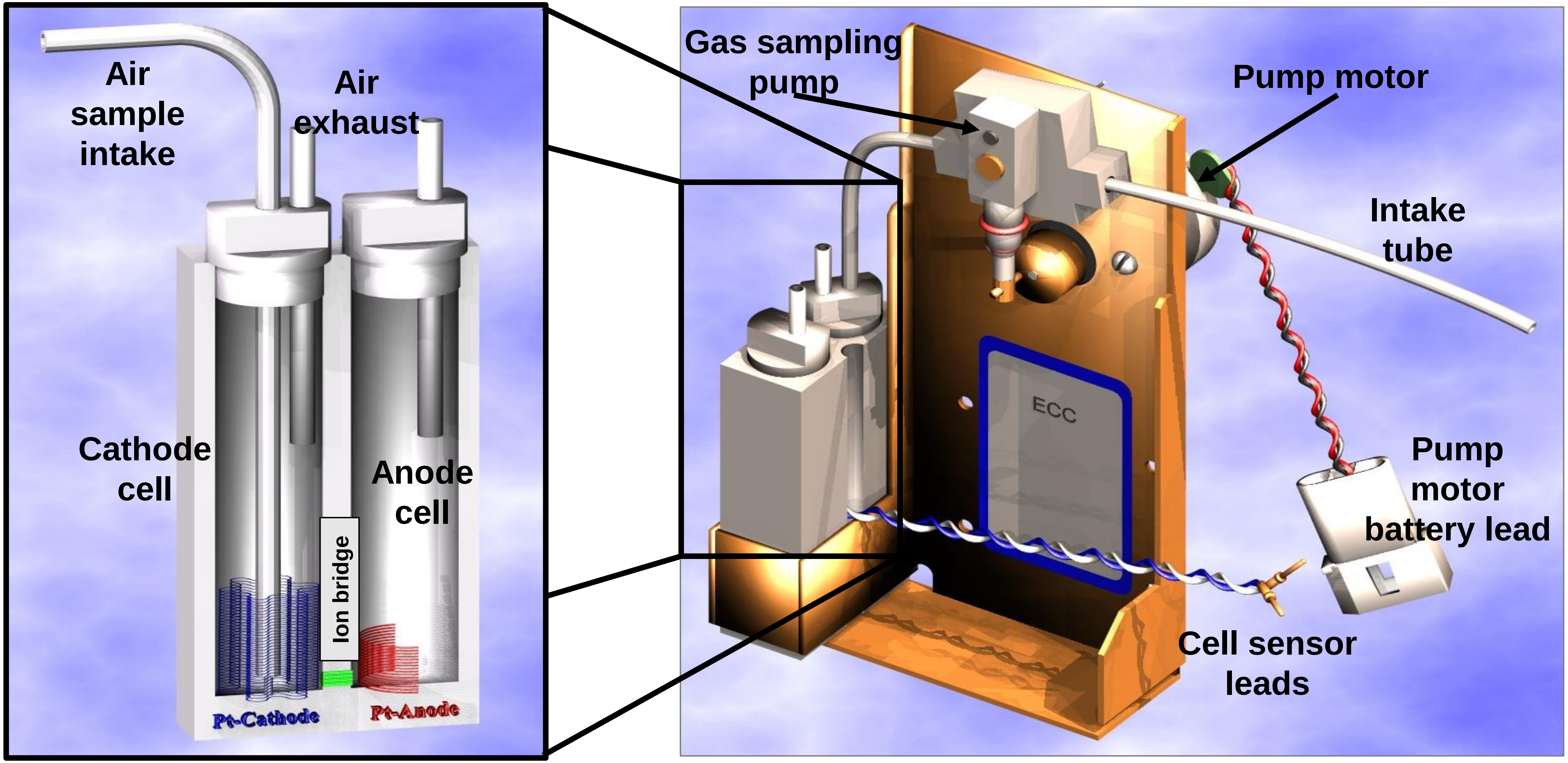
Air sample intake
Air exhaust
Cathode cell
Anode cell
Ion bridge
Pt-Cathode
Pt-Anode
Gas sampling pump
Pump motor
Intake tube
ECC
Pump motor battery lead
Cell sensor leads

Figure 4

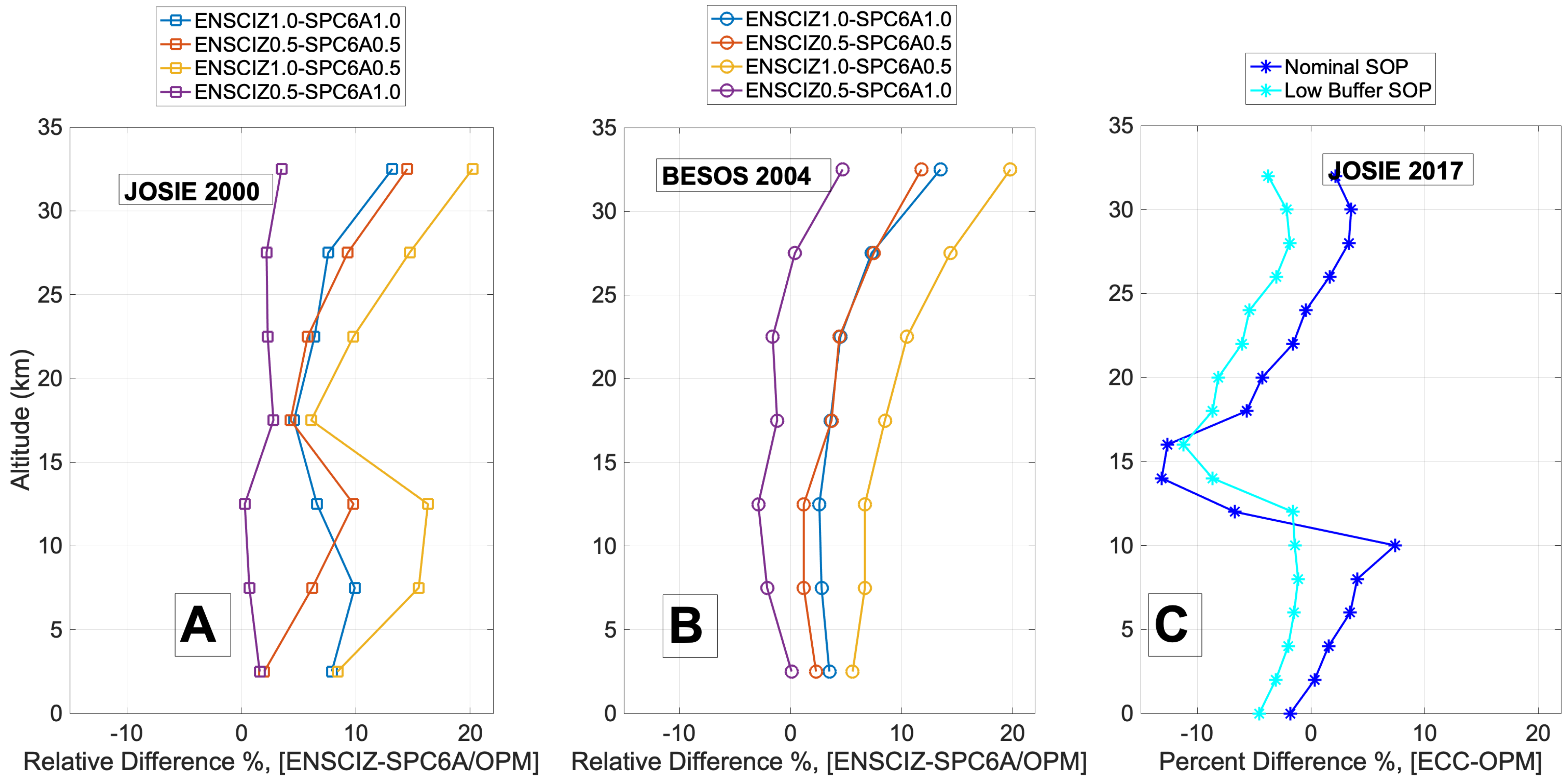
ENSCIZ1.0-SPC6A1.0
ENSCIZ0.5-SPC6A0.5
ENSCIZ1.0-SPC6A0.5
ENSCIZ0.5-SPC6A1.0
JOSIE 2000
A
Altitude (km)
Relative Difference %, [ENSCIZ-SPC6A/OPM]
ENSCIZ1.0-SPC6A1.0
ENSCIZ0.5-SPC6A0.5
ENSCIZ1.0-SPC6A0.5
ENSCIZ0.5-SPC6A1.0
BESOS 2004
B
Relative Difference %, [ENSCIZ-SPC6A/OPM]
Nominal SOP
Low Buffer SOP
JOSIE 2017
C
Percent Difference %, [ECC-OPM]

Figure 5

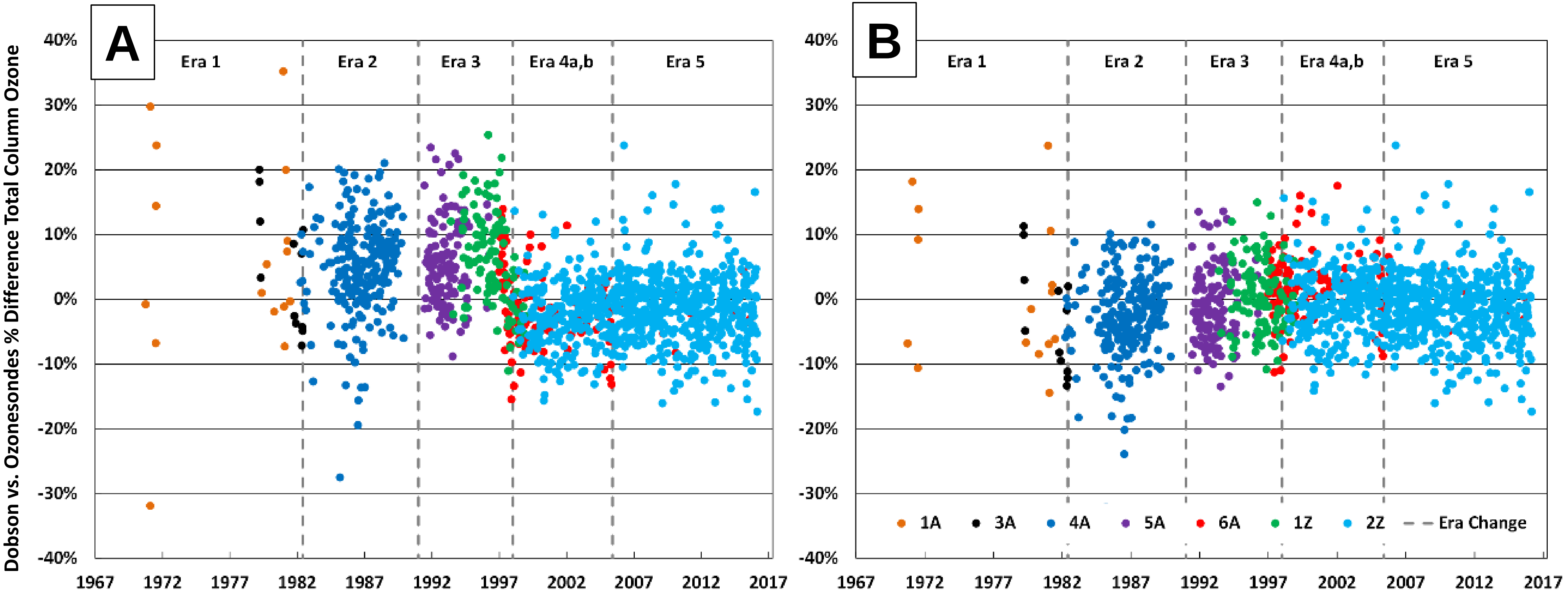
A
B
Era 1
Era 2
Era 3
Era 4a,b
Era 5
Dobson vs. Ozonesondes % Difference Total Column Ozone
40%
30%
20%
10%
0%
-10%
-20%
-30%
-40%
1967
1972
1977
1982
1987
1992
1997
2002
2007
2012
2017
1A
3A
4A
5A
6A
1Z
2Z
Era Change

Figure 6

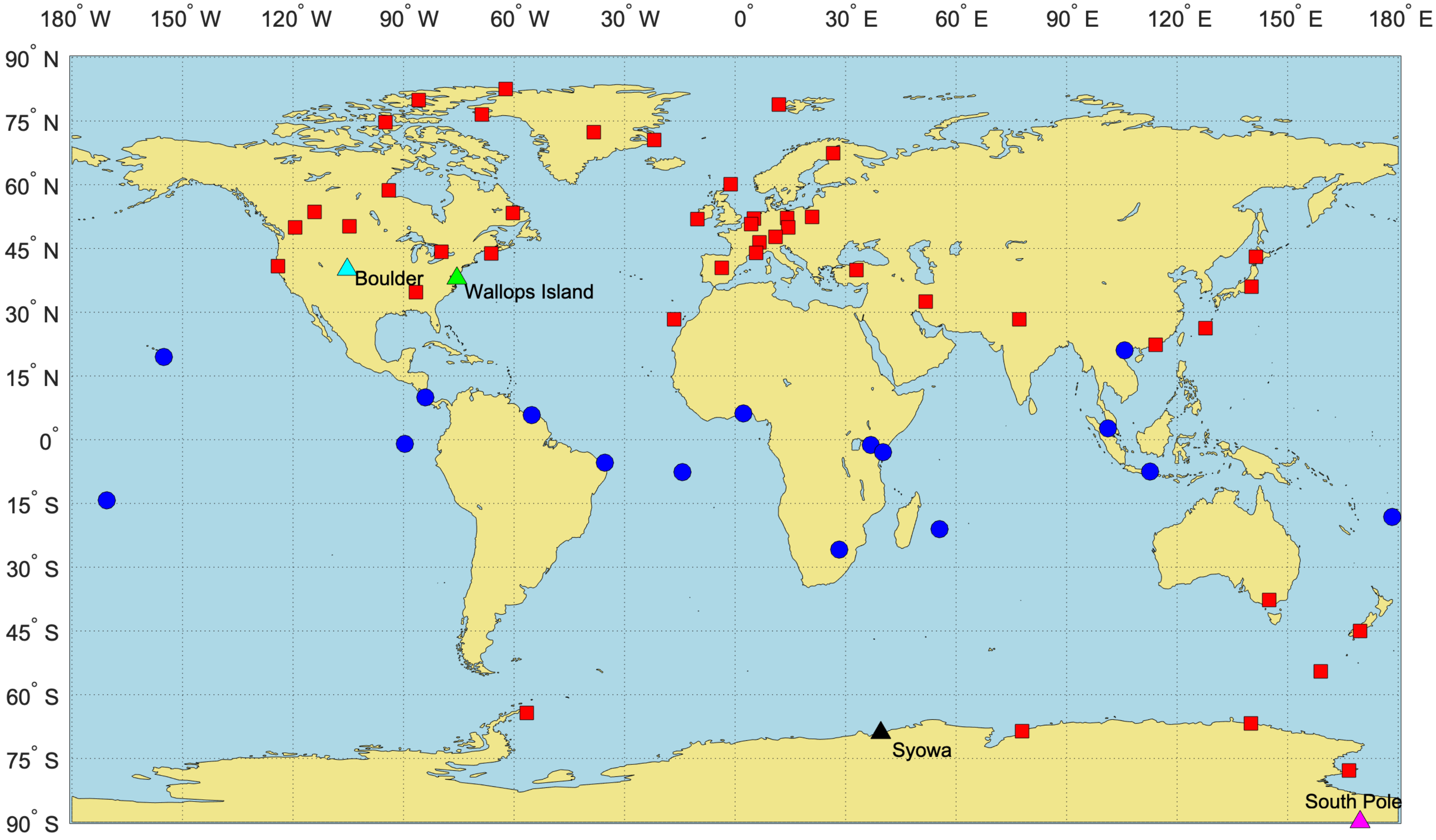

180° W
150° W
120° W
90° W
60° W
30° W
0°
30° E
60° E
90° E
120° E
150° E
180° E
90° N
75° N
60° N
45° N
30° N
15° N
0°
15° S
30° S
45° S
60° S
75° S
90° S
Boulder
Wallops Island
Syowa
South Pole

Figure 7

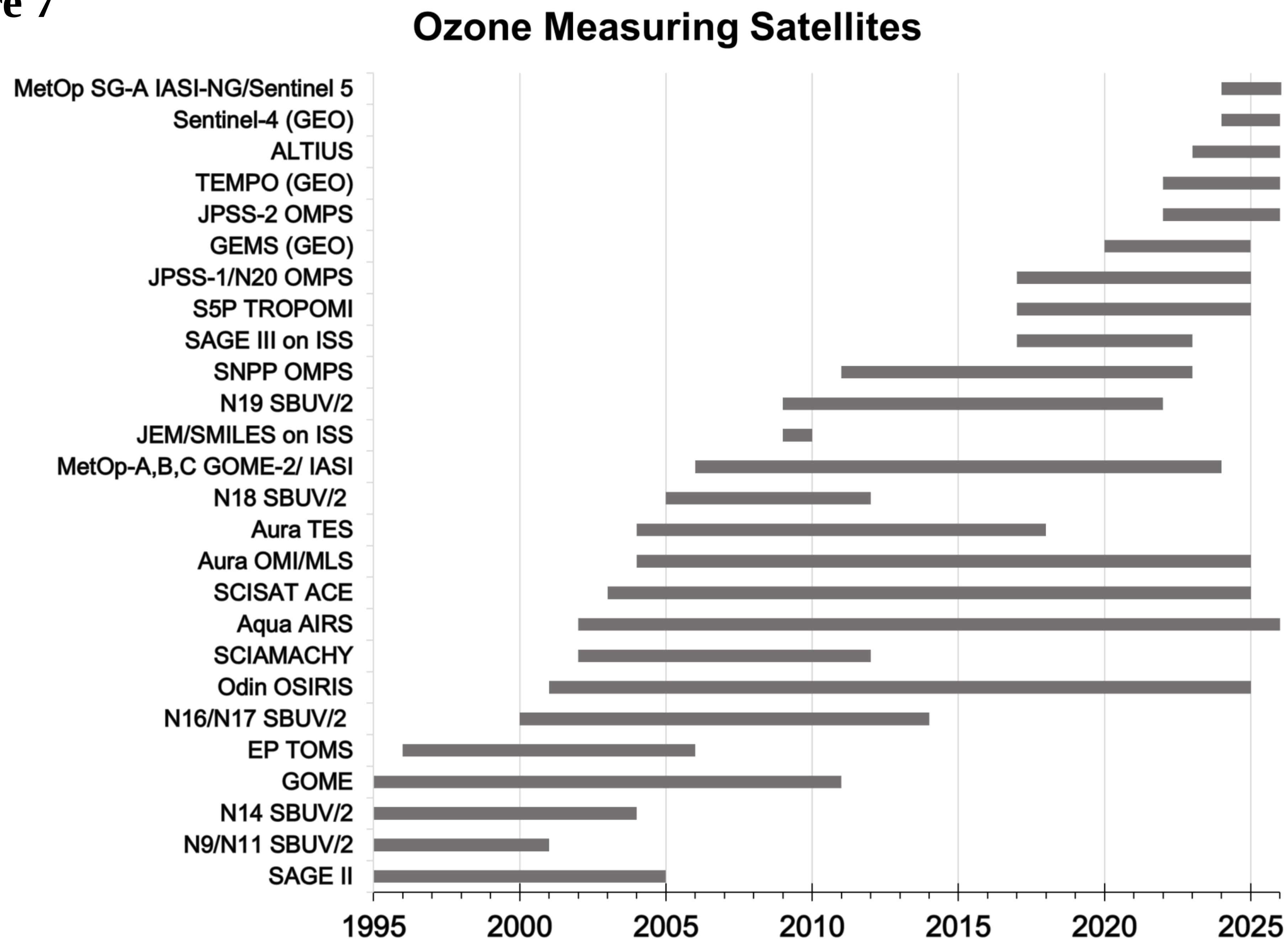

Ozone Measuring Satellites
MetOp SG-A IASI-NG/Sentinel 5
Sentinel-4 (GEO)
ALTIUS
TEMPO (GEO)
JPSS-2 OMPS
GEMS (GEO)
JPSS-1/N20 OMPS
S5P TROPOMI
SAGE III on ISS
SNPP OMPS
N19 SBUV/2
JEM/SMILES on ISS
MetOp-A,B,C GOME-2/ IASI
N18 SBUV/2
Aura TES
Aura OMI/MLS
SCISAT ACE
Aqua AIRS
SCIAMACHY
Odin OSIRIS
N16/N17 SBUV/2
EP TOMS
GOME
N14 SBUV/2
N9/N11 SBUV/2
SAGE II
1995
2000
2005
2010
2015
2020
2025

Figure 8

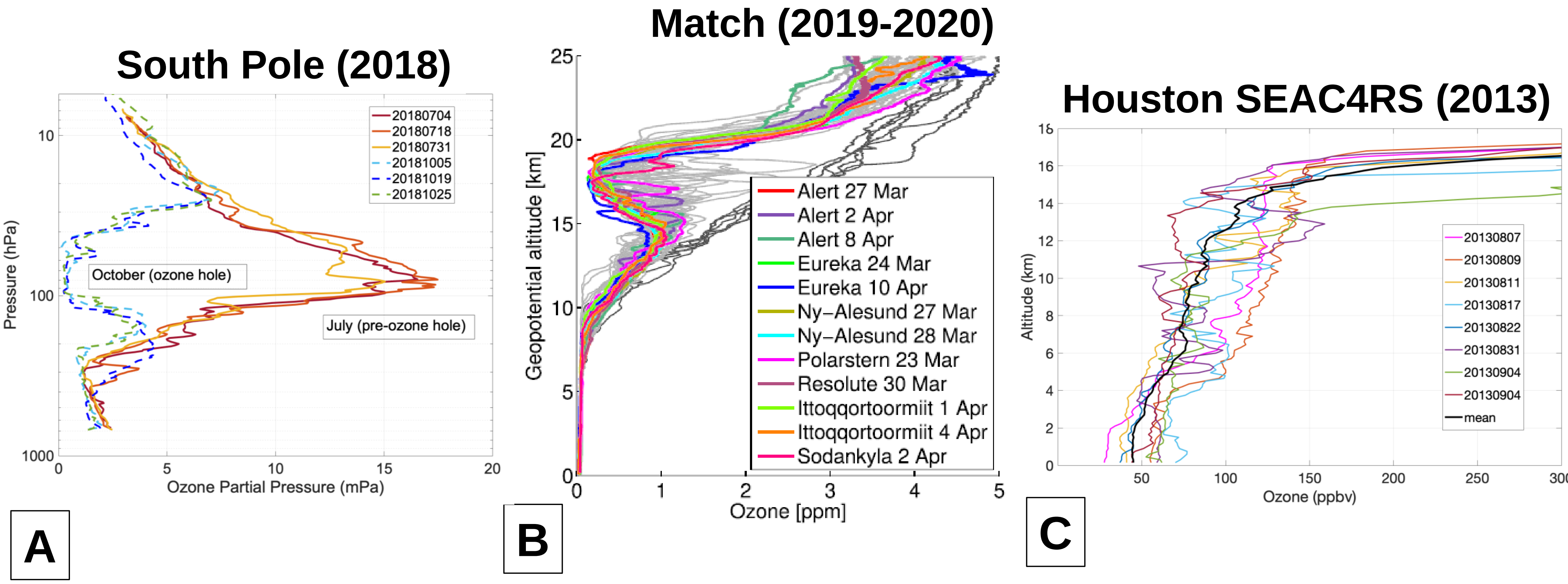
South Pole (2018)
20180704
20180718
20180731
20181005
20181019
20181025
October (ozone hole)
July (pre-ozone hole)
Pressure (hPa)
Ozone Partial Pressure (mPa)
A
Match (2019-2020)
Alert 27 Mar
Alert 2 Apr
Alert 8 Apr
Eureka 24 Mar
Eureka 10 Apr
Ny−Alesund 27 Mar
Ny−Alesund 28 Mar
Polarstern 23 Mar
Resolute 30 Mar
Ittoqqortoormiit 1 Apr
Ittoqqortoormiit 4 Apr
Sodankyla 2 Apr
Geopotential altitude [km]
Ozone [ppm]
B
Houston SEAC4RS (2013)
20130807
20130809
20130811
20130817
20130822
20130831
20130904
20130904
mean
Altitude (km)
Ozone (ppbv)
C

Figure 9

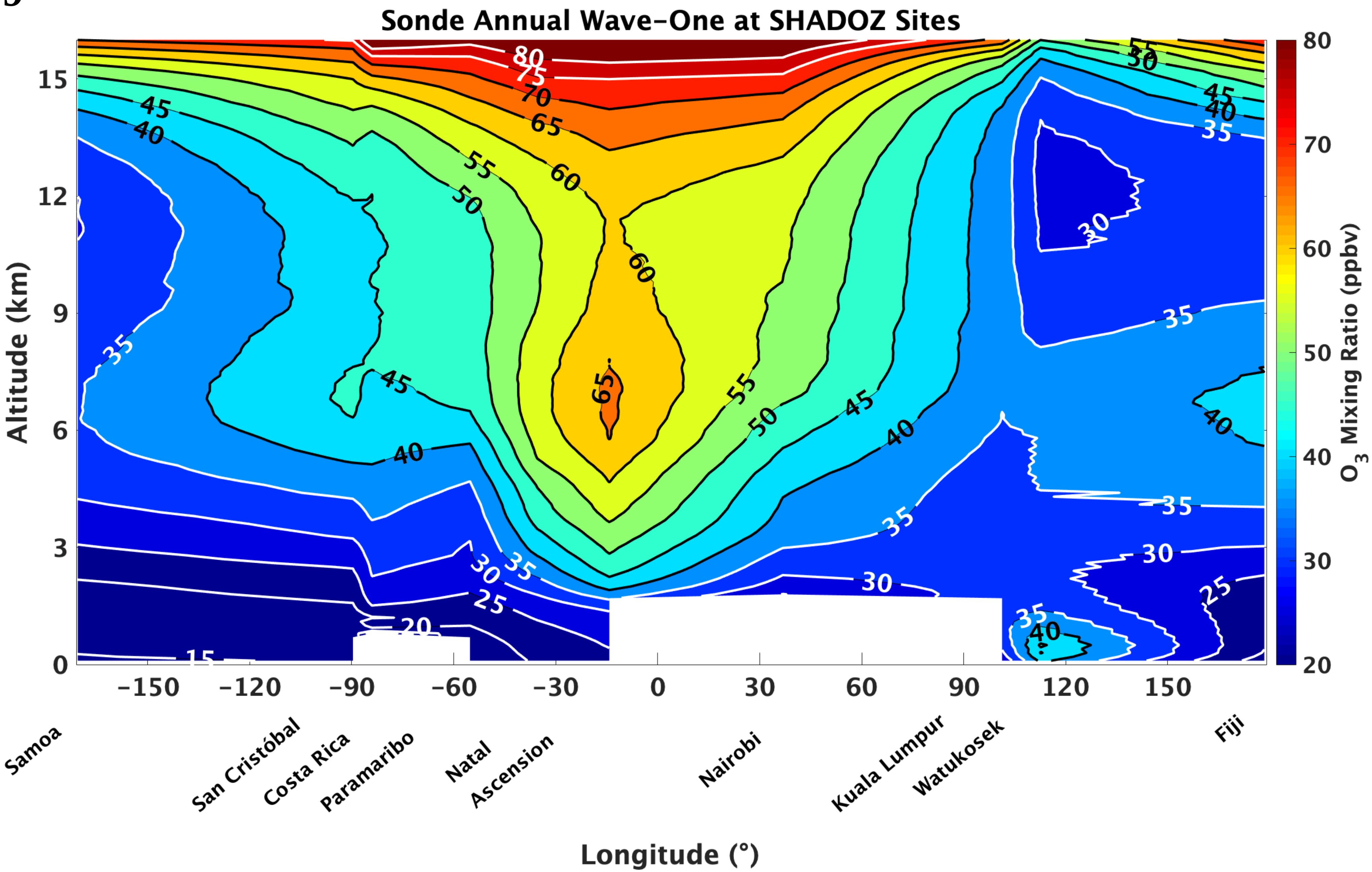

Sonde Annual Wave-One at SHADOZ Sites
Altitude (km)
Longitude (°)
O3 Mixing Ratio (ppbv)
Samoa
San Cristóbal
Costa Rica
Paramaribo
Natal
Ascension
Nairobi
Kuala Lumpur
Watukosek
Fiji

Figure 10

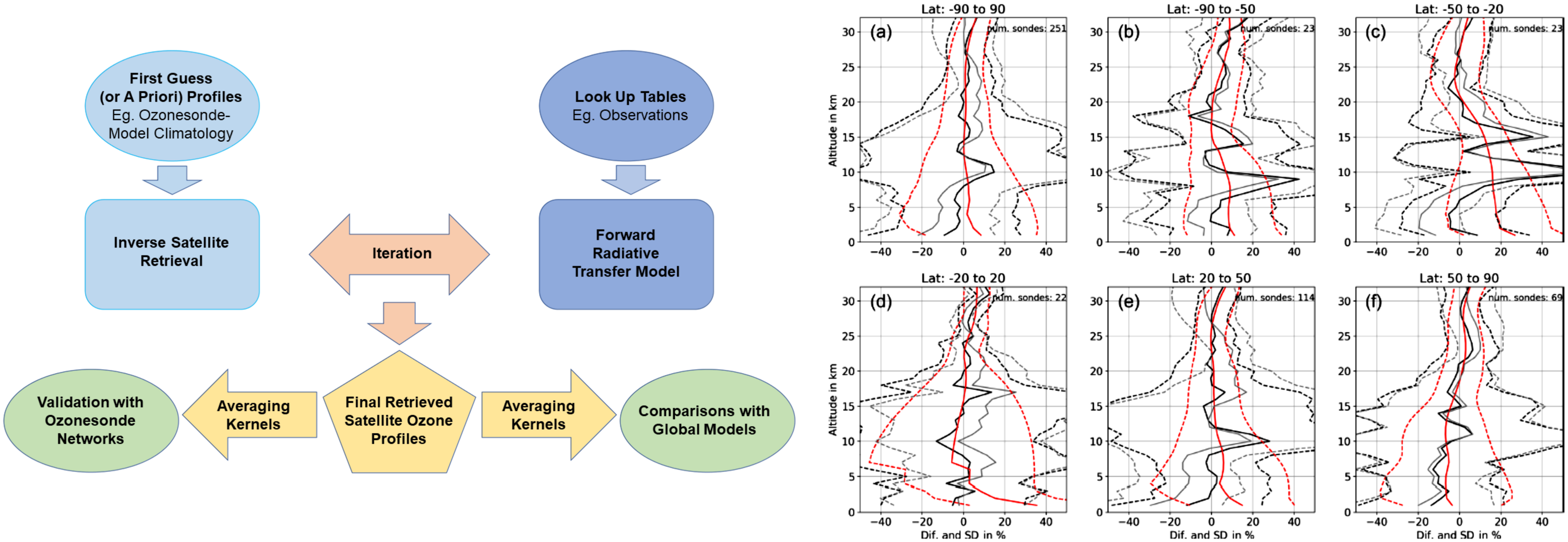
First Guess
(or A Priori) Profiles
Eg. Ozonesonde-
Model Climatology
Look Up Tables
Eg. Observations
Inverse Satellite
Retrieval
Iteration
Forward
Radiative
Transfer Model
Validation with
Ozonesonde
Networks
Averaging
Kernels
Final Retrieved
Satellite Ozone
Profiles
Averaging
Kernels
Comparisons with
Global Models
Lat: -90 to 90
(a)
num. sondes: 251
Lat: -90 to -50
(b)
num. sondes: 23
Lat: -50 to -20
(c)
num. sondes: 23
Lat: -20 to 20
(d)
num. sondes: 22
Lat: 20 to 50
(e)
num. sondes: 114
Lat: 50 to 90
(f)
num. sondes: 69
Altitude in km
Dif. and SD in %

A

B

Figure 11

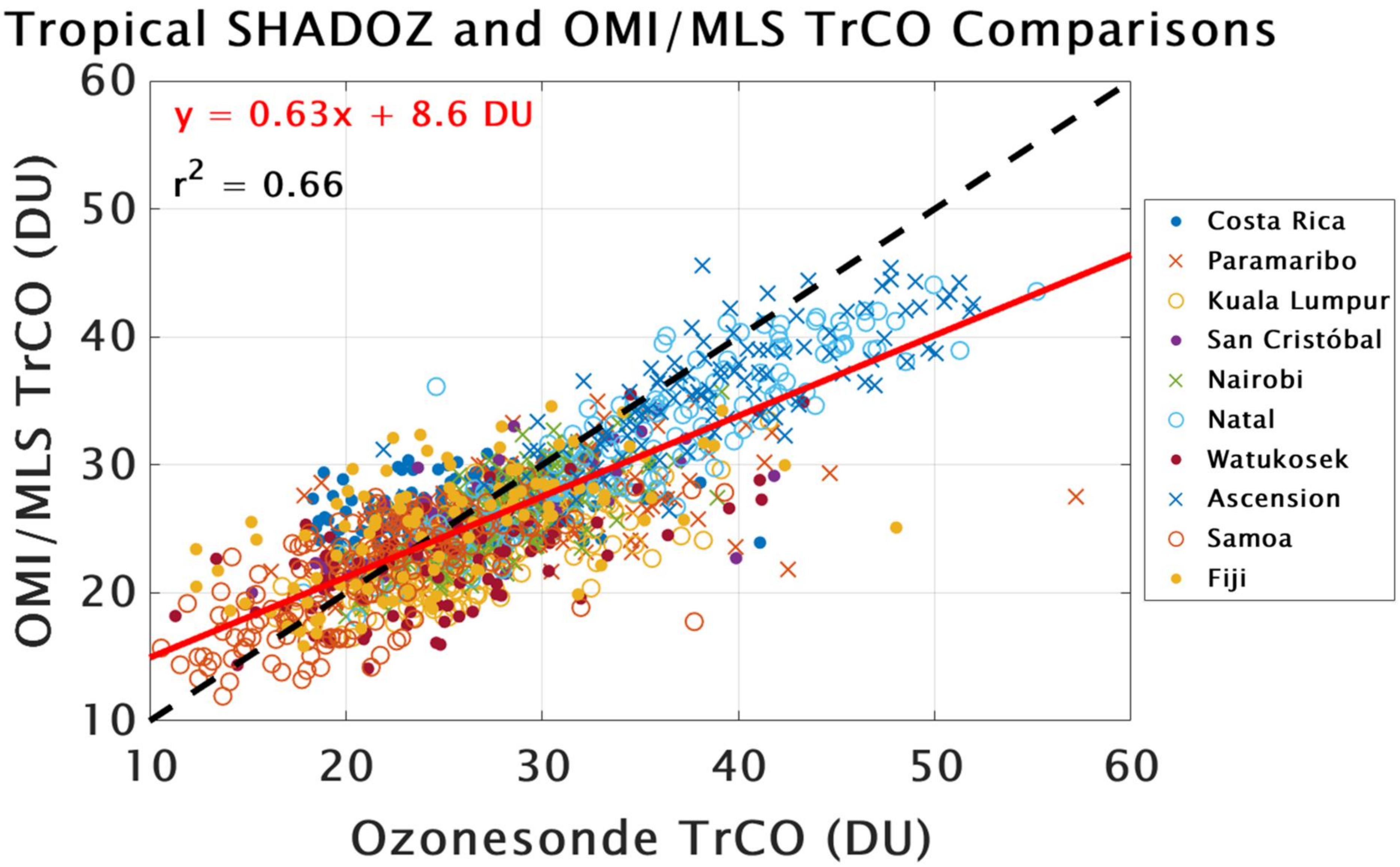

Tropical SHADOZ and OMI/MLS TrCO Comparisons
y = 0.63x + 8.6 DU
r2 = 0.66
OMI/MLS TrCO (DU)
Ozonesonde TrCO (DU)
10
20
30
40
50
60
10
20
30
40
50
60
Costa Rica
Paramaribo
Kuala Lumpur
San Cristóbal
Nairobi
Natal
Watukosek
Ascension
Samoa
Fiji

Figure 12

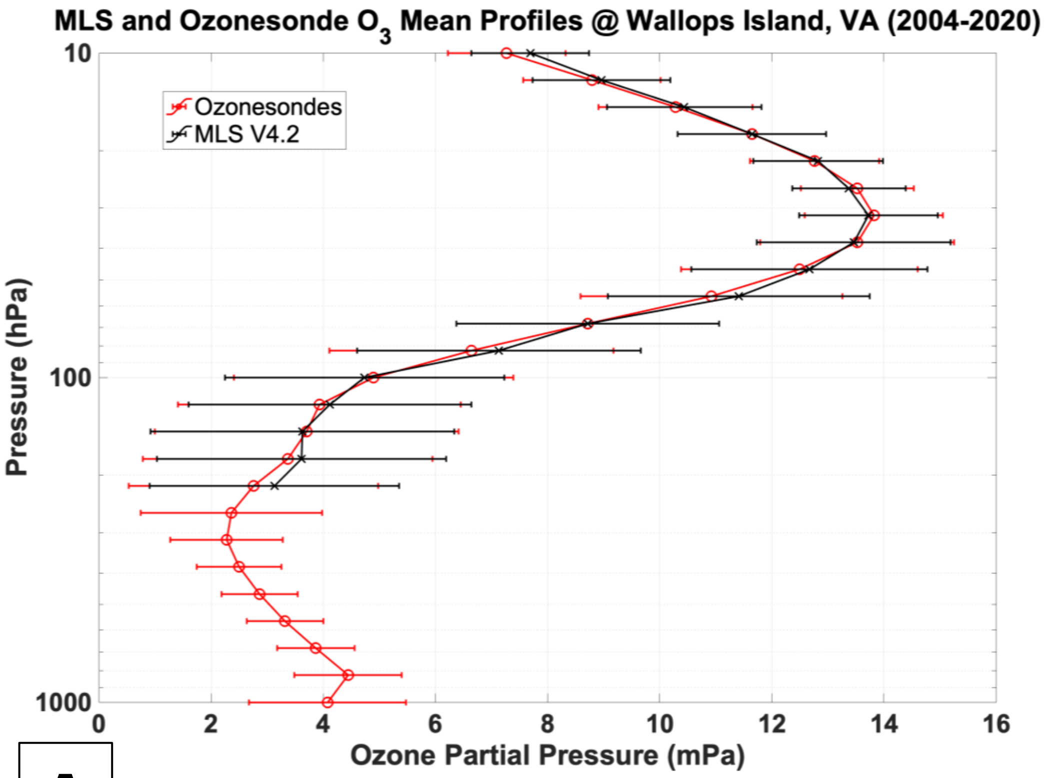
MLS and Ozonesonde O_3 Mean Profiles @ Wallops Island, VA (2004-2020)
Ozonesondes
MLS V4.2
Pressure (hPa)
Ozone Partial Pressure (mPa)

A

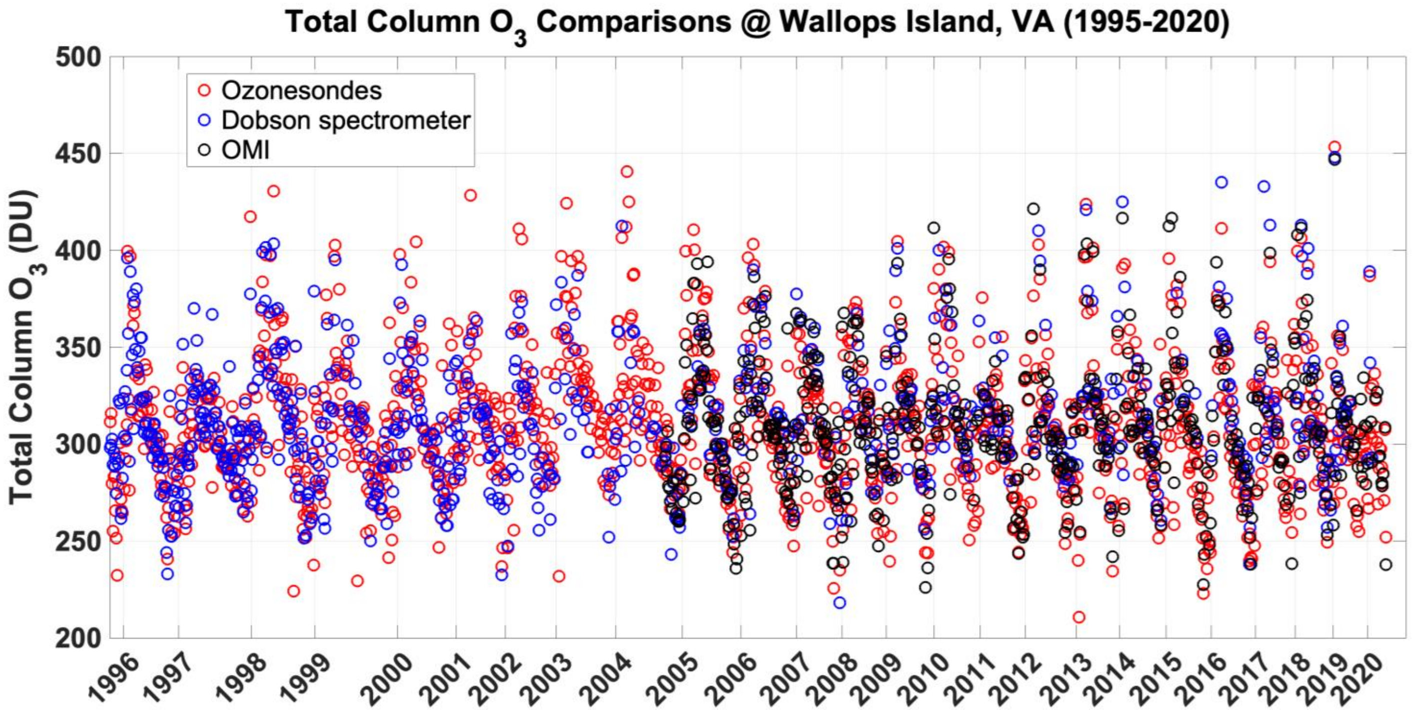
Total Column O_3 Comparisons @ Wallops Island, VA (1995-2020)
Ozonesondes
Dobson spectrometer
OMI
Total Column O_3 (DU)

B

Figure 13

A

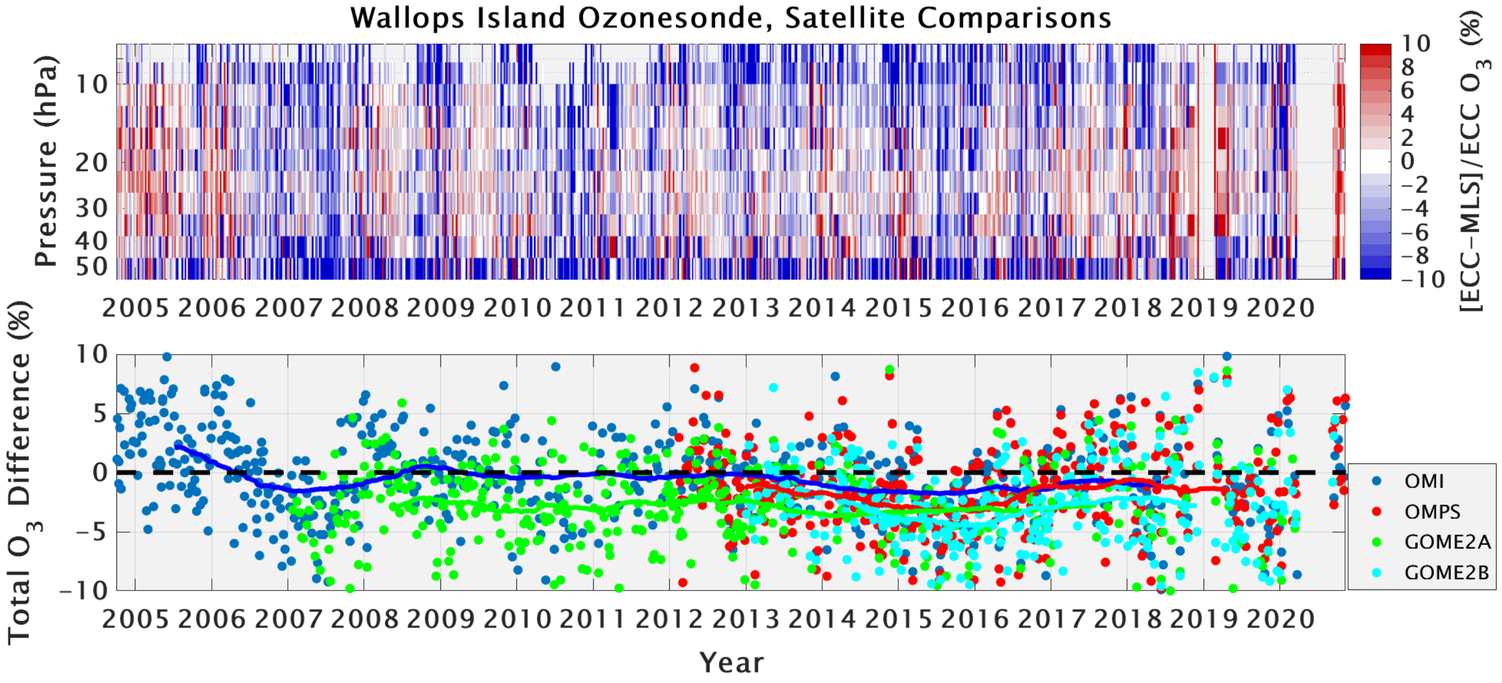
Wallops Island Ozonesonde, Satellite Comparisons
Pressure (hPa)
10
20
30
40
50
10
8
6
4
2
0
−2
−4
−6
−8
−10
[ECC−MLS]/ECC O3 (%)
2005 2006 2007 2008 2009 2010 2011 2012 2013 2014 2015 2016 2017 2018 2019 2020
Total O3 Difference (%)
10
5
0
−5
−10
OMI
OMPS
GOME2A
GOME2B
Year

B

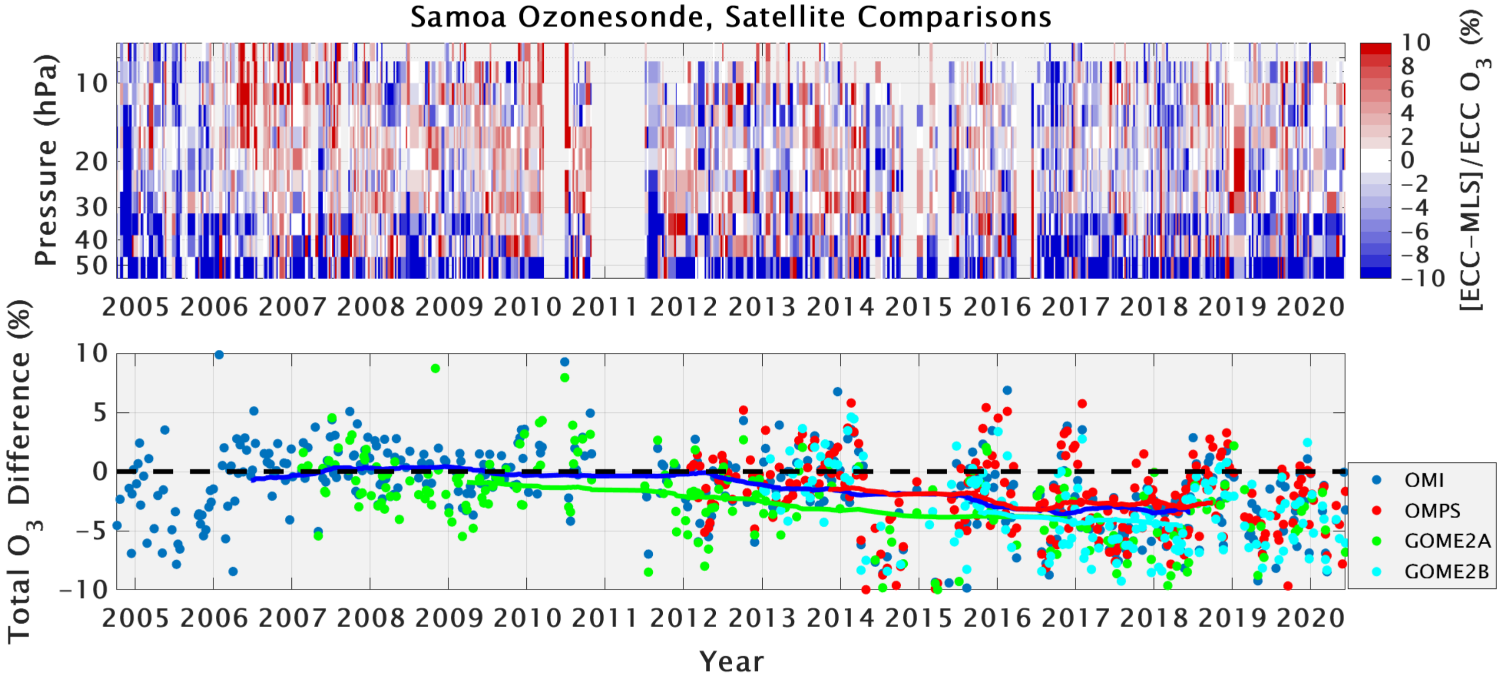
Samoa Ozonesonde, Satellite Comparisons
Pressure (hPa)
10
20
30
40
50
10
8
6
4
2
0
−2
−4
−6
−8
−10
[ECC−MLS]/ECC O3 (%)
2005 2006 2007 2008 2009 2010 2011 2012 2013 2014 2015 2016 2017 2018 2019 2020
Total O3 Difference (%)
10
5
0
−5
−10
OMI
OMPS
GOME2A
GOME2B
Year